A Fixed-Point Algorithm for the AC Power Flow Problem

by

Liangjie Chen

A thesis submitted in conformity with the requirements
for the degree of Master of Applied Science

Edward S. Rogers Department of Electrical and Computer Engineering
University of Toronto

A Fixed-Point Algorithm for the AC Power Flow Problem

Liangjie Chen
Master of Applied Science
Edward S. Rogers Department of Electrical and Computer Engineering
University of Toronto
2022

Abstract

This thesis presents an algorithm that solves the power flow problem for balanced, three phase transmission systems at steady state. This algorithm is an extension of the "fixed-point power flow" algorithm in the literature, which is originally derived for lossless AC transmission systems. We first manipulate the standard power flow equations into an equivalent fixed-point form, from which we derive the extended fixed-point power flow algorithm. We then theoretically study the proposed algorithm on a two-bus system, where we model selected network parameters, e.g., resistive loss, as perturbations to a nominal, lossless system, and derive sufficient solvability conditions. Finally, we validate the algorithm through extensive simulations on test systems of various sizes under different loading scenarios, and compare its convergence behaviors against those of classic power flow algorithms.

To Jesse.

Acknowledgments

First and foremost, I want to thank my supervisor, Professor John Simpson-Porco. While his knowledge, intuition and mathematical rigor greatly helped me solve a myriad of problems I faced over the last two years and grow as a student in general, I could never have finished this thesis without his endless patience and understanding. Knowing that I am far from an ideal student, I consider myself extremely fortunate to have a supervisor like him, and I am grateful for his guidance.

I would also like to thank my committee members, Professors Zeb Tate and Josh Taylor, for providing insightful and valuable feedback on this thesis. In particular, I had the pleasure of working under the supervision of Professor Tate during my undergraduate studies, and that experience was largely what inspired me to pursue graduate studies. I thank him for his encouragements and mentorship during that time, and his help during my scholarship applications and coursework afterwards.

I would not be who or where I am if not for the hard work and sacrifices of my parents, 王淑荣 and 陈枫华, and I owe everything I have to you. I dedicate this thesis to my brother Jesse, who had to endure my presence at home over the first year and half of the pandemic, and whom I have probably driven crazy on multiple occasions. I am also indebted to my extended family in China, who have loved and believed in me since day one.

To my friends and colleagues at the Systems Control Group, thank you for making me feel included and welcomed with the many memes, chaotic discussions, and (sometimes traumatic) social events. My thanks also extend to the lab dog Akela, whose visits always make my day.

Last but certainly not least, I would like to thank Amy for being the most supportive and loving partner I could ever wish for. Thank you for keeping me sane and always being there for me during the last two years. You inspire me to better myself everyday.

Contents

List of Figures

List of Tables

Chapter 1

Introduction

1.1 Problem Motivation

A fundamental problem that underpins many power system analyses and operations is the power flow problem, which describes the flow and balance of power in a synchronous AC power system at steady state, and (usually) its relationship with the voltage at each bus in the system. The power flow problem is formulated by a set of coupled nonlinear equations—known as the power flow equations—that enforces Kirchhoff's laws and Ohm's law, subject to physical constraints [1]. The power flow problem can be difficult to solve due to the inherent nonlinearity in the power flow equations, and typically no analytic solution is possible. However, solving the power flow problem is essential for the grid operators to control the power system effectively and respond to contingency events safely.

For balanced three-phase transmission systems at steady state, the standard approach to accurately solve the power flow problem is to use an iterative algorithm such as Newton-Raphson. However, these algorithms usually demand initial conditions in a sufficiently small neighborhood of the desired solution in order to converge to it, and it can be difficult to satisfy this requirement since there exists no systematic process for finding such initial conditions. Furthermore, when these algorithms fail, it could be due to the inherent problem infeasibility given the system parameters, the numerical instability of the algorithms, or poor initial conditions for the algorithms. Therefore, a robust and reliable algorithm that solves the power flow problem is highly desirable.

A recently developed research direction produced a novel and particularly robust fixed-point based algorithm to solve the power flow problem in the *lossless* or *decoupled* contexts [2]–[4]. While typical transmission systems have small losses, their presence can fundamentally change the physical behavior of the system as well as

the solvability of the power flow problem [5]. Similarly, to accurately solve the full power flow problem, the coupling between active and reactive power in the power flow equations cannot be ignored. As such, in this thesis we seek to extend this line of research to incorporate network losses, coupling and other physically realistic modelling aspects not present in the original works, and derive the *extended* Fixed-Point Power Flow (FPPF) algorithm to solve the AC power flow problem.

1.2 Literature Review

There has been a litany of studies on the power flow equations tracing back to the 1960s, and the relevant literature loosely fall under two main categories. The first category concerns the derivation of necessary and/or sufficient conditions for the existence and uniqueness of the solution(s) to the power flow equations. For example, Korsak was among the first to show the non-uniqueness of power flow solutions in both lossless and lossy systems [6]. Wu and Kumagai used a version of the Leray-Schauder fixed-point theorem to study on the existence of solutions in the security region for the lossless power flow equations [7], [8]. Ilić et al. developed sufficient but conservative solvability conditions for the lossy decoupled active and reactive power flow equations in polar coordinates, and showed their similarities to nonlinear resistive circuits [9], [10]. More recently, Molzahn et al. derived a sufficient condition for the insolvability of power flow equations by studying the feasibility of a semidefinite program. Simpson-Porco et al. derived a sufficient condition for the solvability of the lossless reactive power flow equation in [11], which is closely connected to the phenomenon of voltage collapse. This result is analogous to the investigation of decoupled active power flow equation by Dörfler et al. in their more general discussion of synchronization in coupled oscillator networks [12]. In contrast to standard formulation of power flow equations in the reals, Cui and Sun proposed a sufficient condition of power flow equation solvability in the complex domain using a fixed-point argument, though it relies on a model of generator buses that differs from the standard PV bus model in transmission networks [13]. For distribution systems, Bolognani and Zampieri gave a sufficient condition for the existence and uniqueness of the complex-valued power flow solution using the Banach fixed-point theorem, though it requires the impedance matrix rather than the conventional admittance matrix of the network [14]. Aside from these examples, there have also been a diverse range of other relaxations and/or approximations of power flow equations, which are surveyed in [15].

The second category focuses on the algorithms that solve the power flow equations as well as the analysis of these algorithms. For instance, many have applied algorithms that solve general systems of nonlinear equations to the power flow problem. Meisel

and Barnard appear to be the first to apply fixed-point theoretic techniques to analyze Newton-Raphson and Gauss-Seidel algorithms applied to the power flow problem [16]. A few years later, Wu developed a sufficient condition on the convergence of Stott's fast decoupled load flow algorithm that is dependent on the system topology, similarly using a fixed-point theoretic argument [17]. More recently, Wang et al. proposed a fixed-point theoretic reformulation of the complex-valued power flow equations that can be used to certify the existence and uniqueness of the solution, as well as an algorithm that solves the power flow problem in distribution networks [18]. Bernstein and Dall'Anese then derived a computationally efficient linearization of this fixed-point reformulation in the unbalanced three-phase context [19]. For balanced transmission systems, Simpson-Porco developed fixed-point based algorithms for the decoupled active power flow equation and the lossless coupled power flow equations by rewriting them into an equivalent fixed-point form, and analyzed the convergence of the sequence of voltages under the fixed-point mapping [2]–[4]. Other approaches and algorithms originate from domains such as optimization and control theory. For example, Dvijotham et al. proposed an algorithm that solves the lossless power flow equations based on the connection between power flow equations and energy functions, and gave a convergence condition based on the convexity of the energy function [20]. In radial distribution networks, Dvijotham et al. also showed the equivalence of algorithms developed in the convex relaxation, energy function, and fixed-point theoretic frameworks under some assumptions about the system parameters such as balanced network and uniform R/X ratio [21].

In summary, while there have been numerous studies on the power flow equations and its solution(s) to further understand their properties—in particular using a fixed-point theoretic approach, lossy and coupled power flow equations remain challenging to analyze and solve. Furthermore, there seems to be little interest in incorporating physically realistic modelling of system components such as phase-shifting transformers and the Π-model of transmission lines, which undoubtedly increase the complexity of the analysis, though doing so would offer additional practical benefits.

1.3 Contributions and Organization

The most significant results in this thesis are as follows:

- In Chapter 3, we develop a novel vectorization scheme for the standard lossy power flow equations that accommodates the distributed slack bus model, and it culminates in an equivalent fixed-point reformulation of the standard power flow equations in Theorem 4.1. In particular, we prove one of the key equivalence condition using a property of the asymmetrically weighted incidence matrix,

which is constructed in Chapter 2. Finally, we introduce the extended FPPF algorithm based on the fixed-point reformulation in Algorithm 1.

- In Proposition 5.2, we provide sufficient conditions for the existence and uniqueness of the desired high voltage solution to the two-bus power flow problem, and show that the proposed extended FPPF algorithm is guaranteed to converge to it. This result relies on Theorems 5.1–5.2, where we reproduce the sufficient condition for the *lossless* FPPF algorithm to be a contraction on a compact invariant set, which contains the high voltage solution to the lossless two-bus power flow problem.
- In Chapter 6, we numerically test the extended FPPF algorithm and demonstrate its robustness over the standard algorithms on a large set of test cases with various sizes, loading profiles and initial conditions. We also show its limitations due to an implicit constraint from the fixed-point reformulation.
- As a tangential contribution, we develop some novel rank properties for the asymmetrically weighted incidence matrix in Appendix A.

This thesis is organized as follows:

- In Chapter 2, we present the required background materials on the mathematical tools and the transmission network models used in this thesis.
- In Chapter 3, we set up the vectorized power flow equations using the distributed slack bus model for subsequent reformulation.
- In Chapter 4, we reformulate the vectorized power flow equations into an equivalent fixed-point form, and present the extended FPPF algorithm.
- In Chapter 5, we analyze the FPPF algorithm on a two-bus system, and provide sufficient conditions for the existence and uniqueness of the desired solution.
- In Chapter 6, we present comprehensive numerical simulations of the FPPF algorithm on standard test cases.
- In Chapter 7, we provide a conclusion of this thesis and avenues for future work.
- In Appendix A, we present some novel rank properties of the asymmetrically weighted incidence matrix.
- In Appendix B, we provide an example for the vectorized power flow equations developed in Chapter 3.3.

Chapter 2

Background

In this chapter, we present the relevant background information on the mathematical tools and electrical network modelling used in the main body of this thesis.

When stating a known theorem or lemma in this Chapter, we indicate the source of the statement and/or the proof without reproducing the proof. Some notations and constants used in Sections 2.1 and 2.2 may not extend to later sections (including Section 2.3), where they are redefined; for example, m denotes the cardinality of the edge set $\mathcal{E}$ of a generic graph in Section 2.2, but is redefined in Section 2.3 to denote the cardinality of the generator bus set.

2.1 Mathematical Preliminaries

We start by presenting some relevant results from matrix algebra and analysis based on [22]–[25]. These include the classes of diagonally dominant and M-matrices, the pseudoinverse of a matrix, and the induced norm of a matrix. When a matrix is used to represent a linear operator, it is written with respect to the standard basis, where the i-th basis element is denoted by $\mathbb{e}_i$. We also use $\mathbb{0}_n, \mathbb{0}_{n\times m}, \mathbb{1}_n$ and I_n to denote the n-dimensional zero vector, the $n \times m$ zero matrix, the n-dimensional vector of all ones, and the $n \times n$ identity matrix, respectively. We omit these subscripts when the dimensions are unimportant or can be easily inferred.

Let $\mathbb{F}$ denote an arbitrary field, which is usually taken to be the real or complex numbers denoted as $\mathbb{R}$, $\mathbb{C}$, respectively. Depending on the context, $|\cdot|$ denotes the absolute value of a real number, the magnitude of a complex number, or the cardinality of a set. The matrix $M \in \mathbb{F}^{n\times n}$ is *diagonally dominant* if for $i \in \{1, ..., n\}$,

$$|M_{ii}| \geq \sum_{j=1,\, j\neq i}^{n} |M_{ij}|,$$

and is *strictly diagonally dominant* if the inequality above holds strictly. If $M \in \mathbb{F}^{n\times n}$ is a strictly diagonally dominant matrix, then M is invertible; M is also positive definite if $M_{ii} > 0$ and $M_{ij} = M_{ji}$ for all $i, j \in \{1, ...n\}$ [23, Theorem 6.1.10].

Let $\rho(\cdot)$ denote the spectral radius of a matrix. A matrix $M \in \mathbb{R}^{n\times n}$ is a *Z-matrix* if $M_{ij} \leq 0$ for all $i, j \in \{1, ...n\}$ such that $i \neq j$. It is an *M-matrix* if there exists a nonnegative matrix $P \in \mathbb{R}^{n\times n}$ such that $M = sI - P$ for some $s \geq \rho(P)$. If $s > \rho(B)$, then M is a *nonsingular M-matrix*. If $M \in \mathbb{R}^{n\times n}$ is a nonsingular M-matrix, then the inverse M^{-1} is nonnegative [25, Theorem 2.3 N_{38}].

Let M^{H} denote the Hermitian transpose of the matrix M. A *pseudoinverse* of a matrix $M \in \mathbb{F}^{n\times m}$, denoted by $M^{\dagger}$, is an $m \times n$ matrix that satisfies the following conditions: (i) both $MM^{\dagger}$ and $M^{\dagger}M$ are Hermitian, (ii) $MM^{\dagger}M = M$, and (iii) $M^{\dagger}MM^{\dagger} = M^{\dagger}$. If $M \in \mathbb{F}^{n\times m}$ has full column rank, then $M^{\dagger}$ is the *left inverse* of M and satisfies $M^{\dagger}M = I_m$, and it can be explicitly written as $\left(M^{\mathsf{H}}M\right)^{-1} M^{\mathsf{H}}$. If M has full row rank, then $M^{\dagger}$ is the *right inverse* of M and satisfies $MM^{\dagger} = I_n$, and it can be explicitly written as $M^{\mathsf{H}}\left(MM^{\mathsf{H}}\right)^{-1}$.

Finally, given ℓ_p norms $\|\cdot\|_a$ in $\mathbb{R}^m$ and $\|\cdot\|_b$ in $\mathbb{R}^n$, the *induced norm* of a matrix $M \in \mathbb{F}^{n\times m}$ is

$$\|M\|_{a\to b} \coloneqq \sup_{\|x\|_a \leq 1} \|Mx\|_b.$$

For our purposes, the ℓ_∞ norm is of particular interest, and it is defined as

$$\|v\|_\infty \coloneqq \max_{i\in\{1,\ldots,n\}} |v_i|$$

for any $v \in \mathbb{R}^n$. Note that the ℓ_∞ norm can be used to measure the absolute value of the greatest element-wise difference between two vectors. From [23, Example 5.6.5], the induced ℓ_∞ norm of an $n \times n$ matrix M can be computed by

$$\|M\|_\infty = \max_{i\in\{1,\ldots,n\}} \sum_{j=1}^{n} |M_{ij}|.$$

Next, we turn our attention to the functions and sets in $\mathbb{R}^n$. Standard definitions of (i) continuous, Lipschitz continuous and differentiable functions and conditions for continuity and differentiability, (ii) convex and invariant set, and (iii) elementary topology in $\mathbb{R}^n$, e.g., open/closed/compact sets can be found in standard textbooks such as [26]–[29] and are not repeated here. An important result from real analysis that is crucial for our subsequent discussions in Chapter 5 is the implicit function theorem, stated below.

Theorem 2.1 (Theorem 5, [30])**.** *Consider a continuously differentiable (C^1) function $f : \mathcal{U} \subset \mathbb{R}^n \times \mathbb{R}^m \to \mathbb{R}^n$, where $\mathcal{U}$ is open. Partition the Jacobian matrix of f evaluated*

at any $(x, y) \in \mathcal{U}$ *as*

$$J(x,y) = \left[\begin{array}{c|c} J_x(x,y) & J_y(x,y) \end{array}\right] = \left[\begin{array}{c|c} \dfrac{\partial f_i}{\partial x_j}(x,y) & \dfrac{\partial f_i}{\partial y_k}(x,y) \end{array}\right]_{\substack{1\leq i,j\leq n \\ 1\leq k\leq m}}.$$

Suppose that there exists a point $(x_0, y_0) \in \mathcal{U}$ *such that* $f(x_0, y_0) = \mathbb{0}_n$*. If* $J_x(x_0, y_0)$ *is invertible, then there exists open sets* $\mathcal{X} \subset \mathbb{R}^n$ *and* $\mathcal{Y} \subset \mathbb{R}^m$*, such that* $x_0 \in \mathcal{X}$ *and* $y_0 \in \mathcal{Y}$*, and there exists a unique* C^1 *function* $g : \mathcal{Y} \to \mathcal{X}$ *satisfying* $g(y_0) = x_0$*, and,* $f(g(y), y) = \mathbb{0}$ *for all* $y \in \mathcal{Y}$*.*

Intuitively, this theorem provides a sufficient condition for local solvability of $f(x, y) = \mathbb{0}$. If the condition is satisfied, then the zeros of f near the known solution is locally the graph of an implicit function of the parameterizing variable y.

Finally, we introduce two well-known fixed-point theorems and a sufficient condition that certifies a C^1 function is a contraction based on its Jacobian matrix. Since the fixed-point power flow algorithm discussed in the subsequent chapters is iterative in nature, fixed-point theorems play a significant role in analyzing the algorithm's convergence behavior. The point $\bar{x} \in \mathbb{R}^n$ is a *fixed point* of a function $f : \mathbb{R}^n \to \mathbb{R}^n$ if $\bar{x} = f(\bar{x})$. For simplicity, we make the following notational shorthand: given any $x \in \mathbb{R}^n$, for $k = 1, 2, ...$ we recursively define $x_k \coloneqq f(x_{k-1})$, where $x_0 \coloneqq x$; thus, we may also say that x_k is a fixed point of f if $x_{k+1} = x_k$.

The first fixed-point theorem is Brouwer's fixed-point theorem in $\mathbb{R}^n$, which states that a continuous function mapping a convex and compact set to itself has at least one fixed point in this set [27, Theorem 52]. However, this theorem only certifies the existence of the fixed point, but it does not help us construct the fixed point or certify its uniqueness. To achieve both, we require the Banach fixed-point theorem, which states that a globally Lipschitz function f mapping $\mathbb{R}^n$ to $\mathbb{R}^n$ with Lipschitz constant strictly less than 1 has a unique fixed point, and that for every $x \in \mathbb{R}^n$, the sequence $\{x_i\}_{i\in\mathbb{Z}_{\geq 0}}$ converges to the fixed point [31, Theorem 1.1]. When the condition is satisfied for a given ℓ_p norm, we call f a *contraction* in the ℓ_p norm.

Note that the requirement for f to be a contraction on all of $\mathbb{R}^n$ restricted to a closed f-invariant subset of $\mathbb{R}^n$. A set $\mathcal{S} \subset \mathbb{R}^n$ is *f-invariant* if $f(\mathcal{S}) \subseteq \mathcal{S}$. If f can be shown to be a contraction on this closed subset, then it must contain the unique fixed point $\bar{x}$. Furthermore, let $J(x)$ denote the Jacobian of f evaluated at a point x. If $\|J(x)\|_p < 1$ for all x in a convex and compact f-invariant set, then f is a contraction in the ℓ_p norm on this set [32, Theorem 2].

For our purposes, we are interested in both certifying a C^1 function f is a contraction on some compact and convex f-invariant set $\mathcal{S} \subset \mathbb{R}^n$, and obtaining the unique fixed point $\bar{x} \in \mathcal{S}$. Thus, we need to first show that f is a contraction (or give

conditions on when f is a contraction) on $\mathcal{S}$ by evaluating the induced norm of its Jacobian matrix at every point in $\mathcal{S}$. Next, by the Banach fixed-point theorem, we may start at an arbitrary point (the "initial condition") $x_0 \in \mathcal{S}$, and iteratively apply f to obtain the sequence $\{x_1, x_2, ...\}$ until $\|x_{n+1} - x_n\|$ is sufficiently small, i.e., x_{n+1} well-approximates the fixed point $\bar{x}$. Figure 2.1 demonstrates this process.

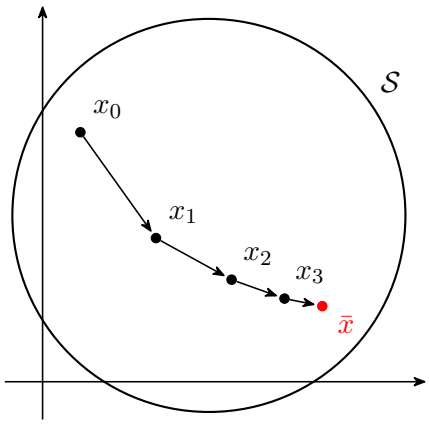

Figure 2.1: An example sequence of $\{x_i\}$ that converges to the fixed point $\bar{x}$

2.2 Algebraic Graph Theory

Since a balanced transmission network at steady state can be modelled as a graph, tools from algebraic graph theory are extremely important for the results in this thesis. We first provide the relevant definitions of different types of graphs and some of their relevant properties, then introduce some matrices that can be used to describe the graphs. For a comprehensive treatment on algebraic graph theoretic results relevant to electrical network theory and applications, see [24].

Graphs

A *finite* and *simple* graph $\mathcal{G}$ is a pair $(\mathcal{N}, \mathcal{E})$, where $\mathcal{N}$ and $\mathcal{E} \subseteq \mathcal{N} \times \mathcal{N}$ are both finite sets of nodes and edges, and without any self-loops (to be defined next). A *subgraph* $\mathcal{G}'$ of $\mathcal{G}$ is a pair $(\mathcal{N}', \mathcal{E}')$ where $\mathcal{N}' \subseteq \mathcal{N}$ and $\mathcal{E}' \subseteq \mathcal{E}$. Let $n = |\mathcal{N}|$, $m = |\mathcal{E}|$ denote the number of nodes and edges in $\mathcal{G}$, respectively. Without loss of generality, we let $\mathcal{N} = \{1, ..., n\}$, and we enumerate the edge set to be $\mathcal{E} = \{e_1, ..., e_m\}$ with the index set $\mathcal{I}_E \coloneqq \{1, ..., m\}$. The *degree* of node i in a graph, denoted by $\deg(i)$, is the number of edges incident to i. Every edge connecting node i and j in a graph can be assigned a nonzero weight $w_{ij} \in \mathbb{F}$ from some field $\mathbb{F}$. As a convention, if any edge weight is not ± 1, then the graph is *weighted*.

A *directed* graph is one such that the elements of $\mathcal{E}$ are ordered pairs of nodes,

denoted as (i, j), where i is the source node and j is the sink node; equivalently, the edge (i, j) "leaves" node i and "enters" node j. An *undirected* graph is one such that the elements of $\mathcal{E}$ are unordered pairs of nodes, denoted as $\{i, j\}$, which are without the notion of source or sink node. That is, $\{i, j\} \in \mathcal{E}$ if and only if $\{j, i\} \in \mathcal{E}$. An edge (i, j) or $\{i, j\}$ is called a *self loop* if $i = j$. We may also assign an "edge number" k from the edge index set $\mathcal{I}_E$, i.e., the k-th edge can be written as e_k or equivalently, (i, j) (resp. $\{i, j\}$) in a directed (resp. undirected) graph[1]. An undirected graph $\mathcal{G}$ is *connected* if there exists a sequence of edges in $\mathcal{E}$ connecting every node to every other node, and a directed graph $\mathcal{G}^\sigma$ is *weakly connected* if its underlying undirected graph $\mathcal{G}$ is connected. A (weakly) connected graph is *radial* if $m = n-1$, and *meshed* if $m > n - 1$.

Every undirected graph can be made into a directed graph by assigning a direction to each edge. We denote the directed graph constructed from an undirected graph $\mathcal{G} = (\mathcal{N}, \mathcal{E})$ with the orientation σ by $\mathcal{G}^\sigma = (\mathcal{N}, \mathcal{E}^\sigma)$. Similarly, every directed graph $\mathcal{G}^\sigma$ induces an "underlying undirected graph" $\mathcal{G}$ if the direction of every edge in $\mathcal{E}^\sigma$ is removed. Note that we use the notation $\mathcal{G}$ to represent both directed and undirected graphs when the context is clear. We only differentiate the two by using both $\mathcal{G}$ and $\mathcal{G}^\sigma$ if one induces the other in the same scope of discussion.

Next, we introduce the notion of the bidirected graph. It is less commonly used than the simple undirected or directed graph, but it has desirable properties of both, which are insufficient for our modelling purposes when there is a phase-shifting transformer in the transmission network[2].

Definition 2.1 (p.10, [5])**.** A *bidirected* graph is a graph $\mathcal{G} = (\mathcal{N}, \mathcal{E})$ where the edges are directed, and $(i, j) \in \mathcal{E}$ if and only if $(j, i) \in \mathcal{E}$. Exactly one of (i, j) and (j, i) has the "forward" direction (called the"forward edge" in short), where the other one has the "backward" direction (called the "backward edge" in short), which can be chosen arbitrarily.

When it is necessary for us to distinguish the bidirected graphs from the standard (un)directed graphs, for $k \in \mathcal{I}_E$, we use e_k^+ to denote the k-th forward edge (i, j) and use e_k^- to denote the k-th backward edge (j, i). For our purposes, when a bidirected graph is unweighted, we are only interested in the forward edges of a bidirected graph. Thus, we may focus on the induced directed graph formed by removing all the edges in the backward direction in the bidirected graph. As such, when the context is clear, we simply drop the $\cdot^+$ superscript, and use e_k to denote the forward edges only. However, when a bidirected graph is weighted, both forward and backward edge

[1] While the edge set is usually unordered, it is helpful to have the edge numbers for the construction of the node-edge incidence matrix discussed later.

[2] See Section 2.3 for more detailed discussions.

weights are important and neither is omitted. In addition, the forward and backward edge weights can be different, though we require that both are nonzero like the edge weights in a standard weighted (un)directed graph. Finally, to ensure the consistency of the size of edge set $\mathcal{E}$, we slightly abuse the notation and use m to also denote $|\mathcal{E}|$ for a bidirected graph. That is, we consider the forward and backward edges to make up a single "edge" entity in a bidirected graph; the alternative interpretation is that we do not "double count" the number of edges in a bidirected graph[3].

Figures 2.2–2.3 demonstrate the difference between edges in the undirected, directed and bidirected graph in both unweighted and weighted contexts. For the bidirected graph, the edge with forward direction is drawn in black and the edge with backward direction is drawn in gray.

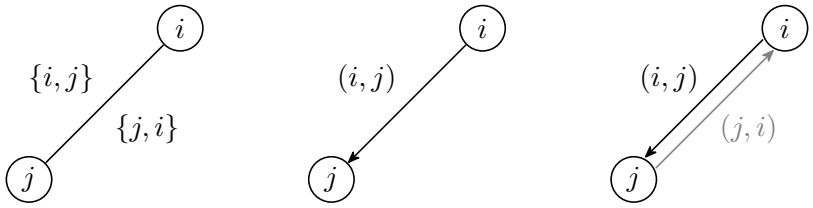

Figure 2.2: An edge in an undirected (left), directed (center), and bidirected (right) graph

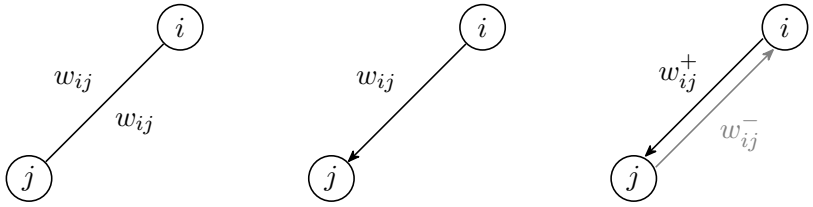

Figure 2.3: A weighted edge in an undirected (left), directed (center), and bidirected (right) graph

Recall the notions of *degree* and *connectedness* in standard (un)directed graphs defined at the beginning. These definitions can also be extended to bidirected graphs. Since the degree of a node in a bidirected graph concerns only the number of incident edges to it and has nothing to do with their weights, as mentioned before, we can focus on the induced directed graph (obtained by removing the backward edges). That is, for every node i in a bidirected graph, $\deg(i) = \deg(i')$, where i' is the corresponding node in the induced directed graph. Similarly, since the notion of connectedness does not depend on edge weights, a bidirected graph is weakly connected if and only if its induced directed graph is weakly connected. In the subsequent discussion, unless

[3]This caveat is admittedly somewhat ambiguous, but the most important reason to define the bidirected graphs (in particular, the ones with different forward and backward edge weights) this way is to facilitate our construction of the asymmetrically weighted incidence matrix, to be discussed next.

otherwise specified, $\mathcal{G}$ is connected if $\mathcal{G}$ is undirected, and weakly connected if $\mathcal{G}$ is (bi)directed, which implies that $m \geq n - 1$ [33].

Of particular importance to our algorithm formulation in Chapter 4 are the cycles in a graph and the related concepts. A subgraph $\mathcal{G}'$ of an graph (undirected, directed or bidirected) is called a *cycle* if every node in $\mathcal{G}'$ has even degrees, and it is furthermore a *circuit* if it is connected and every node i satisfies $\deg(i) = 2$. The *edge space* of a graph $\mathcal{G}$ is $\mathcal{E}_\kappa(\mathcal{G}) \coloneqq \kappa^m$, where κ is the field

- $\{0, 1\}$ if $\mathcal{G}$ is undirected and unweighted,
- $\{-1, 0, 1\}$ if $\mathcal{G}$ is (bi)directed and unweighted, and
- $\mathbb{R}$ or $\mathbb{C}$ if $\mathcal{G}$ is weighted (though it is beyond the scope of this thesis).

Thus, we can represent an unweighted cycle (in an undirected, directed or bidirected graph) as an m-dimensional vector $\mathbf{c} \in \mathcal{E}_\kappa(G)$, which we call a *$\kappa$-cycle* to distinguish it from the subgraph-based definition earlier. Similarly, circuits can be written in vector form as κ-circuits. The k-th element of $\mathbf{c}$ are nonzero and takes value from the field κ if and only if the i-th (forward) edge is in the cycle. The *cycle space* of a graph $\mathcal{G}$ is the set $\mathcal{C}_\kappa(\mathcal{G}) \coloneqq \{\mathbf{c} : \mathbf{c} \text{ is a } \kappa\text{-cycle of } \mathcal{G}\}$ with dimension $c = m - n + 1$, known as the *cycle dimension*. A *cycle basis* spans $\mathcal{C}_\kappa(G)$, and it is a minimal set of k-circuits such that any κ-cycle can be written as a linear combination of the κ-circuits in the basis.

To demonstrate these concepts above, consider the directed graph in Figure 2.4 (adapted from [33, Figure 3]). The four subgraphs in Figure 2.5 are circuits that form a cycle basis; as such, $c = 4$. Pick the cycle orientation to be clockwise, then the κ-cycle representation of the cycle in Figure 2.5(a) is $[0 \quad 0 \quad 0 \quad -1 \quad -1 \quad 0 \quad 0 \quad 1]^\mathsf{T}$, since only the edges e_4, e_5 and e_8 are in the cycle and thus the 4th, 5th and 8th elements are nonzero. Note that the κ-cycle representation of a cycle is not unique. If $\mathcal{G}$ is instead an unweighted bidirected graph, we have the same results since we only care about the induced directed graph if $\mathcal{G}$ is unweighted.

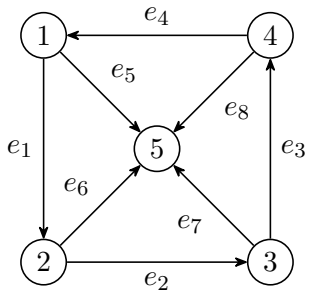

Figure 2.4: A directed graph $\mathcal{G}$ with cycles

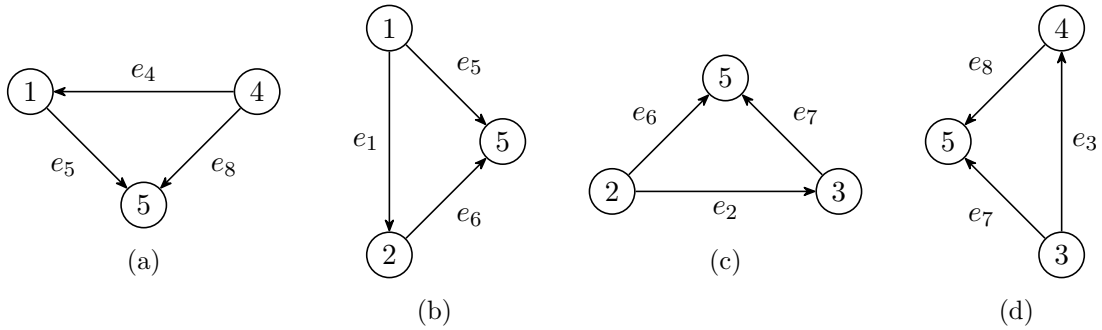

Figure 2.5: A cycle basis for $\mathcal{G}$ with 4 circuits

Graph Matrices

We are now ready to describe graphs and their properties using tools from matrix algebra. Once again, we assume that the graph—whether undirected, directed, bidirected, and/or weighted—is (weakly) connected. We focus on two main graph matrices: the node-edge incidence matrix A and the edge-cycle incidence matrix C. We also introduce some properties relevant to our discussion.

Given an unweighted (bi)directed graph $\mathcal{G} = (\mathcal{N}, \mathcal{E})$, the *node-edge incidence matrix* (or simply *incidence matrix*) of $\mathcal{G}$, denoted by $A \in \mathbb{R}^{n \times m}$, is defined elementwise as[4]

$$A_{ik} \coloneqq \begin{cases} 1 & \text{if node } i \text{ is the source node of edge } e_k \\ -1 & \text{if node } i \text{ is the sink node of edge } e_k \\ 0 & \text{otherwise} \end{cases}, \tag{2.1}$$

for all $i \in \mathcal{N}$ and $k \in \mathcal{I}_E$.

Furthermore, we can define the nonnegative "from" and "to" incidence matrices A^+, A^- such that $A = A^+ - A^-$, and $A^+_{ik} = 1$ if and only if $A_{ik} = 1$, and $A^-_{ik} = 1$ if and only if $A_{ik} = -1$. There does not seem to be a standard nomenclature in the literature for the matrices A^+, A^-, but several instances of them can be found in [2], [3], [5], [34], [35], where the matrices A^+, A^- (or their transpose) are variously called the "from"/"to" connection matrix, "heads"/"tails" matrix, etc.

If $\mathcal{G}$ is undirected, then its incidence matrix is denoted by $|A|$, and is constructed by applying absolute value entry-wise to any induced directed graph's incidence matrix A. That is, $|A|_{ij} = 1$ if and only if $A_{ij} \neq 0$, and 0 otherwise. Using the "from"/"to" incidence matrices discussed above, we can also write $|A| = A^+ + A^-$.

Let $y \coloneqq A^\mathsf{T} x \in \mathbb{R}^m$ for an arbitrary $x \in \mathbb{R}^n$. Then for all $k \in \mathcal{I}_E$, $y_k = x_i - x_j$, where $(i, j) = e_k \in \mathcal{E}$ [2, Section I-C]; as a result, $\ker A^\mathsf{T} = \operatorname{span}\{\mathbb{1}_n\}$. It is a standard result that $\operatorname{rank}(A) = \operatorname{rank}(|A|) = n - 1$ [36, Theorems 7.2, 9.6]; as a result, $\ker A$ is

[4]Some texts define the incidence matrix as the transpose of A defined here.

trivial if and only if the graph is radial.

Now, let $\mathcal{G}$ be a weighted directed graph. Given a vector of nonzero edge weights $w \in \mathbb{R}^m$ and let $[w]$ denote the diagonal matrix with w on its main diagonal, we can also define the *weighted incidence matrix*, denoted by $\mathrm{T} \coloneqq A[w] \in \mathbb{R}^{n\times m}$. Similar to (2.1), T can be alternatively constructed entry-wise, but we omit the details since they are unimportant. The matrix T also has rank $n-1$, since a nontrivial $v \in \mathbb{R}^m$ is in $\ker A$ if and only if $[w]^{-1}v \in \ker \mathrm{T}$, and $[w]^{-1}$ exists since the weights are nonzero.

Finally, we define the *asymmetrically weighted incidence matrix*, denoted by Γ, for a bidirected graph where the edge weights w_{ij} may not be equal to w_{ji}. There does not seem to be any standard nomenclature for this matrix in the literature, and to the best of our knowledge, it only appeared in the proof of [5, Theorem 3], whose authors did not give it a particular name. This matrix is central to the power flow equation vectorization process in Chapter 3.

Definition 2.2 (Asymmetrically weighted incidence matrix)**.** Given two vectors of nonzero edge weights $w^+, w^- \in \mathbb{R}^m$, where w_k^+ represents the weight of the forward edge k and w_k^- represents the weight of the backward edge k, the *asymmetrically weighted incidence matrix* is constructed as

$$\Gamma \coloneqq A^+[w^+] - A^-[w^-], \tag{2.2a}$$

or element-wise as

$$\Gamma_{ik} \coloneqq \begin{cases} w_k^+ & \text{if } i \text{ is the source node of the forward edge } e_k \\ -w_k^- & \text{if } i \text{ is the sink node of the forward edge } e_k \\ 0 & \text{otherwise} \end{cases}. \tag{2.2b}$$

Note that Γ always has the same sparsity pattern as T and A, and Γ reduces to T when $w^+ = w^-$. However, it is not true that Γ is always rank-deficient like A or T; see Appendix A for an in-depth treatment on its rank properties. Here, we present a novel property of Γ that is useful in the proof of Lemma 4.1.

Lemma 2.1. *Suppose that w^+, w^- are both element-wise strictly positive. If there exists a nonzero $x \in \mathbb{R}^n$ such that $\Gamma^{\mathsf{T}} x = \mathbb{0}_m$, then x is element-wise strictly positive or strictly negative.*

Proof. Let $\tau_k \in \mathbb{R}^n$ denote the k-th column of Γ, which represents the edge $e_k = (i,j) \in \mathcal{E}$ and weights w_k^+, w_k^-. If $\Gamma^{\mathsf{T}} x = \mathbb{0}_m$, then for all $k \in \mathcal{I}_E$, $\langle \tau_k, x\rangle = w_k^+ x_i - w_k^- x_j = 0$. Since w_k^+, w_k^- are both strictly positive, x_i, x_j must be both strictly positive, strictly negative, or zero, and we need to show that the last case is impossible. Assuming towards contradiction that there exists an edge $e_k = (i,j)$ that results in

$x_i = x_j = 0$ but overall, x is not the zero vector $\mathbb{0}_n$. If $\mathcal{G}$ only contains two nodes, then $e_k = e_1$, $x = [x_1 \quad x_2]^\mathsf{T} = [0 \quad 0]^\mathsf{T}$, and we arrive at the contradiction immediately. In general, if $\deg(i) = 1$, then $\deg(j) > 1$ since $\mathcal{G}$ is weakly connected, i.e., there exists some forward edge $e_\ell = (j, h)$ or (h, j). Since $\langle \tau_\ell, x \rangle = 0$ as well, $x_i = x_j = 0$ implies $x_h = 0$. The same logic applies if both nodes i, j have degrees larger than 1. Thus, by weak connectivity of $\mathcal{G}$, if $x_i = x_j = 0$, then it would propagate to the rest of the graph and result in $x = \mathbb{0}_n$, which is a contradiction. Thus, x must be element-wise strictly positive or strictly negative. □

Next, we introduce the edge-cycle incidence matrix and its relevant properties. Given a graph $\mathcal{G} = (\mathcal{N}, \mathcal{E})$ with cycle space $\mathcal{C}_\kappa(\mathcal{G})$ and cycle dimension c, the *edge-cycle incidence matrix* (or *cycle matrix* in short) $C \in \kappa^{m \times c}$ corresponding to some cycle basis is a matrix whose columns are the κ-cycle vectors in the cycle basis. Note that the elements of C depends on the choice of cycle basis, but it always has full column rank by construction. For any unweighted (bi)directed graph $\mathcal{G}$, $\ker A = \mathcal{C}_\kappa(\mathcal{G})$ [2, Section I-C]; as a result, $AC = \mathbb{0}_{n \times c}$.

2.3 Transmission System Modelling

In this section, we discuss some relevant concepts on AC transmission system and its modelling. Basic definitions and expositions on these topics, as well as the AC power flow problem can be found on standard textbooks such as [1, Chapters 4-6] and [37, Chapter 2], and are not repeated here.

2.3.1 Graph Model

Consider a balanced AC transmission system at synchronous steady state, modelled as a weakly connected, weighted bidirected graph $\mathcal{G} = (\mathcal{N}, \mathcal{E})$, where $\mathcal{N} = \{1, ..., n, n+1, ..., n+m\}$ is the set of buses and $\mathcal{E} \subseteq \mathcal{N} \times \mathcal{N}$ is the set of branches. We assume that $\mathcal{G}$ has no self-loops, and the parallel branches between any two buses, if they exist, are modelled as a single equivalent branch[5].

[5] In our numerical experiments in Chapter 6, we keep multiple branches (if they exist) as is, since one or more of these parallel branches may be marked as "offline". Note that this assumption does not refer to the forward/backward direction of the edges, since $\mathcal{G}$ is bidirected.

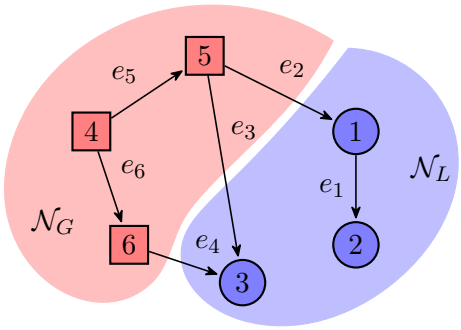

Figure 2.6: Graph model of a simple transmission system

We adopt the notations used in [3] and partition the bus set $\mathcal{N}$ into the set of load buses (or PQ buses) $\mathcal{N}_L = \{1, ..., n\}$ and the set of generator buses (or PV buses) $\mathcal{N}_G = \{n+1, ..., n+m\}$; Figure 2.6 demonstrates an example, where nodes 1 to 3 represent load buses and nodes 4 to 6 represent generator buses. Each bus $i \in \mathcal{N}$ is associated with four physical quantities of interest: voltage magnitude V_i, phase angle θ_i, real power injection P_i, and reactive power injection Q_i. We adopt the convention that a positive P_i or Q_i represents a real or reactive power *generation*, whereas a negative value represents *consumption* or *demand*. For load buses, P_i, Q_i are known and V_i, θ_i are unknown. For generator buses, P_i, V_i are known and Q_i, θ_i are unknown.

We can vectorize the quantities associated with each bus and partition the vectors according to the $\mathcal{N}_L$ and $\mathcal{N}_G$ subsets as

$$P = \begin{bmatrix} P_L \\ \hline P_G \end{bmatrix}, \quad Q = \begin{bmatrix} Q_L \\ \hline Q_G \end{bmatrix}, \quad V = \begin{bmatrix} V_L \\ \hline V_G \end{bmatrix}, \quad \theta = \begin{bmatrix} \theta_L \\ \hline \theta_G \end{bmatrix}. \tag{2.3}$$

The edge set $\mathcal{E}$ is partitioned into $\mathcal{E}^{\ell\ell}$, $\mathcal{E}^{g\ell}$ and $\mathcal{E}^{gg}$, the set of branches connecting load bus to another load bus, generator bus to another load bus, and generator bus to another generator bus, respectively. Without loss of generality, we assume that current flows from generators to load. For notational simplicity, we use $\mathbb{1}_{gg}, \mathbb{0}_{gg}$ and I_{gg} to denote the vector of all ones, zeros and the identity matrix of the size $|\mathcal{E}^{gg}|$, respectively; constants with dimensions of the size of the other two subsets of $\mathcal{E}$ follow the same pattern.

Recall that the *unweighted* incidence matrix A of a bidirected graph is the same as that of its induced directed graph. Using the node and edge set partitions, we can readily partition the unweighted incidence matrix A of the bidirected graph model of

a transmission system as

$$A = \left[\begin{array}{c} A_L \\ \hline A_G \end{array}\right] = \left[\begin{array}{c|c|c} A_L^{\ell\ell} & A_L^{g\ell} & \mathbb{0} \\ \hline \mathbb{0} & A_G^{g\ell} & A_G^{gg} \end{array}\right], \tag{2.4}$$

and similarly for the matrices $|A|, A^+, A^-$ and their weighted versions. Recall the assumption that currents flow from generators into loads, $A_L^{g\ell}$ is nonnegative, and $A_G^{g\ell}$ is nonpositive. The zero blocks in A are due to the fact that $\mathcal{E}_{\ell\ell}$ contain only branches connecting load buses to load buses, and similarly for $\mathcal{E}_{gg}$.

2.3.2 The Admittance Matrix

Consider the standard Π-model of a branch in Figure 2.7 (adapted from [35, Figure 3.1]), which can be modelled as a forward edge $(i, j) \in \mathcal{E}$ in the transmission system modelled as a weakly connected, weighted bidirected graph $\mathcal{G}$. Let $\mathbf{j}$ denote the unit imaginary number. The branch admittance is $y_{ij} = 1/z_{ij} = g_{ij} - \mathbf{j}b_{ij}$, where $g_{ij} \geq 0$ is the conductance and $b_{ij} > 0$ is the susceptance. The line-charging susceptance is $b_{c_{ij}} \in \mathbb{R}$, and the complex transformer turns ratio is $\tau_{ij} = t_{ij}\exp(\mathbf{j}\theta_{s_{ij}})$, where t_{ij} is the transformer turns ratio, $\theta_{s_{ij}}$ is the phase shift, and $\exp(\cdot)$ denotes the exponential function. While we can easily accommodate nonzero shunt conductance in the branches, we assume that they are negligibly small. The model in [35, Chapter 3.2] also adopts this assumption.

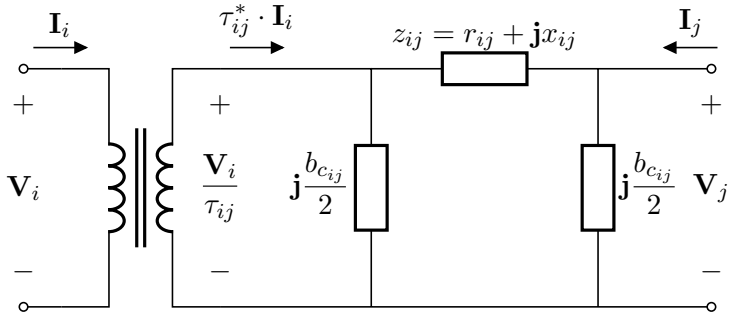

Figure 2.7: Standard Π-model of the branch (i, j)

The branch admittance matrix for the branch (i, j) can be computed as

$$\begin{bmatrix} Y_{\mathrm{ff}}^{(i,j)} & Y_{\mathrm{ft}}^{(i,j)} \\ Y_{\mathrm{tf}}^{(i,j)} & Y_{\mathrm{tt}}^{(i,j)} \end{bmatrix} := \begin{bmatrix} \dfrac{y_{ij} + \mathbf{j}\frac{b_{c_{ij}}}{2}}{t_{ij}^2} & -\dfrac{y_{ij}}{\tau_{ij}^*} \\ -\dfrac{y_{ij}}{\tau_{ij}} & y_{ij} + \mathbf{j}\frac{b_{c_{ij}}}{2} \end{bmatrix}, \tag{2.5}$$

where "f" denotes the *from* end, and "t" denotes the *to* end of a branch [35], and $\cdot^*$ denotes the complex conjugate. The asymmetry of the branch admittance matrix is due to the phase-shifting transformer in the branch (i, j); if $\tau \in \mathbb{R}$, then $Y_{\text{ft}}^{(i,j)} = Y_{\text{tf}}^{(i,j)}$. If furthermore $\tau_{ij} = 1\angle 0$, i.e., the branch (i, j) is a simple transmission line, then $Y_{\text{ft}}^{(i,j)} = Y_{\text{tf}}^{(i,j)}$ and $Y_{\text{ff}}^{(i,j)} = Y_{\text{tt}}^{(i,j)}$.

We can also write the entries of (2.5) in rectangular coordinates as

$$Y_{\text{ff}}^{(i,j)} = \frac{g_{ij}}{t_{ij}^2} + \mathbf{j}\frac{1}{t_{ij}^2}\left(-b_{ij} + \frac{b_{c_{ij}}}{2}\right) \tag{2.6a}$$

$$Y_{\text{ft}}^{(i,j)} = \frac{-g_{ij}\cos\theta_{\text{s}_{ij}} - b_{ij}\sin\theta_{\text{s}_{ij}}}{t_{ij}} + \mathbf{j}\frac{-g_{ij}\sin\theta_{\text{s}_{ij}} + b_{ij}\cos\theta_{\text{s}_{ij}}}{t_{ij}} \tag{2.6b}$$

$$Y_{\text{tf}}^{(i,j)} = \frac{-g_{ij}\cos\theta_{\text{s}_{ij}} + b_{ij}\sin\theta_{\text{s}_{ij}}}{t_{ij}} + \mathbf{j}\frac{g_{ij}\sin\theta_{\text{s}_{ij}} + b_{ij}\cos\theta_{\text{s}_{ij}}}{t_{ij}} \tag{2.6c}$$

$$Y_{\text{tt}}^{(i,j)} = g_{ij} + \mathbf{j}\left(-b_{ij} + \frac{b_{c_{ij}}}{2}\right) \tag{2.6d}$$

Let $Y_{\text{ff}}, Y_{\text{ft}}, Y_{\text{tf}}, Y_{\text{tt}} \in \mathbb{C}^{|\mathcal{E}|}$ be vectors containing the appropriate entries in (2.6a)–(2.6d). Then, the system admittance matrix is an $(n+m) \times (n+m)$ complex matrix defined as

$$Y = A^+[Y_{\text{ff}}](A^+)^\mathsf{T} + A^+[Y_{\text{ft}}](A^-)^\mathsf{T} + A^-[Y_{\text{tf}}](A^+)^\mathsf{T} + A^-[Y_{\text{tt}}](A^-)^\mathsf{T} + [Y_{\text{sh}}], \tag{2.7}$$

where $Y_{\text{sh}} \in \mathbb{C}^{n+m}$ represents the shunt elements at the buses.

The admittance matrix can be separated into real and imaginary parts as $Y = G + \mathbf{j}B$, where G is the *conductance matrix* and B is the *susceptance matrix*. In particular, it is useful for B to be partitioned by the load/generator bus set as

$$B = \left[\begin{array}{c|c} B_{LL} & B_{LG} \\ \hline B_{GL} & B_{GG} \end{array}\right].$$

Lastly, we introduce two standing assumptions that the rest of this thesis relies on, as well as the rationales for establishing them.

Assumption 2.1. The submatrix $B_{LL} \in \mathbb{R}^{n\times n}$ is strictly diagonally dominant and thus invertible.

Assumption 2.1 is related to [3, Assumption 2.2], and implies that the shunt capacitors at the buses must not overcompensate the network. The difference between the two assumptions is that we do not require B_{LL} to be negative definite as well, which is due to the fact that we allow phase-shifting transformers to be in networks, due to which we may lose the symmetry of B_{LL}. That is, we recover the original

assumption if there are no phase-shifting transformers in the network. The existence of B_{LL}^{-1} follows from our discussion in Section 2.1 on strictly diagonally dominant matrices. However, since a matrix can be negative definite but not strictly diagonally dominant, e.g.,

$$\begin{bmatrix} -2 & 3 \\ 3 & -7 \end{bmatrix},$$

our assumption is stricter and does not hold on some test cases in Chapter 6. However, this is not a significant issue since B_{LL} is always invertible on these test cases, which is required for the numerical experiments.

Assumption 2.2. For all $(i, j) \in \mathcal{E}$, the associated off-diagonal entries B_{ij}, B_{ji} are strictly positive.

For Assumption 2.2 to hold, we must have

$$\min_{(i,j)\in\mathcal{E}} \left\{ \frac{-g_{ij}\sin\theta_{\mathrm{s}_{ij}} + b_{ij}\cos\theta_{\mathrm{s}_{ij}}}{t_{ij}}, \quad \frac{g_{ij}\sin\theta_{\mathrm{s}_{ij}} + b_{ij}\cos\theta_{\mathrm{s}_{ij}}}{t_{ij}} \right\} > 0.$$

For all $(i, j) \in \mathcal{E}$, realistically speaking $g_{ij} \geq 0$, $b_{ij} > 0$, $t_{ij} > 0$ and $\theta_{\mathrm{s_{ij}}} \in (-\frac{\pi}{2}, \frac{\pi}{2})$, so we must have

$$\frac{b_{ij}}{g_{ij}} > \tan\theta_{\mathrm{s}_{ij}},$$

for all $(i, j) \in \mathcal{E}$. Thus, Assumption 2.2 holds in cases where both phase shift $\theta_{\mathrm{s}_{ji}}$, and the branch R/X ratio are small; when phase shift is large, then the R/X ratio must be made sufficiently small to compensate the difference. On the test cases in Chapter 6, this assumption nearly always holds, except for the RTE systems.

Remark 2.1. Assumptions 2.1–2.2 imply that $B_{ij} \geq 0$ and $B_{ii} < 0$ for all $1 \leq i, j \leq n$. Thus, $-B_{LL}$ is also a nonsingular M-matrix [3, Appendix A], and it follows from our discussion in Section 2.1 that $-B_{LL}^{-1}$ is a nonnegative matrix.

Chapter 3

The Power Flow Equations

In this chapter, we set up the problem by first stating the standard power flow equations with the distributed slack bus formulation. Then, we develop the open-circuit solution to the power flow equations, and introduce a novel vectorization scheme for the power flow equations using the algebraic graph theoretic tools from Chapter 2.

3.1 The Distributed Slack Bus Model

We continue from the discussion in Chapter 2.3, where a balanced transmission network at steady state is modelled as a weakly connected bidirected graph.

In classic power system textbooks, the power flow problem in lossy networks requires a single slack bus to compensate for the transmission loss, and it is also used as the phase angle reference [1], [37], [38]. However, since transmission systems often span over large geographical areas, it is physically unrealistic to assign all the network loss to be compensated by a single generator. In addition, some commercial power system simulation software such as PowerWorld already support the distributed slack bus model in the power flow computations. As such, we adopt the distributed slack bus model studied in [39] for our formulation of the power flow equations, and show that this model is in fact a generalization of the traditional single slack bus model.

To start, we denote the subset of distributed slack buses as $\mathcal{N}_G^{\text{slack}} \subseteq \mathcal{N}_G$, in which each distributed slack bus $i \in \mathcal{N}_G^{\text{slack}}$ is associated with a known participation factor $\alpha_i > 0$ such that $\sum \alpha_i = 1$. In particular, for all $i \in \mathcal{N}_G^{\text{slack}}$, $P_i = \bar{P}_i + \alpha_i P_{\text{slack}}$, where $\bar{P}_i$ is the scheduled real power generation and is known, and $P_{\text{slack}} \geq 0$ is the unknown total network loss in the system to be computed. Clearly, when $P_{\text{slack}} = 0$, the network is lossless and α effectively becomes irrelevant. We also assume that no generator output limits are violated, so all the participation factors α_i stay constant, and no PV bus changes to the PQ bus as a result.

Since we formulate the power flow equations in terms of nodal power injections, we can additionally define $\alpha_i \coloneqq 0$ for all $i \in \mathcal{N} \setminus \mathcal{N}_G^{\text{slack}}$. Then, each bus (regardless of generator or load) is associated with a nonnegative participation factor. Thus, we can overload the notation and write $P_i = \bar{P}_i$ for all $i \in \mathcal{N} \setminus \mathcal{N}_G^{\text{slack}}$. That is, the participation factor can be partitioned into the load bus and generator bus subsets, similar to (2.3):

$$\alpha = \begin{bmatrix} \mathbb{0}_n \\ \hline \alpha_G \end{bmatrix}.$$

Using rectangular coordinates for the admittance matrix entries and polar coordinates for the nodal voltages, the power flow equations for the system [1, Equations 6.4.12-13] are given by

$$\bar{P}_i + \alpha_i P_{\text{slack}} = V_i \sum_{j=1}^{n+m} V_j (G_{ij} \cos(\theta_i - \theta_j) + B_{ij} \sin(\theta_i - \theta_j)), \qquad i \in \mathcal{N} \tag{3.1a}$$

$$Q_i = V_i \sum_{j=1}^{n+m} V_j (G_{ij} \sin(\theta_i - \theta_j) - B_{ij} \cos(\theta_i - \theta_j)), \qquad i \in \mathcal{N}_L \tag{3.1b}$$

where $\bar{P} \in \mathbb{R}^{n+m}$, $Q_L \in \mathbb{R}^n$, $V_G \in \mathbb{R}^m$ and $\alpha \in \mathbb{R}^{n+m}$ as well as the entries of G, B matrices are known and fixed. The objective is to solve for the phase θ_i at all $n+m$ generator and load buses, the voltage magnitude V_i at the n load buses, such that (3.1) holds. Thus, we have $2n+m$ equations with $2n+m$ unknowns. The generator bus reactive power injections $Q_G \in \mathbb{R}^m$ and the the total network loss $P_{\text{slack}} \geq 0$ can be computed as by-products in the end.

As mentioned before, the power flow problem is typically stated with a single slack bus doubled as the phase angle reference ($\theta_i = 0$ at this bus), and its voltage magnitude is fixed to be 1.0 p.u. Thus, the Newton-Raphson algorithm applied to the power flow equations does not require the slack bus's known voltage magnitude and phase. In addition, the total network loss is all compensated by the single slack bus after the algorithm terminates, so the active power injection at the slack bus is also omitted from the formulation [1, Equation 6.6.1]. However, with the distributed slack bus formulation used here, we cannot simply remove the equations corresponding to the slack buses to compute the rest of the bus voltages, but we can still eliminate the *a priori* unknown P_{slack} in the calculation as follows. Let $f_{P,i}(V, \theta)$ be a shorthand

for the right-hand side of (3.1a), then in vector form, we have

$$\bar{P} + \alpha P_{\text{slack}} = f_P(V, \theta) \coloneqq \begin{bmatrix} f_{P,1}(V,\theta) \\ \vdots \\ f_{P,n+m}(V,\theta) \end{bmatrix}.$$

We make a transformation to the active power flow equation to eliminate P_{slack}, given that the participation factor vector $\alpha \in \mathbb{R}^{n+m}$ is known. Let $R \in \mathbb{R}^{(n+m)\times(n+m-1)}$ be a matrix whose columns form an orthonormal basis for the orthogonal complement of the subspace spanned by α, denoted by $\alpha^{\perp}$. That is, $R^{\mathsf{T}}\alpha = \mathbb{0}_{n+m-1}$. Left-multiply both sides of (3.1a) by R^{T}, then it can be transformed into a system of $n+m-1$ nonlinear equations

$$R^{\mathsf{T}}\bar{P} = R^{\mathsf{T}} f_P(V, \theta), \tag{3.2}$$

which encapsulate the original active power flow equation (3.1a) but no longer has the variable α or P_{slack} in it. The matrix R can be thought of as a "compression" matrix that transforms the original active power flow equations into one without the slack variable.

Remark 3.1. Since R has orthonormal columns and full column rank, R^{T} has a right inverse $\left(R^{\mathsf{T}}\right)^{\dagger}$ such that $R^{\mathsf{T}}\left(R^{\mathsf{T}}\right)^{\dagger} = I_{n+m-1}$.

Remark 3.2. By the fundamental theorem of linear algebra,

(i) since $\operatorname{rank}(R) = n+m-1$, $\ker R$ is trivial, and

(ii) since $\ker R^{\mathsf{T}} = \operatorname{span}\{\alpha\}$, $\operatorname{im} R = \operatorname{span}\{\alpha\}^{\perp}$.

After we solve for θ and V with the transformed active power flow equation (3.2) and the reactive power flow equation (3.1b), we can recover P_{slack} by simply taking the sum of the left and right hand side of (3.1a) and use the fact that $\mathbb{1}_{n+m}^{\mathsf{T}}\alpha = 1$ to obtain

$$P_{\text{slack}} = \mathbb{1}_{n+m}^{\mathsf{T}}\left(\bar{P} - f_P(V,\theta)\right). \tag{3.3}$$

Before we move on, we show that this transformation can readily handle the single slack bus formulation as a special case. Without loss of generality, let the $(n+1)$-th bus (the first generator bus in $\mathcal{N}_G$) be the only slack bus, then $\alpha = \mathbb{e}_{n+1}$, and we can pick the matrix R to be

$$\begin{bmatrix} \mathbb{e}_1 & \cdots & \mathbb{e}_n & \mathbb{e}_{n+2} & \cdots & \mathbb{e}_{n+m} \end{bmatrix},$$

which is equivalent to the removal of the equation corresponding to the single slack bus from (3.1a).

3.2 The Open-Circuit Solution

In this section, we develop the notion of the *open-circuit load voltage*, which is used later as a normalization factor for bus voltages variables we need to solve for.

Definition 3.1 (Definition 1, [3])**.** The *open-circuit load voltage* $V_L^\circ \in \mathbb{R}^n$ is defined as

$$V_L^\circ = -B_{LL}^{-1} B_{LG} V_G. \tag{3.4}$$

The vector V_L° is known and fixed, since B_{LL}, B_{LG} and V_G are known. We can also extend this definition and additionally define the *open-circuit voltage*

$$V^\circ \coloneqq \begin{bmatrix} V_L^\circ \\ V_G \end{bmatrix} \in \mathbb{R}_{>0}^{n+m},$$

which is known since V_G contains the strictly positive, fixed generator voltage magnitudes. The fact that V° is positive element-wise is not trivial, and we focus on the elements in V_L° since V_G are the generator setpoints and it would be unrealistic for them to not be positive. For V_L°, note that the submatrix B_{LG} only contains the off-diagonal entries of B, and is a nonnegative matrix that does not have a zero row or column if Assumption 2.2 holds and the network $\mathcal{G}$ is weakly connected. In addition, $-B_{LL}^{-1}$ is a nonnegative matrix by Remark 2.1. Thus, V_L° must be strictly positive as well.

We can also define the *normalized* load voltage vector $v \in \mathbb{R}^n$ as

$$v \coloneqq [V_L^\circ]^{-1} V_L, \tag{3.5}$$

and the original V_L can be recovered via $[V_L^\circ]v$. Note that we may extend this normalization scheme for all bus voltage magnitudes V° as

$$g(v) \coloneqq [V^\circ]^{-1} V = \begin{bmatrix} v \\ \mathbb{1}_m \end{bmatrix} \iff [V^\circ] g(v) = [g(v)] V^\circ = V. \tag{3.6}$$

The variable v is crucial to the ensuing discussion since we can compute the unknown load voltage magnitudes V_L if and only if we know v. This normalization scheme also allows us to work with a more "centered" variable v.

With Definition 3.1, we are ready to extend the open-circuit solution stated in [3, Proposition 3.1] to the lossy system result below.

Proposition 3.1 (Open-circuit solution)**.** When $\bar{P} = \mathbb{0}_{n+m}$ and $Q_L = \mathbb{0}_n$, $(\theta, V_L) = (\mathbb{0}_{n+m}, V_L^\circ)$ is a solution to (3.1). In addition, $P_{\text{slack}} = \mathbb{1}_{n+m}^\mathsf{T} [V^\circ] G V^\circ$.

Proof. We can verify that $(\theta, V_L) = (\mathbb{0}_{n+m}, V_L^\circ)$ is a solution to (3.1a)–(3.1b) by direct substitution. When $\theta = \mathbb{0}_{n+m}$, $\sin(\theta_i - \theta_j) = 0$ and $\cos(\theta_i - \theta_j) = 1$ for all $i, j \in \mathcal{N}$. Thus, (3.1) reduces to

$$P_i = V_i \sum_{j=1}^{n+m} V_j G_{ij}, \qquad i \in \mathcal{N}$$
$$Q_i = -V_i \sum_{j=1}^{n+m} V_j B_{ij}, \qquad i \in \mathcal{N}_L$$

which can be vectorized as

$$P = [V]GV, \tag{3.7a}$$
$$Q_L = -[V_L] \begin{bmatrix} B_{LL} & B_{LG} \end{bmatrix} \begin{bmatrix} V_L \\ V_G \end{bmatrix}. \tag{3.7b}$$

With V_G known and V_L° nonzero, if $V_L = V_L^\circ$, then (3.7b) becomes

$$\begin{aligned} Q_L &= -[V_L^\circ] \begin{bmatrix} B_{LL} & B_{LG} \end{bmatrix} \begin{bmatrix} -B_{LL}^{-1} B_{LG} V_G \\ V_G \end{bmatrix} \\ &= -[V_L^\circ] \left(-B_{LL} B_{LL}^{-1} B_{LG} V_G + B_{LG} V_G \right) = \mathbb{0}_n, \end{aligned}$$

that is, $(\theta, V_L) = (\mathbb{0}_{n+m}, V_L^\circ)$ solves the reactive power flow equation (3.7b) given that $Q_L = \mathbb{0}_n$. Finally, given that $\bar{P} = \mathbb{0}_{n+m}$, we can verify that $(\theta, V_L) = (\mathbb{0}_{n+m}, V_L^\circ)$ is a solution to the active power flow equation (3.7a) since the distributed slack bus compensation $P_{\text{slack}} = \mathbb{1}_{n+m}^\mathsf{T}[V^\circ]GV^\circ$ satisfies the active power balance. □

Given the network losses and the resulting nonzero P_{slack}, the name "open-circuit solution" is admittedly somewhat of a misnomer compared to the open-circuit solution given in the lossless context, where there is truly zero active power flow in the network. However, this idea is a standard construction in several other papers with fixed-point theoretic analysis of the power flow equations in both lossless and lossy contexts, e.g., [14], [18], [19]. However, as in the lossless case, the construction of the open-circuit voltage magnitude V_L° here is still important as an normalizing factor for the fixed-point reformulation and analysis in the subsequent chapters.

3.3 Vectorization of the Power Flow Equations

Recall that the power flow equations (3.1) are written as scalar equations of the form $g_i(x) = c_i$ for each bus i in the system. Looking ahead, our goal in Chapter 4.1 is to

manipulate (3.1) into an equivalent fixed-point form $f(x) = x$, where f is no longer scalar in general. Thus, to bridge the gap between what we have and our goal in the next chapter, we need to vectorize the scalar equations (3.1) in this section. First, we introduce a few notations generalized or adapted from [3].

Definition 3.2 (Branch stiffness matrices)**.** Given the normalized voltage magnitudes and the off-diagonal entries of the conductance and susceptance matrices G and B, the branch stiffness matrices are the following semidefinite diagonal matrices

$$\begin{aligned} D_G^+ &= \left[V_i^\circ V_j^\circ G_{ij}\right]_{(i,j)\in\mathcal{E}}, \qquad & D_G^- &= \left[V_i^\circ V_j^\circ G_{ji}\right]_{(i,j)\in\mathcal{E}} \\ D_B^+ &= \left[V_i^\circ V_j^\circ B_{ij}\right]_{(i,j)\in\mathcal{E}}, \qquad & D_B^- &= \left[V_i^\circ V_j^\circ B_{ji}\right]_{(i,j)\in\mathcal{E}} \end{aligned} \tag{3.8}$$

Since the off-diagonal elements of G are typically nonpositive, D_G^+ and D_G^- are generally negative semidefinite. In addition, by Assumption 2.2, D_B^+ and D_B^- are positive definite. Note that if the system contains no phase-shifting transformers, then $D_B^+ = D_B^-$ and $D_G^+ = D_G^-$, in which case we drop the $\cdot^+, \cdot^-$ superscripts and use the notations D_B and D_G instead. These matrices can be interpreted as the (asymmetrical) forward and backward edge weights in the graph model of the transmission system, and are in fact what inspired the construction of the asymmetrically weighted incidence matrix.

Next, for any forward edge $(i,j) \in \mathcal{E}$, we define the mapping $h_{(i,j)} : \mathbb{R}^n \to \mathbb{R}$ by

$$h_{(i,j)}(v) = \begin{cases} v_i v_j & \text{if } (i,j) \in \mathcal{E}^{\ell\ell} \\ v_j & \text{if } (i,j) \in \mathcal{E}^{g\ell} \\ 1 & \text{if } (i,j) \in \mathcal{E}^{gg} \end{cases}. \tag{3.9a}$$

Then, for all forward edges $(i,j) \in \mathcal{E}$, we can define the vector-valued mapping $h : \mathbb{R}^n \to \mathbb{R}^{|\mathcal{E}|}$ using $h_{(i,j)}$ and the $\mathcal{E}^{\ell\ell}, \mathcal{E}^{\ell g}$, and $\mathcal{E}^{gg}$ edge set partitions as

$$h(v) = \begin{bmatrix} h_{\ell\ell}(v) \\ h_{g\ell}(v) \\ h_{gg}(v) \end{bmatrix} = \begin{bmatrix} \begin{bmatrix} \left(A_L^{\ell\ell,+}\right)^\mathsf{T} v \end{bmatrix} \begin{bmatrix} \left(A_L^{\ell\ell,-}\right)^\mathsf{T} v \end{bmatrix} \\ \begin{bmatrix} \left(A_L^{g\ell,-}\right)^\mathsf{T} v \end{bmatrix} \\ \mathbb{1}_{gg} \end{bmatrix} = \begin{bmatrix} \left(A^+\right)^\mathsf{T} g(v) \end{bmatrix} \left(A^-\right)^\mathsf{T} g(v). \tag{3.9b}$$

Note that $h(\mathbb{1}_n) = \mathbb{1}_{|\mathcal{E}|}$. Combined with the branch stiffness matrices, we have

$$\begin{aligned} \left[V_i V_j G_{ij}\right]_{(i,j)\in\mathcal{E}} &= D_G^+[h(v)], \qquad & \left[V_i V_j B_{ij}\right]_{(i,j)\in\mathcal{E}} &= D_B^+[h(v)], \\ \left[V_i V_j G_{ji}\right]_{(i,j)\in\mathcal{E}} &= D_G^-[h(v)], \qquad & \left[V_i V_j B_{ji}\right]_{(i,j)\in\mathcal{E}} &= D_B^-[h(v)]. \end{aligned} \tag{3.10}$$

To vectorize the active power equation, we first rewrite the right-hand side of the

active power flow equation (3.1a) as

$$V_i^2 G_{ii} + \sum_{\substack{j=1 \\ j\neq i}}^{n+m} V_i V_j G_{ij} \cos(\theta_i - \theta_j) + \sum_{\substack{j=1 \\ j\neq i}}^{n+m} V_i V_j B_{ij} \sin(\theta_i - \theta_j)), \qquad i \in \mathcal{N} \tag{3.11}$$

and we vectorize the three terms in (3.11) one by one. Observe that the first term contains the diagonal entries of the conductance matrix G, whereas the second and third terms contain the off-diagonal elements of G and B.

For the first term in (3.11), we can first extract the diagonal entries of G into the diagonal matrix $[G_{ii}]$. Then, the $V_i^2 G_{ii}$ terms can be vectorized as $[V][G_{ii}]V$, and can be further rewritten in terms of the normalized load voltage magnitude v and the map $g(\cdot)$ using (3.6) as

$$[V^\circ][g(v)][G_{ii}][V^\circ]g(v). \tag{3.12a}$$

For the second term in (3.11), we first collect the branch-wise phase differences $\theta_i - \theta_j$, and vectorize them as $A^\mathsf{T}\theta$ as discussed in Chapter 2.2. Let $\mathbf{cos}\,(\cdot)$ denote the element-wise cosine function, then we can vectorize all $\cos(\theta_i - \theta_j)$ terms as $\mathbf{cos}\left(A^\mathsf{T}\theta\right)$. Since cosine is an even function, $\cos(\theta_i - \theta_j) = \cos(\theta_j - \theta_i)$, and we need not worry about the sign mismatch due to whether the branch (i, j) or (j, i) is in the forward direction. However, if the branch (i, j) contains a phase shifting transformer, then $G_{ij} \neq G_{ji}$, and this is precisely why we defined both D_G^+ and D_G^- in (3.8): suppose that we had not differentiated between the D_G^+ and D_G^- and only defined a diagonal D_G according to the branches in the forward direction, i.e., $D_G = D_G^+$. If the edge (j, i) is in the forward direction, then the j-th summand in the second term of the i-th equation of (3.11) would be $V_i V_j G_{ij} \cos(\theta_i - \theta_j)$. However, vectorizing the second term with D_G alone would result in $V_i V_j G_{ji} \cos(\theta_i - \theta_j)$, which is incorrect unless the branch (i, j) does not contain a phase-shifting transformer. Thus, we need to work with both D_G^+ and D_G^- defined above. Finally, since (3.11) describes the *nodal* power injection and has n equations, and the vectorization $\mathbf{cos}\left(A^\mathsf{T}\theta\right)$ describes the *branch* phase difference and has $|\mathcal{E}|$ equations, we use the incidence matrix and its "from" and "to" partitions to capture the summation, and vectorize the second term in (3.11) as

$$\left(A^+ D_G^+ + A^- D_G^-\right)[h(v)]\,\mathbf{cos}\left(A^\mathsf{T}\theta\right), \tag{3.12b}$$

where the $[h(v)]$ term transforms the normalized voltage magnitudes back to the actual bus voltage magnitudes, as demonstrated by (3.10).

Finally, for the third term in (3.11), denote $\mathbf{sin}\,(\cdot)$ as the element-wise sine function similarly as before, but now we need to be careful about the signs since the sine function is odd. Note that the j-th summand in the third term of the i-th equation of

(3.11) contains $\sin(\theta_i - \theta_j)$, and recall that the corresponding element in $\mathbf{sin}\left(A^\mathsf{T}\theta\right)$ is $\sin(\theta_i - \theta_j)$ if (i,j) is the forward edge and $\sin(\theta_j - \theta_i) = -\sin(\theta_i - \theta_j)$ if (j,i) is the forward edge. Thus, there needs to be additional negative signs to cancel out these sign mismatches. Therefore, we can vectorize the third term of (3.11) as

$$\left(A^+ D_B^+ - A^- D_B^-\right)[h(v)]\,\mathbf{sin}\left(A^\mathsf{T}\theta\right). \tag{3.12c}$$

The subtraction in (3.12c) "corrects" all the sign mismatches due to the $\mathbf{sin}\,(\cdot)$ function being odd.

If none of the branches in the system contains a phase shifting transformer, then G and B are symmetric, $D_G^+ = D_G^-$, $D_B^+ = D_B^-$, and (3.12b)–(3.12c) simply reduce to $|A|D_G[h(v)]\,\mathbf{cos}\left(A^\mathsf{T}\theta\right)$ and $AD_B[h(v)]\,\mathbf{sin}\left(A^\mathsf{T}\theta\right)$. However, in general, using the asymmetrically weighted incident matrix constructed in Section 2.2, we can define[1]

$$\begin{aligned} \Gamma_B &\coloneqq A^+ D_B^+ - A^- D_B^-, \qquad & |\Gamma_B| &\coloneqq A^+ D_B^+ + A^- D_B^-, \\ \Gamma_G &\coloneqq A^+ D_G^+ - A^- D_G^-, \qquad & |\Gamma_G| &\coloneqq A^+ D_G^+ + A^- D_G^-. \end{aligned} \tag{3.13}$$

Finally, left multiply on both sides of the vectorized transformed active power flow equation (3.2) by R^T, we can rewrite it as

$$\begin{aligned} R^\mathsf{T}\bar{P} = {} & R^\mathsf{T}[V^\circ][g(v)][G_{ii}][V^\circ]g(v) \\ & + R^\mathsf{T}|\Gamma_G|[h(v)]\,\mathbf{cos}\left(A^\mathsf{T}\theta\right) + R^\mathsf{T}\Gamma_B[h(v)]\,\mathbf{sin}\left(A^\mathsf{T}\theta\right). \end{aligned} \tag{3.14}$$

Next, similar to (3.11), we first write the reactive power flow equation (3.1b) as

$$Q_i = -V_i^2 B_{ii} + \sum_{\substack{j=1 \\ j\neq i}}^{n+m} V_i V_j G_{ij}\sin(\theta_i - \theta_j) - \sum_{\substack{j=1 \\ j\neq i}}^{n+m} V_i V_j B_{ij}\cos(\theta_i - \theta_j), \tag{3.15}$$

for all $i \in \mathcal{N}_L$. Since we only care about the first n reactive power flow equations corresponding to the load buses, we take the top n rows of the relevant matrices. Let $[B_{ii}]_L$ denote the $n \times n$ diagonal matrix formed by the diagonal elements of B corresponding to the load buses, and let $\Gamma_{G_L}, \Gamma_{B_L}$ denote the top $n \times |\mathcal{E}|$ submatrix of Γ_G, Γ_B, respectively, as shown in (3.16).

$$[B_{ii}] = \begin{bmatrix} [B_{ii}]_L & \mathbb{0} \\ \mathbb{0} & [B_{ii}]_G \end{bmatrix}, \qquad \Gamma_G = \begin{bmatrix} \Gamma_{G_L} \\ \Gamma_{G_G} \end{bmatrix}, \qquad \Gamma_B = \begin{bmatrix} \Gamma_{B_L} \\ \Gamma_{B_G} \end{bmatrix}. \tag{3.16}$$

We can then vectorize (3.15) using the Definition 3.2 and the maps (3.9a)–(3.9b)

[1] The notation $|\Gamma_B|$ does not imply that $|\Gamma_B|$ is constructed by taking the absolute value of Γ_B elementwise, but comes from the analogous relationship between A and $|A|$ written using A^+ and A^-.

from before as

$$Q_L = -[V_L^\circ][v][B_{ii}]_L[V_L^\circ]v + \Gamma_{G_L}[h(v)]\,\mathbf{sin}\left(A^\mathsf{T}\theta\right) - |\Gamma_{B_L}|[h(v)]\,\mathbf{cos}\left(A^\mathsf{T}\theta\right) \tag{3.17}$$

using similar arguments as the vectorization of the active power flow equations.

An example that demonstrates the vectorization scheme (3.14) and (3.17) for a simple system is provided in Appendix B.

Chapter 4

The Fixed-Point Power Flow Algorithm

In this chapter, we develop the fixed-point power flow (FPPF) algorithm, the main algorithmic result of this thesis. In Section 4.1, we reformulate the vectorized power flow equations derived in Chapter 3 into a fixed-point form, and show that the solution to the reformulation is equivalent to the solution to the original power flow equations. In Section 4.2, we present the FPPF algorithm from the fixed-point reformulation.

4.1 The Fixed-Point Reformulation

In this section, we manipulate the vectorized power flow equations (3.14) and (3.17) into an equivalent fixed point form. First, we introduce a few more definitions and construct some useful quantities.

Let $C \in \{-1, 0, 1\}^{|\mathcal{E}| \times n_c}$ be the cycle matrix of $\mathcal{G}$, where $n_c = |\mathcal{E}| - (n + m - 1)$ is the cycle dimension. Recall from the construction of the cycle matrix in Chapter 2.2 that the columns of C form an orthonormal basis of $\ker A$. In addition, we define

$$M_B \coloneqq R^{\mathsf{T}} \Gamma_B \in \mathbb{R}^{(n+m-1) \times |\mathcal{E}|}, \tag{4.1}$$

using the Γ_B matrix defined in (3.13). Let $K \in \mathbb{R}^{|\mathcal{E}| \times n_c}$ be a sparse matrix whose columns form a basis[1] of $\ker M_B$, which implies $M_B K = \mathbb{0}$. That K must have n_c linearly independent columns is nontrivial, and relies on the fact that M_B has full row rank to be proved in Lemma 4.1 in the next section. Since we interpreted the R matrix to act as a compression matrix in Chapter 3.1, we can interpret M_B to be the compressed asymmetrically weighted incidence matrix (with weights associated with

[1] This is not necessarily an *orthonormal* basis, which would generally make K dense and computationally inefficient; see Chapter 6.1 for more details.

the branch susceptance values), and K can be viewed as a compressed weighted cycle matrix. This interpretation is due to the connection between the fact that $AC = \mathbb{0}$ and the objective that $M_B K = \mathbb{0}$.

Finally, we define the *nodal stiffness matrix* denoted by S [3, Definition 2], which quantifies the strength of load bus interconnections in the network.

Definition 4.1 (Nodal Stiffness Matrix)**.** Given the open circuit load voltage magnitudes V_L° and the submatrix B_{LL}, the *nodal stiffness matrix* is an $n \times n$ invertible matrix defined as

$$S \coloneqq \frac{1}{4}[V_L^\circ] B_{LL} [V_L^\circ].$$

We are now ready to provide the main theoretical results of this chapter, which states the equivalence between the solution to the standard power flow equations and the solution to our fixed-point reformulation to be developed next.

Theorem 4.1 (Fixed-Point Solution to the Lossy Power Flow Equations)**.** *Consider the change of variable $\psi \coloneqq \mathbf{sin}\left(A^\mathsf{T}\theta\right) \in \mathbb{R}^{|\mathcal{E}|}$, the normalized load voltage magnitudes $v \in \mathbb{R}^n$ and some vector $x_c \in \mathbb{R}^{n_c}$. If Assumptions 2.1–2.2 hold, then the following statements are equivalent:*

(i) (V_L, θ) solves the vectorized power flow equations (3.14), (3.17)*.*

(ii) (v, ψ, x_c) satisfy

$$v = \mathbb{1}_n - \frac{1}{4} S^{-1} [v]^{-1} \left(Q_L - \Gamma_{G_L} [h(v)] \psi - |\Gamma_{B_L}| [h(v)] \left(\mathbb{1}_{|\mathcal{E}|} - \eta \right) \right), \tag{4.2a}$$

$$\psi = [h(v)]^{-1} M_B^\dagger R^\mathsf{T} \left(\bar{P} - [V^\circ][g(v)][G_{ii}][V^\circ] g(v) - |\Gamma_G| [h(v)] \eta \right) + [h(v)]^{-1} K x_c, \tag{4.2b}$$

$$\mathbb{0}_{n_c} = C^\mathsf{T} \mathbf{arcsin}\left(\psi\right) \mod 2\pi, \tag{4.2c}$$

where $\eta \coloneqq \sqrt{\mathbb{1}_{|\mathcal{E}|} - [\psi]\psi}$.

The results above are derived in Sections 4.1.1–4.1.2 by considering the active and reactive power flow equations separately to obtain their equivalent fixed-point reformulations. As mentioned in Section 3.1, we do not include P_{slack} as an unknown to be solved since it can be directly computed once the bus voltages are solved for. In addition, note that Theorem 4.1 induces a constraint on ψ: to keep all the variables real-valued, we must have $\|\psi\|_\infty \leq 1$. This implicit constraint turns out to be quite problematic in certain test cases, and we elaborate on this issue in Chapter 6.

When the network is radial, $n_c = 0$ and x_c can be discarded. Thus, we can remove the term $[h(v)]^{-1} K x_c$ from (4.2b) and disregard the constraint (4.2c) in this case. We

do not state the result for radial networks separately since it can be trivially derived from Theorem 4.1.

It is worth noting that, while there are many ways to rewrite the power flow equations from its standard root-finding form to a fixed-point form, we have chosen the particular form in Theorem 4.1 since it is a direct extension of the lossless formulation in [3]. Since the main goal of this thesis is to extend the lossless FPPF algorithm and incorporate losses and other realistic transmission line parameters, it is natural to choose this particular form.

4.1.1 Active Power Flow Equation

Before we show that the vectorized active power flow equation (3.14) can be equivalently manipulated into the fixed-point form given above, we state and prove the following lemma, which is crucial to the proof of the equivalence statement in Theorem 4.1.

Lemma 4.1. *If Assumption 2.2 holds, then M_B has full row rank.*

Proof. Since M_B has full row rank if and only if M_B^T has full column rank, which holds if and only if it has a trivial kernel, we can equivalently prove that $M_B^\mathsf{T} = \Gamma_B^\mathsf{T} R$ has a trivial kernel.

Assume towards contradiction that there exist a nonzero $x \in \ker M_B^\mathsf{T}$, then at least one of the following two cases must be true:

(i) $x \in \ker R$, or

(ii) there exists some $y = Rx$ such that $y \in \ker \Gamma_B^\mathsf{T}$.

We can rule out case (i) due to Remark 3.2(i). For case (ii), suppose that such y exists and is nonzero (if $y = \mathbb{0}$, then we are back to the first case). Denote the k-th column of Γ_B by w_k, then $\Gamma_B^\mathsf{T} y = \mathbb{0}$ if and only if $\langle w_k, y\rangle = 0$ for all $k = 1, ..., |\mathcal{E}|$. By the construction of the branch stiffness matrices D_B^+, D_B^- and Assumption 2.2, for each $e_k = (i, j) \in \mathcal{E}$, w_k contains exactly two nonzero elements at $w_{k,i} = V_i^\circ V_j^\circ B_{ij}$ and $w_{k,j} = -V_i^\circ V_j^\circ B_{ji}$, so $\Gamma_B^\mathsf{T} y = \mathbb{0}$ if and only if $\langle w_k, y\rangle = V_i^\circ V_j^\circ (B_{ij} y_i - B_{ji} y_j) = 0$ for all $k = 1, ..., |\mathcal{E}|$. However, since $V_i^\circ, V_j^\circ > 0$ and $B_{ij}, B_{ji} > 0$, y_i, y_j must be both positive, both negative, or both zero. Recall that in Lemma 2.1, the weak connectivity of the bidirected graph implies that

- if there exists an edge $(i, j) \in \mathcal{E}$ such that $y_i = y_j = 0$, then $y = \mathbb{0}$ must hold, which returns us to case (i) and results in a contradiction;
- the sign of any particular y_i, y_j will propagate to the rest of the elements of y, i.e., $y > \mathbb{0}$ or $y < \mathbb{0}$ element-wise.

However, regardless of whether $y > \mathbb{0}$ or $y < \mathbb{0}$ element-wise, $\alpha_i \geq 0$ implies that $y^\mathsf{T}\alpha \neq 0$ always holds, because we would need at least one sign variation within the elements of y for $y^\mathsf{T}\alpha = \mathbb{0}$ to even be possible. Finally, by Remark 3.2(ii), $y^\mathsf{T}\alpha \neq 0$ implies that $y \notin \operatorname{im} R$, that is, there does not exist a nonzero x such that $y = Rx \in \ker \Gamma_B^\mathsf{T}$ and case (ii) cannot hold. Thus, neither case (i) or case (ii) can hold, and we can conclude that $\ker M_B^\mathsf{T}$ must be trivial. □

Remark 4.1. Since M_B has full row rank, the right inverse of M_B denoted by $M_B^\dagger$ exists, i.e., $M_B M_B^\dagger = I_{n+m-1}$ and we can explicitly write $M_B^\dagger = M_B^\mathsf{T}\left(M_B M_B^\mathsf{T}\right)^{-1}$. If the system is also radial, then $|\mathcal{E}| = n + m - 1$, in which case M_B becomes invertible and we write $M_B^\dagger$ as M_B^{-1} instead.

Now, we rewrite the transformed active power flow equation (3.14) into a fixed-point form. With the change of variable from the phase angles θ to ψ, we have

$$\mathbf{sin}\left(A^\mathsf{T}\theta\right) = \psi, \quad \mathbf{cos}\left(A^\mathsf{T}\theta\right) = \sqrt{\mathbb{1}_{|\mathcal{E}|} - [\psi]\psi},$$

where the square root is understood to be taken element-wise on its argument. Thus, (3.14) becomes

$$R^\mathsf{T}\bar{P} = R^\mathsf{T}[V^\circ][g(v)][G_{ii}][V^\circ]g(v) + R^\mathsf{T}|\Gamma_G|[h(v)]\sqrt{\mathbb{1}_{|\mathcal{E}|} - [\psi]\psi} + M_B[h(v)]\psi, \quad (4.3a)$$

which can be rearranged to isolate the $M_B[h(v)]\psi$ term as

$$M_B[h(v)]\psi = R^\mathsf{T}\bar{P} - R^\mathsf{T}[V^\circ][g(v)][G_{ii}][V^\circ]g(v) - R^\mathsf{T}|\Gamma_G|[h(v)]\sqrt{\mathbb{1}_{|\mathcal{E}|} - [\psi]\psi} \quad (4.3b)$$

If we temporarily assume the right-hand side to be a known vector, then (4.3b) is linear in ψ, and is written in the form of $\mathbf{A}\psi = \mathbf{b}$ with known $\mathbf{A}$ and $\mathbf{b}$. A clear solution candidate for ψ on the left-hand side is thus $\psi = \mathbf{A}^\dagger\mathbf{b}$ such that $\mathbf{A}\mathbf{A}^\dagger = I$. We can check that (4.2b) is the general solution of (4.3b) by substituting it into the left-hand side of (4.3b), which becomes

$$\begin{aligned} M_B[h(v)][h(v)]^{-1}M_B^\dagger R^\mathsf{T}\Big(\bar{P} - [V^\circ][g(v)][G_{ii}][V^\circ]g(v) - |\Gamma_G|[h(v)]\sqrt{\mathbb{1}_{|\mathcal{E}|} - [\psi]\psi}\Big) \\ + M_B[h(v)][h(v)]^{-1}Kx_c. \end{aligned} \quad (4.3c)$$

The left-hand side after substitution (4.3c) is consistent with the right-hand side of (4.3b), since $[h(v)][h(v)]^{-1} = I_{|\mathcal{E}|}$ and $M_B[h(v)][h(v)]^{-1}M_B^\dagger = I_{n+m-1}$ by Lemma 4.1. The first term of (4.2b) is the particular solution, and the second term parameterizes the homogeneous solution with a slack variable x_c, since $M_B K = \mathbb{0}$ by construction.

Finally, let $\mathbf{arcsin}\,(\cdot)$ denote the element-wise arcsine function. If ψ, v are known

and $\psi \in [-1,1]^{|\mathcal{E}|}$, then the change of variable scheme $\mathbf{sin}\left(A^{\mathsf{T}}\theta\right) = \psi$ implies that

$$\mathbf{arcsin}\left(\psi\right) = A^{\mathsf{T}}\theta + 2\pi k \tag{4.4a}$$

for some $k \in \mathbb{Z}^{|\mathcal{E}|}$ [40, Remark 5.3.2]. As discussed in Chapter 2.2, $AC = \mathbb{0}_{(n+m)\times n_c}$, so (4.4a) yields

$$C^{\mathsf{T}}\,\mathbf{arcsin}\left(\psi\right) = C^{\mathsf{T}}\left(A^{\mathsf{T}}\theta + 2\pi k\right) = (AC)^{\mathsf{T}}\theta + 2\pi C^{\mathsf{T}}k = 2\pi C^{\mathsf{T}}k. \tag{4.4b}$$

Since $C \in \{-1,0,-1\}^{|\mathcal{E}|\times n_c}$ and $k \in \mathbb{Z}^{|\mathcal{E}|}$, we must have $C^{\mathsf{T}}k \in \mathbb{Z}^{n_c}$, which implies that $2\pi C^{\mathsf{T}}k \bmod 2\pi = \mathbb{0}_{n_c}$. That is, the "loop flow" constraint (4.2c) must be satisfied, and we elaborate on this requirement in Section 4.2. The cycles in the network necessitate the variable x_c in the formulation, and we expect its magnitude to be small[2].

To summarize, we have shown the equivalence between the fixed-point reformulation and the transformed active power flow equations, as well as the necessity of the constraint (4.2c).

4.1.2 Reactive Power Flow Equation

We make use of [3, Lemma A.3] stated below to derive the fixed-point reactive power flow equation (4.2a).

Lemma 4.2. *If Assumption 2.1 holds, then the following expressions are equivalent:*

(i) $-[V_L^\circ][v][B_{ii}]_L[V_L^\circ]v - |\Gamma_{B_L}|[h(v)]\mathbb{1}_{|\mathcal{E}|}$

(ii) $-[V_L]\left(B_{LL}V_L + B_{LG}V_G\right)$

(iii) $[v][V_L^\circ]B_{LL}[V_L^\circ]\left(\mathbb{1}_n - v\right)$

Proof. Note that when $\theta = \mathbb{0}_{n+m}$, $\mathbf{sin}\left(A^{\mathsf{T}}\theta\right) = \mathbb{0}_{|\mathcal{E}|}$ and $\mathbf{cos}\left(A^{\mathsf{T}}\theta\right) = \mathbb{1}_{|\mathcal{E}|}$, thus, the reactive power flow equation (3.17) becomes

$$Q_L = -[V_L^\circ][v][B_{ii}]_L[V_L^\circ]v - |\Gamma_{B_L}|[h(v)]\mathbb{1}_{|\mathcal{E}|},$$

and the condition $\theta = \mathbb{0}_{n+m}$ is used to develop the open-circuit solution in (3.7b),

$$Q_L = -[V_L]\left(B_{LL}V_L + B_{LG}V_G\right),$$

thus, (i) and (ii) are equivalent. Now, expanding out $[V_L] = [V_L^\circ][v]$ and inserting an

[2] We can corroborate this statement with the numerical tests in Chapter 6, and show that the linear approximation x_c must be $\mathbb{0}_{n_c}$, though the details are not important and omitted here.

additional $B_{LL}B_{LL}^{-1} = I$ term into the equation above, we have

$$\begin{aligned} Q_L &= -[V_L^\circ][v]B_{LL}B_{LL}^{-1}\left(B_{LL}V_L + B_{LG}V_G\right) \\ &= -[V_L^\circ][v]B_{LL}\left([V_L^\circ]v - V_L^\circ\right) = [v][V_L^\circ]B_{LL}[V_L^\circ]\left(\mathbb{1}_n - v\right), \end{aligned}$$

which shows that (ii) and (iii) are equivalent. □

With the nodal stiffness matrix S in Definition 4.1 and the equivalent expressions above, we have

$$-[V_L^\circ][v][B_{ii}]_L[V_L^\circ]v - |\Gamma_{B_L}|[h(v)]\mathbb{1}_{|\mathcal{E}|} = 4[v]S(\mathbb{1}_n - v).$$

Thus, if we add and subtract a $|\Gamma_{B_L}|[h(v)]\mathbb{1}_{|\mathcal{E}|}$ term in (3.17) and again apply the change of variable $\psi = \mathbf{sin}\left(A^\mathsf{T}\theta\right)$, we have

$$\begin{aligned} Q_L &= -[V_L^\circ][v][B_{ii}]_L[V_L^\circ]v - |\Gamma_{B_L}|[h(v)]\mathbb{1}_{|\mathcal{E}|} + \Gamma_{G_L}[h(v)]\psi \\ &\quad + |\Gamma_{B_L}|[h(v)]\mathbb{1}_{|\mathcal{E}|} - |\Gamma_{B_L}|[h(v)]\sqrt{\mathbb{1}_{|\mathcal{E}|} - [\psi]\psi} \\ &= 4[v]S\left(\mathbb{1}_n - v\right) + \Gamma_{G_L}[h(v)]\psi + |\Gamma_{B_L}|[h(v)]\left(\mathbb{1}_{|\mathcal{E}|} - \sqrt{\mathbb{1}_{|\mathcal{E}|} - [\psi]\psi}\right). \end{aligned}$$

Rearrange the equation above and multiply by $\frac{1}{4}S^{-1}[v]^{-1}$ on both sides, we get

$$v = \mathbb{1}_n - \frac{1}{4}S^{-1}[v]^{-1}\left(Q_L - \Gamma_{G_L}[h(v)]\psi - |\Gamma_{B_L}|[h(v)]\left(\mathbb{1}_{|\mathcal{E}|} - \sqrt{\mathbb{1}_{|\mathcal{E}|} - [\psi]\psi}\right)\right),$$

which is precisely (4.2a), and the proof of Theorem 4.1 is complete.

4.2 The Fixed-Point Power Flow Algorithm

We now return to the fixed point reformulation of the power flow equations in lossy networks, and derive the full FPPF algorithm. Recall that the fixed point reformulation for the meshed networks in Section 4.1 is written in the form

$$v = \mathcal{Q}(\psi, v, x_c), \tag{4.5a}$$
$$\psi = \mathcal{P}(\psi, v, x_c), \tag{4.5b}$$
$$\mathbb{0} = \mathcal{C}(\psi, v, x_c), \tag{4.5c}$$

where $\mathcal{Q}, \mathcal{P}$ and $\mathcal{C}$ represent the right-hand side expressions of (4.2) for notational simplicity. As mentioned before, in the case of radial networks, we can remove x_c from (4.5a)–(4.5b) and disregard the constraint (4.5c).

To find the solution, we need to initialize ψ, v, and x_c at some (ψ^0, v^0, x_c^0); at the

k-th step, we substitute the current values of ψ^k, v^k, and x_c^k into right-hand side of (4.5a)–(4.5b), and treat their left-hand side as the next iteration ψ^{k+1}, v^{k+1}, and x_c^{k+1} to be evaluated, e.g., $v^{k+1} = \mathcal{Q}(\psi^k, v^k, x_c^k)$. Similarly, we solve the constraint (4.5c) at every iteration using the most up-to-date values of ψ, v, and x_c. We continue the iterations until the fixed-point equations (4.5a)–(4.5b) and the constraint (4.5c) are all satisfied up to a small tolerance ϵ, as demonstrated in Figure 2.1. These convergence criteria are in practice equivalent to the power balance mismatch criterion typically used in power flow studies.

Since the updates are sequential, in the spirit of [17], at each iteration, we use the already updated variable to evaluate the update of the next variable. In addition, there are three variables in total, so we can choose from six different update orders. For example, we can first evaluate v^{k+1} using ψ^k, v^k and x_c^k, then evaluate ψ^{k+1} using the updated v^{k+1} and the current ψ_k and x_c^k, and finally evaluate x_c^{k+1} using both updated v^{k+1}, ψ^{k+1}, and the current x_c^k. All the update orders lead to convergence under slight modifications to the network R/X ratios on standard test IEEE and PEGASE systems[3], but have slightly different trajectories of power balance mismatches. While these update orders may be empirically similar, they formulate entirely different fixed-point mappings, and thus, any further theoretical analysis must factor the update order into account. We discuss the impact of update order on the convergence behaviors in more detail in Chapter 6.2.

For brevity, the ensuing discussion is based on the following update order. First, we evaluate v^{k+1} using ψ^k, v^k, and x_c^k as

$$v^{k+1} = \mathcal{Q}\left(\psi^k, v^k, x_c^k\right). \tag{4.6a}$$

Then, we compute x_c^{k+1} by solving the constraint (4.5c) using v^{k+1}, ψ^k, and x_c^k. Since the constraint (4.5c) is already in the root-finding form, we may use Newton-Raphson to compute x_c^{k+1} as follows

$$x_c^{k+1} = x_c^k - \left(J_c^k\right)^{-1} \mathcal{C}\left(\psi^k, v^k, x_c^k\right), \tag{4.6b}$$

where J_c^k is the Jacobian matrix of (4.5c) at the k-th iteration, and can be explicitly computed using the chain rule as

$$J_c^k = C^\mathsf{T}\left(I_{|\mathcal{E}|} - [\psi^k]^2\right)^{-1/2} [h(v^{k+1})]^{-1} K. \tag{4.6c}$$

Finally, we evaluate ψ^{k+1} using v^{k+1}, ψ^k, and x_c^{k+1} as

$$\psi^{k+1} = \mathcal{P}\left(\psi^k, v^k, x_c^{k+1}\right). \tag{4.6d}$$

[3]Some update orders fail to converge on certain RTE systems; see Chapter 6 for more details.

We iteratively update these variables until the termination criterion is met, which is the power balance mismatch typically used in power flow algorithms (or if a pre-set maximum iteration limit is reached). To compute the power balance, we simply substitute the computed ψ^{k+1}, v^{k+1} values into (3.14) and (3.17), and evaluate mismatch between the known power injections $R^\mathsf{T}\bar{P}, Q$ on the left-hand side and the results on the right-hand side. In addition, as mentioned previously, if the system is radial, then $n_c = 0$ and we omit steps (4.6b)–(4.6c), and the instances of x_c^k and x_c^{k+1} in (4.6a)–(4.6d) are fixed to be $\mathbb{0}$. The pseudocode for the FPPF algorithm is listed in Algorithm 1, where the initial voltage conditions are the default values in the test system. The construction of the required power flow data and relevant matrices presented in this chapter is discussed in more depth in Chapter 6.

Algorithm 1 The Fixed-Point Power Flow Algorithm (v-x_c-ψ order)

Require: Power flow data, power balance mismatch tolerance ϵ, maximum iteration limit

$v[0] \leftarrow V_L/V_L^\circ$, $\psi[0] \leftarrow \mathbf{sin}\left(A^\mathsf{T}\theta\right)$, $x_c[0] \leftarrow \mathbb{0}_{n_c}$

$k \leftarrow 0$

Compute power balance mismatch with $\psi[0], v[0]$

while power balance mismatch $> \epsilon$ AND $k <$ maximum iteration limit **do**

  update $v[k+1]$ using (4.6a)

  if $n_c > 0$ **then**

    update $x_c[k+1]$ using (4.6b)–(4.6c)

  end if

  update $\psi[k+1]$ using (4.6d)

  Compute power balance mismatch with $\psi[k+1], v[k+1]$

  $k \leftarrow k+1$

end while

return $\psi[k+1]$, $v[k+1]$, power balance mismatch

Chapter 5

Analysis of the Algorithm for the Two-Bus System

In this chapter, we leverage the mathematical tools from Chapter 2 to provide a detailed theoretical analysis for the fixed-point power flow algorithm developed in Chapter 4 on a simple two-bus system.

The two-bus system is a trivial radial system, so we focus on analyzing the FPPF algorithm for radial systems, i.e., without the cycle constraint and slack variable x_c. In Section 5.1, we simplify the vectorized equations into the scalar equations, written with constants specific to the two-bus model, and make several simplifying assumptions on the system parameters. In Section 5.2, we reproduce the theoretical results on a lossless two-bus system presented in [4, Section III-C] with more detailed derivations, which lays the foundation for the analysis of the lossy FPPF algorithm. Finally, in Section 5.3, we generalize the lossless system results to a full, lossy system, and provide a sufficient condition for the existence of a convex and compact invariant set, in which the desired power flow solution exists.

Since the full system not only includes the resistive loss, but also the parameters from the (phase-shifting) transformer and Π model of the transmission line, we refer to the lossless system discussed in Section 5.2 as the "nominal system" to differentiate it from the full system discussed in Section 5.3.

5.1 Problem Setup

Consider the two-bus model in Figure 5.1, where bus 2 is the only generator/slack bus and bus 1 is the load bus, in conformity to our $\mathcal{N}_L, \mathcal{N}_G$ set partition convention. The load is inductive and has a fixed power factor. Since there is exactly one load bus and one generator bus, it holds that $\bar{P}_1 = -\bar{P}_2$, i.e., bus 2 supplies exactly the

known real power consumption at bus 1, plus the transmission line loss P_{slack} to be calculated.

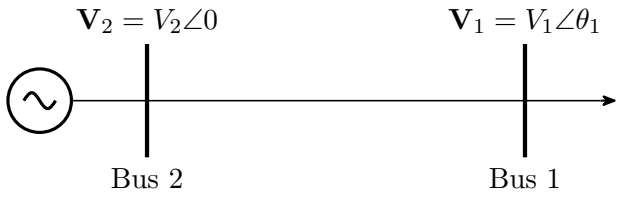

Figure 5.1: Two-bus model

The edge orientation is from bus 1 to bus 2 in the graph model of this system, in accordance with our assumption that the forward edge direction is from the generator buses to load buses. The incidence matrix and its "from" and "to" incidence matrices are $A = [-1 \quad 1]^{\mathsf{T}}$, $A^+ = [0 \quad 1]^{\mathsf{T}}$, and $A^- = [1 \quad 0]^{\mathsf{T}}$. Since bus 2 is the only slack bus, the R matrix in (3.2) can be chosen as $[1 \quad 0]^{\mathsf{T}}$.

The branch is modelled by the standard Π-model (see Figure 2.7), which follows from our discussion in Chapter 2.3. Let the branch admittance be $y = g - \mathbf{j}b$ where $g \geq 0$ and $b > 0$. Let the (small) line-charging susceptance be $b_c \geq 0$, and let the transformer tap ratio be $\tau = t\angle\theta_{\text{s}}$ where $t > 0$ and θ_{s} is small. Based on (2.5), the conductance and susceptance matrix for this system are[1]

$$G = \begin{bmatrix} g & \dfrac{-g\cos\theta_{\text{s}} + b\sin\theta_{\text{s}}}{t} \\ \dfrac{-g\cos\theta_{\text{s}} - b\sin\theta_{\text{s}}}{t} & \dfrac{g}{t^2} \end{bmatrix},$$

$$B = \begin{bmatrix} -b + \dfrac{b_c}{2} & \dfrac{g\sin\theta_{\text{s}} + b\cos\theta_{\text{s}}}{t} \\ \dfrac{-g\sin\theta_{\text{s}} + b\cos\theta_{\text{s}}}{t} & \dfrac{1}{t^2}\left(-b + \dfrac{b_c}{2}\right) \end{bmatrix}.$$

Define $\bar{t} \coloneqq t - 1$ as the shifted magnitude of the transformer tap ratio. For notational simplicity, we also define the following constants:

$$\tilde{g} \coloneqq \frac{g\cos\theta_{\text{s}} - b\sin\theta_{\text{s}}}{\bar{t}+1}, \quad \tilde{b} \coloneqq \frac{b\cos\theta_{\text{s}} + g\sin\theta_{\text{s}}}{\bar{t}+1}, \quad \hat{b} \coloneqq b - \frac{b_c}{2}, \quad \beta \coloneqq \frac{\hat{b}}{\tilde{b}}. \tag{5.1}$$

Realistically speaking, $\tilde{g}, \tilde{b}$ and $\hat{b}$ are all nonnegative constants: $\hat{b} \geq 0$ if and only if $b_c < 2b$, $\tilde{g} \geq 0$ if and only if $g/b \geq \tan(\theta_{\text{s}})$, which is true for $\theta_{\text{s}} \in (-\pi/2, \arctan(g/b)]$[2],

[1] Note that, since the 2-bus system here follows the $\mathcal{N}_L$-$\mathcal{N}_G$ partitioning scheme, the admittance matrix is a permuted version of the one shown in (2.5).

[2] This is a very large interval considering the realistic range of R/X ratios; e.g., if $g/b = 0.2$, then we

and $\tilde{b} \geq 0$ if and only if $b/g \geq \tan(\theta_s)$, which is certainly true if $\tilde{g} \geq 0$. Furthermore, if $\bar{t} \approx 0$, $\theta_s \approx 0$, and $b_c \approx 0$, then $\tilde{g} \approx g$, $\tilde{b} \approx b \approx \hat{b}$, and $\beta \approx 1$. Using these constants, we can extract the following components of the B, G matrices:

$$B_{LL} = -\hat{b}, \quad B_{LG} = \tilde{b}, \quad [G_{ii}] = \begin{bmatrix} g & 0 \\ 0 & \dfrac{g}{t^2} \end{bmatrix}.$$

Next, since the only generator voltage magnitude in this system is $V_2 = 1.0$ p.u., we can compute V_1°, the open-circuit load voltage magnitude as

$$V_1^\circ = -B_{LL}^{-1} B_{LG} V_2 = \frac{\tilde{b}}{\hat{b}} V_2 = \frac{1}{\beta} V_2 = \frac{1}{\beta} V_2^\circ,$$

and write the normalized load voltage magnitude as $v_1 = V_1/V_1^\circ$. Note that $V_2 = V_2^\circ = 1.0$ p.u. The nodal stiffness matrix S can then be computed as

$$S = \frac{1}{4}[V_1^\circ] B_{LL} [V_1^\circ] = -\frac{1}{4}\hat{b}\,(V_1^\circ)^2 = -\frac{1}{4}\tilde{b} V_1^\circ V_2^\circ.$$

The remaining matrices required can be computed as follows:

$$M_B^{-1} = -\left(D_B^-\right)^{-1}, \quad R^\mathsf{T} |\Gamma_G| = D_G^-, \quad |\Gamma_{B_L}| = D_B^-, \quad \Gamma_{G_L} = -D_G^-,$$

where $D_G^- = V_1^\circ V_2^\circ G_{12} = -\tilde{g} V_1^\circ V_2^\circ$ and $D_B^- = V_1^\circ V_2^\circ B_{12} = \tilde{b} V_1^\circ V_2^\circ$. Finally, since the only load bus is bus 1, we can write $v = v_1$, $g(v) = [v_1 \quad 1]^\mathsf{T}$ and $h(v) = v_1$. Combining the results above and noting that $\psi = \sin\left(A^\mathsf{T}\theta\right) = \sin(\theta_2 - \theta_1) = -\sin(\theta_1)$, the fixed-point reformulation in Theorem 4.1 simplifies to

$$\psi = -\left(\frac{\bar{P}_1}{\tilde{b} V_1^\circ V_2^\circ}\right)\frac{1}{v} + \frac{g}{\hat{b}} v - \frac{\tilde{g}}{\tilde{b}}\sqrt{1-\psi^2}, \tag{5.2a}$$

$$v = \left(\frac{Q_1}{\tilde{b} V_1^\circ V_2^\circ}\right)\frac{1}{v} - \frac{\tilde{g}}{\tilde{b}}\psi + \sqrt{1-\psi^2}. \tag{5.2b}$$

Note that (5.2a) reduces exactly to the lossy active power flow fixed-point equation [2, Equation 12] if we additionally assume that $\bar{t} = 0$, $\theta_s = 0$ and $b_c = 0$, i.e., if the branch is modelled as a simple series impedance.

Recall that the normalized load voltage magnitude v introduced in Chapter 3.1 satisfies $v = 1$ when there is no load power demand. If we temporarily assume that the branch connecting bus 1 and 2 is modelled by a simple series impedance, then as the load power demand increases (up to the maximum transferable power), v decreases,

need $\theta_s \in (-90°, 11.3°]$ for $g/b \geq \tan(\theta_s)$ to hold, but θ_s values in test cases found in [35] are often in much smaller intervals.

and thus $v \in (0, 1]$ in this scenario[3]. When the branch is modelled by the full Π-model with a transformer, v is somewhere on the positive real number line, likely around 1 under reasonable assumptions about the Π model and transformer parameters. Thus, unlike ψ which can be positive or negative, v is a "one-sided" variable since it is never negative. If we make a change of variable $x \coloneqq v - 1$, then the values of both ψ and x are expected to be centered around 0. We thus focus on the pair (ψ, x) rather than (ψ, v) in the subsequent analysis, and (5.2b) becomes

$$x = \left(\frac{Q_1}{\tilde{b} V_1^\circ V_2^\circ}\right) \frac{1}{x+1} - \frac{\tilde{g}}{\tilde{b}}\psi + \sqrt{1-\psi^2} - 1. \tag{5.2c}$$

Define the variable $\xi = [\psi \quad x]^\mathsf{T}$, which captures the complex nodal voltage at the load bus, then we can vectorize (5.2a) and (5.2c) as

$$\xi = \begin{bmatrix} \psi \\ x \end{bmatrix} = \begin{bmatrix} -\left(\frac{\bar{P}_1}{\tilde{b} V_1^\circ V_2^\circ}\right) \frac{1}{x+1} + \frac{g}{\tilde{b}}(x+1) - \frac{\tilde{g}}{\tilde{b}}\sqrt{1-\psi^2} \\ \left(\frac{Q_1}{\tilde{b} V_1^\circ V_2^\circ}\right) \frac{1}{x+1} - \frac{\tilde{g}}{\tilde{b}}\psi + \sqrt{1-\psi^2} - 1 \end{bmatrix} =: \begin{bmatrix} \mathcal{P}_\mu(\xi) \\ \mathcal{Q}_\mu(\xi) \end{bmatrix}$$

where $\mu = [g \quad b_c \quad \bar{t} \quad \theta_\mathrm{s}]^\mathsf{T}$. That is, μ contains the resistive loss, the line-charging susceptance, and the (normalized) transformer parameters. When $\mu = \mathbb{0}$, the system reduces to the two-bus system investigated in [4, Section III-C]. Thus, a nonzero μ can be seen as a vector of "perturbations" on the nominal lossless-shuntless-transformerless system ("nominal system" in short). As the elements of μ get further away from $\mathbb{0}$, the solutions to the full system stray further away from the respective solutions to the nominal system.

To simplify the general FPPF algorithm for the two-bus system, we use the most updated ψ in the update of x, then

$$\xi_{k+1} = \begin{bmatrix} \mathcal{P}_\mu(\psi_k, x_k) \\ \mathcal{Q}_\mu(\psi_{k+1}, x_k) \end{bmatrix} = \begin{bmatrix} \mathcal{P}_\mu(\xi_k) \\ \mathcal{Q}_\mu(\mathcal{P}_\mu(\xi_k), x_k) \end{bmatrix} =: F_\mu(\xi_k). \tag{5.3}$$

Note that this is different from the chosen order in Chapter 4.2. However, the main objective of this chapter is to first reproduce the two-bus results in [4], then extend it to the case with the resistive loss and phase-shifting transformer, so we adopt the same update order as [4][4].

Finally, we define the following dimensionless constants that characterize the active

[3] See [37, Chapter 2.2] for a detailed discussion leading up the development of the nose curves.

[4] As we shall see in the next section, this update order is the obvious choice for the nominal system analysis, though the numerical experiments in Chapter 6.2 demonstrate some potentially problematic behaviors.

and reactive power loading margins

$$\tilde{\gamma}_P \coloneqq \frac{\bar{P}_1}{\tilde{b}V_1^\circ V_2^\circ}, \quad \tilde{\gamma}_Q \coloneqq \frac{Q_1}{\tilde{b}V_1^\circ V_2^\circ}, \tag{5.4}$$

which, through the constants $\tilde{b}$, V_1° and V_2°, also encode information on the resistive loss and the transformer parameters. We also define two constants that reflects the system R/X ratio below

$$\rho \coloneqq \frac{g}{\hat{b}} = \frac{g}{b - \frac{b_c}{2}}, \qquad \tilde{\rho} \coloneqq \frac{\tilde{g}}{\tilde{b}} = \frac{g\cos\theta_\mathrm{s} - b\sin\theta_\mathrm{s}}{b\cos\theta_\mathrm{s} + g\sin\theta_\mathrm{s}},$$

such that ρ encodes the shunt information and $\tilde{\rho}$ encodes the phase-shift information.

Assumption 5.1. The constants ρ and $\tilde{\rho}$ are nonnegative.

Satisfying $\rho \geq 0$ is easy since it only requires $g \geq 0$ and $b_c < 2b$, both of which are realistic. However, satisfying $\tilde{\rho} \geq 0$ is a little more delicate, since g is typically much smaller than b, so it does not take a large phase-shift θ_s for $\tilde{\rho}$ to be negative. Intuitively, this means that if g/b is small, then θ_s also needs to be small, and if g/b is large, then θ_s can be large. (Note that the value of $\tilde{\rho}$ is independent of the transformer tap ratio t.) When θ_s is small, $\tilde{\rho}$ is a quasi-linear function of θ_s, and $\tilde{\rho}$ is close to ρ. Lastly, as explained after the introduction of the constants $\tilde{g}, \tilde{b}$, if $\tilde{\rho} \geq 0$, then $\tilde{b} > 0$.

5.2 Nominal System Analysis

In this section, we show that the nominal system possesses two distinct solutions when a crucial assumption on the load bus power consumption is satisfied. Furthermore, we show that the FPPF algorithm is a contraction in a carefully constructed subset of $\mathbb{R}^2$, and it converges to the desired solution in this subset, which has a voltage magnitude near 1.0 p.u. and a small phase angle θ. Once again, while the results from this section are well-known and available in the literature, we reproduce them here to provide the theoretical and notational foundations for the analysis in Section 5.3.

As discussed in the construction of the constants and network parameters in the previous section, when $\mu = \mathbb{0}$, we have that $\hat{b} = \tilde{b} = b > 0$, $\tilde{g} = g = 0$, and $V_1^\circ = V_2^\circ$. In this case, denote the reduced constants $\tilde{\gamma}_P, \tilde{\gamma}_Q$ by γ_P, γ_Q, respectively, and the

FPPF update rule (5.3) reduces to

$$\xi_{k+1} = \begin{bmatrix} \psi_{k+1} \\ x_{k+1} \end{bmatrix} = \begin{bmatrix} -\dfrac{\gamma_P}{x_k + 1} \\ \dfrac{\gamma_Q}{x_k + 1} + \sqrt{1 - \psi_{k+1}^2} - 1 \end{bmatrix} =: F_{\mathbb{0}}(\xi_k). \tag{5.5}$$

When the load draws strictly less than the maximum deliverable power, it is a standard textbook result that (5.5) has two distinct solutions: a "high-voltage" solution and a "low-voltage" solution, with the former being the desired solution [37, Chapter 2]. Our goal is to characterize their locations in the ψ, x plane using a fixed-point theoretic approach for the mapping $F_{\mathbb{0}}$.

As mentioned in the fixed-point theorem discussions in Chapter 2.1, our strategy is to first construct a closed $F_{\mathbb{0}}$ invariant set, then give conditions under which $F_{\mathbb{0}}$ is a contraction in this set. Consequently, we are guaranteed to find the desired high-voltage solution and certify its uniqueness.

5.2.1 Construction of the Invariant Set

We first characterize the invariant set that includes the fixed points, i.e., solutions to the power flow equations. Define the compact and convex set

$$\mathcal{A}(k_1, k_2) \coloneqq \{\xi : |\psi| \leq k_1, |x| \leq k_2\}, \tag{5.6}$$

which is a closed box in $\mathbb{R}^2$ centered at the origin, parameterized by some unknown $k_1, k_2 > 0$ to be determined[5]. The $F_{\mathbb{0}}$-invariance of $\mathcal{A}(k_1, k_2)$ can be established by showing that any $\xi_k \in \mathcal{A}(k_1, k_2)$ implies $\xi_{k+1} \in \mathcal{A}(k_1, k_2)$ for all $k \in \mathbb{Z}_{\geq 0}$. Note that, since we require $|\psi| \leq 1$ in order to recover θ with the arcsine function, we require $k_1 \leq 1$; since the denominator of ψ_{k+1} is $x_k + 1$, we require $k_2 < 1$ to prevent division by zero in (5.5).

Assumption 5.2 (Section III-C, [4])**.** The constants γ_P, γ_Q satisfy $0 < 4\gamma_P^2 - 4\gamma_Q < 1$; equivalently, $0 < \frac{1}{4} + \gamma_Q - \gamma_P^2 < \frac{1}{4}$.

Assumption 5.2 characterizes the permissible loading margins, states that the load is inductive, and implies that $\gamma_P, \gamma_Q \leq 0$ and cannot be both zero[6]. Figure 5.2 shows the permissible region of γ_P, γ_Q levels, where the circles indicate the infeasible extrema. This assumption is crucial for our subsequent analyses.

[5] Since $\mu = \mathbb{0}$ implies that there is no transformer in the system, for the load to draw power, it must be true that $v \in (0, 1)$, i.e., $x \in [-k_2, 0)$. However, for the sake of symmetry of $\mathcal{A}(k_1, k_2)$ and the subsequent analysis of the full lossy system when $\mu \neq \mathbb{0}$, we let $x \in [-k_2, k_2]$.

[6] When $\gamma_P = \gamma_Q = 0$, it is precisely the open-circuit case which is perfectly valid. However, here we are interested in the case where there is a strictly positive active power injection at the generator bus.

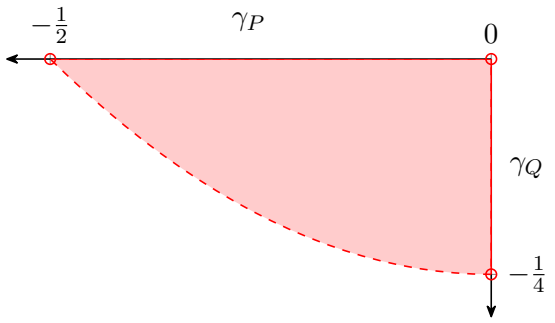

Figure 5.2: The permissible region of γ_P, γ_Q values

We now derive the condition for $\mathcal{A}(k_1, k_2)$ to be an $F_{\mathbb{0}}$-invariant set. From (5.5), $\mathcal{A}(k_1, k_2)$ is $F_{\mathbb{0}}$-invariant if and only if for all $\xi_k \in \mathcal{A}(k_1, k_2)$,

$$\left| -\frac{\gamma_P}{x_k + 1} \right| \leq k_1, \tag{5.7a}$$

$$\left| \frac{\gamma_Q}{x_k + 1} + \sqrt{1 - \psi_{k+1}^2} - 1 \right| \leq k_2. \tag{5.7b}$$

For (5.7a), first note that since $-\gamma_P \geq 0$ and $x_k + 1 > 0$ for all $x_k \in [-k_2, k_2]$ by construction, $-\gamma_P/(x_k + 1) \geq 0$. (Similarly, we can conclude that $\gamma_Q/(x_k + 1) \geq 0$ for all $x_k \in [-k_2, k_2]$.) Thus, we only need to consider the upper bound on the inequality, which is

$$\frac{-\gamma_P}{x_k + 1} \leq k_1.$$

The "worst case" for the inequality above is attained when the denominator is minimized. Since $x_k \in [-k_2, k_2]$ and $k_2 < 1$, if we want to guarantee (5.7a) holds, then we must require

$$\frac{-\gamma_P}{-k_2 + 1} \leq k_1 \implies k_1(1 - k_2) \geq -\gamma_P, \tag{5.8}$$

which implies that k_1 increases or decreases as the choice of fixed k_2 increases or decreases. Solving for the boundary condition with equality, the smallest possible k_1 required is

$$k_1^{\min} := \frac{-\gamma_P}{1 - k_2}, \tag{5.9}$$

when k_2 is fixed. Note that, since the maximum possible value for k_1 is 1, the choice of k_2 must satisfy $k_2 \leq 1 + \gamma_P$. Consequently, characterizing k_1, k_2 such that $\mathcal{A}(k_1, k_2)$ is $F_{\mathbb{0}}$-invariant depends on k_2. Thus, in the ensuing analysis, we first derive the desired interval where k_2 exists, then define the interval where k_1 exists with a fixed k_2, and finally we obtain the $F_{\mathbb{0}}$-invariant set $\mathcal{A}(k_1, k_2)$.

Derivation of k_2

For (5.7b), first note that since all $\psi \in [-1, 1]$, $\sqrt{1-\psi_{k+1}^2} - 1$ must be nonpositive. Then, since $\gamma_Q/(x_k+1)$ is nonpositive as well for all $x \in [-k_2, k_2]$, the upper bound on the inequality constraint in (5.7b) is always satisfied, so we only need to find a k_2 that satisfies the lower bound of (5.7b), which is

$$\frac{\gamma_Q}{x_k+1} + \sqrt{1-\left(\frac{\gamma_P}{x_k+1}\right)^2} - 1 \geq -k_2.$$

Similar to before, the worst case that the inequality above must satisfy is attained when $x_k = -k_2$. Thus, we require

$$\frac{\gamma_Q}{1-k_2} + \sqrt{1-\left(\frac{\gamma_P}{1-k_2}\right)^2} - 1 \geq -k_2$$

which holds if and only if

$$(1-k_2)^4 - (2\gamma_Q+1)(1-k_2)^2 + \gamma_Q^2 + \gamma_P^2 \leq 0. \tag{5.10}$$

Note that (5.10) is a quadratic inequality in $(1-k_2)^2$. At the boundaries of (5.10),

$$(1-k_2)_\pm^2 = \frac{1}{2} + \gamma_Q \pm \sqrt{\frac{1}{4} + \gamma_Q - \gamma_P^2}.$$

The roots $(1-k_2)_\pm^2$ are real and takes two distinct values if and only if Assumption 5.2 holds. Furthermore, $(1-k_2)_\pm^2$ are real if and only if k_2 is real, since the square root of $(1-k_2)_\pm^2$ is real if and only if $\gamma_P^2 + \gamma_Q^2 \geq 0$, which is trivially true. Thus, since $k_2 < 1$, the boundaries of (5.10) correspond to the following roots

$$k_2^- \coloneqq 1 - \sqrt{\frac{1}{2} + \gamma_Q + \sqrt{\frac{1}{4} + \gamma_Q - \gamma_P^2}}, \tag{5.11a}$$

$$k_2^+ \coloneqq 1 - \sqrt{\frac{1}{2} + \gamma_Q - \sqrt{\frac{1}{4} + \gamma_Q - \gamma_P^2}}, \tag{5.11b}$$

where $0 < k_2^- < k_2^+ < 1$, and any $k_2 \in [k_2^-, k_2^+]$ satisfies (5.10), which in turn creates a bound such that every $x_k \in [-k_2, k_2]$ satisfies the second invariance condition (5.7b).

Recall from (5.9) that the choice of k_2 must also satisfy $k_2 \leq 1 + \gamma_P$ for there to be a k_1 such that any $\psi_k \in [-k_1, k_1]$ satisfies the first invariance condition (5.7a). Thus, we must choose k_2 such that $k_2^- \leq k_2 \leq \min\{k_2^+, 1+\gamma_P\}$. To simplify the upper bound, we show that $k_2^+ = \min\{k_2^+, 1+\gamma_P\}$ by assuming towards contradiction that

$1 + \gamma_P \le k_2^+$. We then have

$$1 + \gamma_P \le 1 - \sqrt{\frac{1}{2} + \gamma_Q + \sqrt{\frac{1}{4} + \gamma_Q - \gamma_P^2}} \iff \sqrt{\frac{1}{4} + \gamma_Q - \gamma_P^2} \le \gamma_P^2 - \gamma_Q - \frac{1}{2}.$$

If Assumption 5.2 holds, then $\gamma_P^2 - \gamma_Q < 1/4$, so the statement $1 + \gamma_P \le k_2^+$ implies that $\sqrt{1/4 + \gamma_Q - \gamma_P^2} < 0$, which is a contradiction. Thus, $k_2^+ = \min\{k_2^+, 1 + \gamma_P\}$.

Derivation of k_1

Next, from (5.9), we can compute $k_1^{\min}$, the corresponding smallest possible k_1 that satisfies (5.8). Then, any $\psi_k \in [-k_1, k_1]$ such that $k_1 \in [k_1^{\min}, 1]$ will satisfy the first $F_{\mathbb{0}}$-invariance condition (5.7a). In particular, since $k_1^{\min}$ decreases as k_2 decreases, we denote the smallest $k_1^{\min}$ as

$$k_1^- := -\frac{\gamma_P}{1 - k_2^-} = \frac{-\gamma_P}{\sqrt{\frac{1}{2} + \gamma_Q + \sqrt{\frac{1}{4} + \gamma_Q - \gamma_P^2}}}, \tag{5.12}$$

The invariant set $\mathcal{A}(k_1, k_2)$

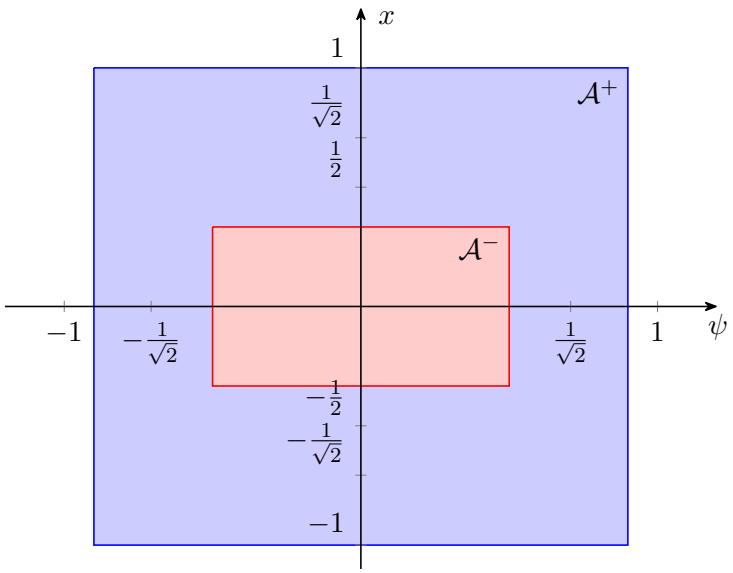

Figure 5.3: Example of the sets $\mathcal{A}^+$ and $\mathcal{A}^-$; any closed ℓ_∞ norm ball in between $\mathcal{A}^+$ and $\mathcal{A}^-$ is also an $F_{\mathbb{0}}$-invariant set

In summary, we have found the intervals where k_1, k_2 respectively exists, such that $\mathcal{A}(k_1, k_2)$ is $F_{\mathbb{0}}$-invariant. In particular, Figure 5.3 shows an example of the largest

and the smallest $F_{\mathbb{0}}$-invariant sets, which are

$$\mathcal{A}^+ \coloneqq \{\xi : |\psi| \leq 1, |x| \leq k_2^+\},$$
$$\mathcal{A}^- \coloneqq \{\xi : |\psi| \leq k_1^-, |x| \leq k_2^-\},$$

respectively. We are in particular interested in the smallest $F_{\mathbb{0}}$-invariant set $\mathcal{A}^-$ since it contains the desired high-voltage solution. We state the result thus far on the $F_{\mathbb{0}}$-invariant set in Theorem 5.1 and Corollary 5.1; the latter of which is a special case of [4, Theorem 5.1].

Theorem 5.1. *The set $\mathcal{A}(k_1, k_2)$ is $F_{\mathbb{0}}$-invariant for any $k_2 \in [k_2^-, k_2^+]$ and $k_1 \in [k_1^-, 1]$, with k_2^-, k_2^+ defined in* (5.11a)*, and k_1^- defined in* (5.12) *given the choice of k_2, if and only if Assumption 5.2 holds.*

Corollary 5.1. *If Assumption 5.2 holds, then the lossless power flow equation* (5.5) *is solvable, and the high-voltage solution is $\bar{\xi}^+ \coloneqq [k_1^- \ -k_2^-]^\mathsf{T} \in \mathcal{A}^-$.*

Proof. Since $\mathcal{A}(k_1, k_2)$ is a compact convex set and $F_{\mathbb{0}}$ is C^1 and thus continuous on $\mathcal{A}(k_1, k_2)$, there must be at least one fixed point $\bar{\xi} \in \mathcal{A}(k_1, k_2)$ by Brouwer's fixed point theorem. We can verify that $\bar{\xi}^+$ is a fixed point of (5.5) by direct substitution. Recall that $v = 1 + x$ by construction, so $\bar{x} = -k_2^-$ implies that $\bar{v}$ is close to 1, and $\bar{\xi}^+$ is thus the desired high-voltage solution. □

We now characterize the intervals where the bounds k_1^-, k_2^- and k_2^+ live in. Since the loading margins γ_P, γ_Q determine the range of k_2^- and k_2^+, we characterize them as follows. Maximizing k_2^- is equivalent to minimizing $1/2 + \gamma_Q + \sqrt{1/4 + \gamma_Q - \gamma_P^2}$, whose infimum is attained when $-\gamma_Q + \gamma_P^2 = 1/4$ and $\gamma_Q = -1/4$. Thus, Assumption 5.2 implies that $k_2^- \in (0, 1/2)$. Similarly, minimizing k_2^- is equivalent to maximizing $1/2 + \gamma_Q - \sqrt{1/4 + \gamma_Q - \gamma_P^2}$, whose supremum is attained when $-\gamma_Q + \gamma_P^2 = 1/4$ and $\gamma_Q = 0$. Thus, $k_2^+ \in (1/\sqrt{2}, 1)$. We can also show by direct computation that $k_1^- \in (0, 1/\sqrt{2})$ based on (5.12). These points are shown on Figure 5.3 as well.

Consequently, when recovering the normalized voltage solution $\bar{v}$ from $\bar{x}$, the low voltage solution denoted by $\bar{v}^-$ takes values in the interval $(0, 1-1/\sqrt{2})$, and the high-voltage solution denoted by $\bar{v}^+$ takes values in the interval $(1/2, 1)$, which implies that $\bar{v}^- < \bar{v}^+$, and we have the two distinct solutions as claimed at the beginning of this section.

5.2.2 Condition for Contractivity

Having shown the existence of the desired high-voltage solution, we now seek to derive a sufficient condition for $F_{\mathbb{0}}$ to be a contraction in the smallest $F_{\mathbb{0}}$-invariant set $\mathcal{A}^-$, which establishes the uniqueness of the high-voltage solution in Corollary 5.1.

Theorem 5.2. *If Assumption 5.2 holds, then $F_{\mathbb{0}}$ is a contraction on $\mathcal{A}^-$ in the ℓ_∞ norm.*

Proof. First, we compute Jacobian of $F_{\mathbb{0}}$ evaluated at any $\xi_k \in \mathcal{A}^-$ as

$$J(\xi_k) = \begin{bmatrix} \frac{\partial \mathcal{P}_{\mathbb{0}}}{\partial \psi_k} & \frac{\partial \mathcal{P}_{\mathbb{0}}}{\partial x_k} \\ \frac{\partial \mathcal{Q}_{\mathbb{0}}}{\partial \psi_k} & \frac{\partial \mathcal{Q}_{\mathbb{0}}}{\partial x_k} \end{bmatrix} = \begin{bmatrix} 0 & \frac{\gamma_P}{(x_k+1)^2} \\ 0 & -\frac{\gamma_Q}{(x_k+1)^2} + \frac{\gamma_P^2}{(x_k+1)^2\sqrt{(x_k+1)^2-\gamma_P^2}} \end{bmatrix}. \quad (5.13)$$

It is easy to show that the partial derivative terms in (5.13) are continuous for all $x_k \in [-k_2^-, k_2^-]$, since each of them are the results of elementary operations of standard continuous functions in x_k. Thus, if there exists a constant $d < 1$ such that $\|J(\xi_k)\|_\infty \leq d$ for all $\xi_k \in \mathcal{A}^-$, then $F_{\mathbb{0}}$ is a contraction in $\mathcal{A}^-$. For any $\xi_k \in \mathcal{A}^-$, recall that the ℓ_∞ matrix norm of $J(\xi_k)$ can be computed as

$$\|J(\xi_k)\|_\infty = \max\left\{ \frac{-\gamma_P}{(x_k+1)^2},\ -\frac{\gamma_Q}{(x_k+1)^2} + \frac{\gamma_P^2}{(x_k+1)^2\sqrt{(x_k+1)^2-\gamma_P^2}} \right\}. \quad (5.14)$$

Fix any γ_P, γ_Q such that Assumption 5.2 is satisfied, then each of the two elements of (5.14) are maximized when the denominator $(x_k+1)^2$ is minimized, i.e., $x_k = -k_2^-$. Then, $F_{\mathbb{0}}$ is a contraction on $\mathcal{A}^-$ if there exist some $d_1, d_2 < 1$ such that the following inequalities hold:

$$\frac{-\gamma_P}{(1-k_2^-)^2} \leq d_1, \quad (5.15a)$$

$$-\frac{\gamma_Q}{(1-k_2^-)^2} + \frac{\gamma_P^2}{(1-k_2^-)^2\sqrt{(1-k_2^-)^2-\gamma_P^2}} \leq d_2. \quad (5.15b)$$

Substituting the definition of k_2^- in (5.11a) into (5.15a), then the left-hand side of (5.15a) becomes

$$\frac{-\gamma_P}{\frac{1}{2}+\gamma_Q+\sqrt{\frac{1}{4}+\gamma_Q-\gamma_P^2}} < \frac{-\gamma_P}{\frac{1}{2}+\gamma_Q} < 1,$$

which is true if and only if Assumption 5.2 holds, since it states that $\sqrt{1/4+\gamma_Q-\gamma_P^2}$ is real and positive, and implies that $-\gamma_P \in (0, 1/2)$ and $\gamma_Q \in (-1/4, 0)$. For (5.15b),

its left-hand side becomes

$$\frac{-\gamma_Q}{\frac{1}{2}+\gamma_Q+\sqrt{\frac{1}{4}+\gamma_Q-\gamma_P^2}} + \frac{\gamma_P^2}{\left(\frac{1}{2}+\gamma_Q+\sqrt{\frac{1}{4}+\gamma_Q-\gamma_P^2}\right)\sqrt{\frac{1}{2}+\gamma_Q+\sqrt{\frac{1}{4}+\gamma_Q-\gamma_P^2}-\gamma_P^2}},$$

Similar as before, an upper bound on the expression above is

$$\frac{-\gamma_Q}{\frac{1}{2}+\gamma_Q}+\frac{\gamma_P^2}{\left(\frac{1}{2}+\gamma_Q\right)\sqrt{\frac{1}{2}+\gamma_Q-\gamma_P^2}} < \frac{-\gamma_Q+2\gamma_P^2}{\frac{1}{2}+\gamma_Q} < \frac{\frac{1}{4}+\gamma_P^2}{\frac{1}{2}+\gamma_Q} < 1,$$

which, again, holds if and only if Assumption 5.2 holds. Therefore, from the sequence of strict inequalities above, there exist constants $d_1, d_2 < 1$ such that $\|J(\xi_k)\|_\infty \leq \max\{d_1, d_2\} < 1$, and we can conclude that $F_{\mathbb{0}}$ is a contraction on $\mathcal{A}^-$. □

In summary, we have constructed an $F_{\mathbb{0}}$-invariant set of interest, $\mathcal{A}^-$, and we have shown the desired high-voltage solution is unique and exists on the boundary of $\mathcal{A}^-$. We have also shown that the FPPF algorithm is a contraction on the $\mathcal{A}^-$ set if the critical loading margin assumption 5.2 holds. Note that these are known results that we have simply stated in the language of invariant sets and contraction mappings. In the next section, we extend them to investigate the location of the high-voltage solution in the ψ-x space by including the resistive loss, the branch Π-model and transformer parameters in the problem.

5.3 Full System Analysis

Now, we shift our focus back to the FPPF algorithm on a full, lossy two-bus system, and similarly show that we can construct an invariant set based on $\mathcal{A}^-$, and give a sufficient condition for contractivity.

Consider the update rule for the full FPPF algorithm (5.3), written using the constants defined in Section 5.1 as

$$\xi_{k+1} = F_\mu(\xi_k) = \begin{bmatrix} \dfrac{-\tilde{\gamma}_P}{x_k+1}+\rho\,(x_k+1)-\tilde{\rho}\sqrt{1-\psi_k^2} \\ \dfrac{\tilde{\gamma}_Q}{x_k+1}-\tilde{\rho}\psi_{k+1}+\sqrt{1-\psi_{k+1}^2}-1 \end{bmatrix} = \begin{bmatrix} \psi_{k+1} \\ x_{k+1} \end{bmatrix}. \tag{5.16}$$

We proceed by assuming that Assumptions 5.1–5.2 hold, which imply that the loading

margins $\tilde{\gamma}_P, \tilde{\gamma}_Q$ defined in (5.4) are nonpositive and are not both zero. Recall that

$$\tilde{\gamma}_P = \frac{\bar{P}_1}{\tilde{b}V_1^\circ V_2^\circ} = \frac{b}{b}\left(\frac{\bar{P}_1}{\tilde{b}\frac{1}{\beta}\left(V_2^\circ\right)^2}\right) = \frac{b\beta}{\tilde{b}}\frac{\bar{P}_1}{b\left(V_2^\circ\right)^2} = \frac{b\beta}{\tilde{b}}\gamma_P =: k_\mu \gamma_P,$$

where $k_\mu \geq 0$ is also implied by Assumption 5.1. We can similarly show that $\tilde{\gamma}_Q = k_\mu \gamma_Q$. Observe that k_μ does not depend on the conductance g, and approaches 1 as the remaining elements of μ approach 0.

5.3.1 Construction of the Invariant Set

Similar to the steps we took in Section 5.2, we first construct a closed F_μ-invariant set, in which the high-voltage solution exists. Let $\epsilon_1 = \epsilon_1(\mu, \gamma_P, \gamma_Q)$ and $\epsilon_2 = \epsilon_2(\mu, \gamma_P, \gamma_Q)$. Denote the set $\mathcal{A}_\epsilon(k_1, k_2) \coloneqq \mathcal{A}(k_1 + \epsilon_1, k_2 + \epsilon_2)$, then we can define $\mathcal{A}_\epsilon^- \coloneqq \mathcal{A}_\epsilon(k_1^- + \epsilon_1, k_2^- + \epsilon_2)$. Intuitively, this set is "slightly expanded" from $\mathcal{A}^-$ (on which $F_{\mathbb{0}}$ is a contraction, as shown in the previous section) when the μ parameters are nonzero. We now derive the conditions on ϵ_1, ϵ_2 such that $\mathcal{A}_\epsilon^-$ is F_μ-invariant.

The set $\mathcal{A}_\epsilon^-$ is F_μ-invariant if and only if for every $\xi_k \in \mathcal{A}_\epsilon^-$,

$$|\psi_{k+1}| = \left|\frac{-k_\mu\gamma_P}{x_k+1} + \rho\left(x_k+1\right) - \tilde{\rho}\sqrt{1-\psi_k^2}\right| \leq k_1^- + \epsilon_1, \tag{5.17a}$$

$$|x_{k+1}| = \left|\frac{k_\mu\gamma_Q}{x_k+1} - \tilde{\rho}\psi_{k+1} + \sqrt{1-\psi_{k+1}^2} - 1\right| \leq k_2^- + \epsilon_2. \tag{5.17b}$$

Unlike in the $F_{\mathbb{0}}$ case in Section 5.2, neither terms inside the absolute value in (5.17a)–(5.17b) are sign-definite without further restrictions on μ and loading margins γ_P, γ_Q. Thus, we need to keep the absolute value and bound both the upper and lower bounds simultaneously.

We start with the inequality (5.17a), and recall from Section 5.2 that $k_1^- \coloneqq -\gamma_P/(1-k_2^-)$. Since $|\psi_k| \leq k_1^- + \epsilon_1$ and $|x_k| \leq k_2^- + \epsilon_2$,

$$\begin{aligned}
|\psi_{k+1}| &= \left|\frac{-k_\mu\gamma_P}{x_k+1} + \rho\left(x_k+1\right) - \tilde{\rho}\sqrt{1-\psi_k^2}\right| \\
&\leq \frac{-k_\mu\gamma_P}{x_k+1} + \rho\left(x_k+1\right) + \tilde{\rho}\sqrt{1-\psi_k^2} \\
&\leq \frac{-k_\mu\gamma_P}{1-k_2^- - \epsilon_2} + \rho\left(1+k_2^-+\epsilon_2\right) + \tilde{\rho} \\
&= k_1^- + \frac{-k_\mu\gamma_P}{1-k_2^- - \epsilon_2} + \frac{\gamma_P}{1-k_2^-} + \rho\left(1+k_2^-+\epsilon_2\right) + \tilde{\rho}
\end{aligned}$$

That is, if ϵ_1, ϵ_2 satisfies

$$\frac{-k_\mu \gamma_P}{1 - k_2^- - \epsilon_2} + \frac{\gamma_P}{1 - k_2^-} + \rho\left(1 + k_2^- + \epsilon_2\right) + \tilde{\rho} \leq \epsilon_1 \tag{5.18a}$$

then any $|\psi_k| \leq k_1^- + \epsilon_1$ implies $|\psi_{k+1}| \leq k_1^- + \epsilon_1$. Note that we also need $\epsilon_2 < 1 - k_2^-$ to prevent division by zero in (5.18a).

Next, the left-hand side of the inequality (5.17b) can be upper bounded as

$$\begin{aligned}
|x_{k+1}| &= \left| \frac{k_\mu \gamma_Q}{x_k + 1} - \tilde{\rho}\psi_{k+1} + \sqrt{1 - \psi_{k+1}^2} - 1 \right| \\
&\leq \frac{-k_\mu \gamma_Q}{x_k + 1} + \left| \sqrt{1 - \psi_{k+1}^2} - 1 - \tilde{\rho}\psi_{k+1} \right| \\
&\leq \frac{-k_\mu \gamma_Q}{1 - k_2^- - \epsilon_2} + \left| \sqrt{1 - \left(k_1^- + \epsilon_1\right)^2} - 1 - \tilde{\rho}\left(k_1^- + \epsilon_1\right) \right| \\
&\leq \frac{-k_\mu \gamma_Q}{1 - k_2^- - \epsilon_2} + 1 - \sqrt{1 - \left(k_1^- + \epsilon_1\right)^2} + \tilde{\rho}\left(k_1^- + \epsilon_1\right) \\
&= k_2^- + \frac{-k_\mu \gamma_Q}{1 - k_2^- - \epsilon_2} + \left(1 - k_2^-\right) + \tilde{\rho}\left(k_1^- + \epsilon_1\right) - \sqrt{1 - \left(k_1^- + \epsilon_1\right)^2},
\end{aligned}$$

so if ϵ_1, ϵ_2 satisfies

$$\frac{-k_\mu \gamma_Q}{1 - k_2^- - \epsilon_2} + \left(1 - k_2^-\right) + \tilde{\rho}\left(k_1^- + \epsilon_1\right) - \sqrt{1 - \left(k_1^- + \epsilon_1\right)^2} \leq \epsilon_2, \tag{5.18b}$$

then any $|x_k| \leq k_2^- + \epsilon_2$ implies $|x_{k+1}| \leq k_2^- + \epsilon_2$. To keep the square root term above real-valued, we also require $\epsilon_1 \in [-1 - k_1^-, 1 - k_1^-]$, although since $\epsilon_1 \geq 0$ by construction, we simply require that $\epsilon_1 \leq 1 - k_1^-$.

Note that since we made several bounding steps in the inequalities above, the bounds (5.18) may be quite conservative, with (5.18a) especially so due to the first inequality step, which is made with triangle inequality. This conservatism can be improved with additional mild assumptions on the magnitudes of ρ and $\tilde{\rho}$, but we do not pursue that path here.

To summarize the steps thus far, if there exist nonnegative $\epsilon \coloneqq (\epsilon_1, \epsilon_2)$ such that it satisfies (5.18), then $\mathcal{A}_\epsilon^-$ is an F_μ-invariant set and it contains at least one solution to the power flow problem. However, in the current form of the problem, we must solve a feasibility problem using the inequalities (5.18) to find a desired ϵ. Wile numerically there exists a wide range of feasible ϵ (especially with a sufficiently small μ), the feasibility problem is difficult to analytically assess. Since any ϵ that satisfies (5.18)

at the boundary, i.e., the system of nonlinear equations

$$\frac{-k_\mu \gamma_P}{1-k_2^- - \epsilon_2} + \frac{\gamma_P}{1-k_2^-} + \rho\left(1 + k_2^- + \epsilon_2\right) + \tilde{\rho} = \epsilon_1 \tag{5.19a}$$

$$\frac{-k_\mu \gamma_Q}{1-k_2^- - \epsilon_2} + \left(1 - k_2^-\right) + \tilde{\rho}\left(k_1^- + \epsilon_1\right) - \sqrt{1 - \left(k_1^- + \epsilon_1\right)^2} = \epsilon_2 \tag{5.19b}$$

trivially satisfy the inequalities (5.18) themselves, we may proceed by focusing on solving the boundary equations (5.19).

Before going back to the question of when the set $\mathcal{A}_\epsilon^-$ is F_μ-invariant, we make one more note to show that $\mathcal{A}_\epsilon^-$ is a well-defined extension of the $\mathcal{A}^-$ set for the nominal system.

Proposition 5.1. When $\mu = \mathbb{0}$, $\epsilon = \mathbb{0}$ solves (5.19) and thus (5.18), which implies that the set $\mathcal{A}_\epsilon^-$ reduces to $\mathcal{A}^-$ as the mapping F_μ reduces to $F_{\mathbb{0}}$.

Proof. Let $\mu = \mathbb{0}$, then (5.19) can be simplified and rearranged as

$$\frac{-\gamma_P}{1-k_2^- - \epsilon_2} + \frac{\gamma_P}{1-k_2^-} - \epsilon_1 = 0, \tag{5.20a}$$

$$\frac{-\gamma_Q}{1-k_2^- - \epsilon_2} + \left(1 - k_2^-\right) - \sqrt{1 - \left(k_1^- + \epsilon_1\right)^2} - \epsilon_2 = 0. \tag{5.20b}$$

It is trivial to verify that $\epsilon = \mathbb{0}$ is a solution to (5.20a) by direct substitution, which results in

$$\frac{-\gamma_P}{1-k_2^-} + \frac{\gamma_P}{1-k_2^-} = 0.$$

However, verifying that it is also a solution to (5.20b) requires some work: substitute $\epsilon = \mathbb{0}$ and the explicit expression of k_1^- (5.12) into (5.20b), then its left-hand side becomes

$$\frac{-\gamma_Q}{1-k_2^-} + (1 - k_2^-) - \sqrt{1 - \frac{\gamma_P^2}{\left(1-k_2^-\right)^2}}. \tag{5.21a}$$

By construction,

$$\frac{-\gamma_Q}{1-k_2^-} + (1 - k_2^-) + \sqrt{1 - \frac{\gamma_P^2}{\left(1-k_2^-\right)^2}} \tag{5.21b}$$

is strictly positive (note the plus sign before the square root term above rather than the minus sign in (5.21a)). That is, (5.21a) equals zero if and only if the expression below equals zero:

$$\left(\frac{-\gamma_Q}{1-k_2^-} + (1 - k_2^-) - \sqrt{1 - \frac{\gamma_P^2}{\left(1-k_2^-\right)^2}}\right)\left(\frac{-\gamma_Q}{1-k_2^-} + (1 - k_2^-) + \sqrt{1 - \frac{\gamma_P^2}{\left(1-k_2^-\right)^2}}\right).$$

The expression above simplifies to

$$\begin{aligned}
&\frac{\gamma_Q^2}{\left(1-k_2^-\right)^2}+\left(1-k_2^-\right)^2-2\gamma_Q-\left(1-\frac{\gamma_P^2}{\left(1-k_2^-\right)^2}\right)\\
&=\frac{\gamma_Q^2+\gamma_P^2}{\gamma_Q+\frac{1}{2}+\sqrt{\frac{1}{4}+\gamma_Q-\gamma_P^2}}+\gamma_Q+\frac{1}{2}+\sqrt{\frac{1}{4}+\gamma_Q-\gamma_P^2}-2\gamma_Q-1\\
&=\frac{\gamma_Q^2+\gamma_P^2}{\sqrt{\frac{1}{4}+\gamma_Q-\gamma_P^2}+\gamma_Q+\frac{1}{2}}+\sqrt{\frac{1}{4}+\gamma_Q-\gamma_P^2}-\left(\gamma_Q+\frac{1}{2}\right)\\
&=\frac{\gamma_Q^2+\gamma_P^2+\frac{1}{4}+\gamma_Q-\gamma_P^2-\left(\gamma_Q+\frac{1}{2}\right)^2}{\sqrt{\frac{1}{4}+\gamma_Q-\gamma_P^2}+\gamma_Q+\frac{1}{2}}=0.
\end{aligned}$$

Thus, $\epsilon=\mathbb{0}$ also solves (5.20b), and $\mathcal{A}_\epsilon^-$ reduces to $\mathcal{A}^-$ when $\mu=\mathbb{0}$. □

Similar to the way we rearranged the equations in the proof above, we rewrite the general boundary condition (5.19) into a root-finding form with $E:\mathcal{D}_\epsilon\times\mathbb{R}^4\to\mathbb{R}^2$ defined as

$$E(\epsilon,\mu)=\begin{bmatrix}\dfrac{-k_\mu\gamma_P}{1-k_2^--\epsilon_2}+\dfrac{\gamma_P}{1-k_2^-}+\rho\left(1+k_2^-+\epsilon_2\right)+\tilde{\rho}-\epsilon_1\\ \dfrac{-k_\mu\gamma_Q}{1-k_2^--\epsilon_2}+\left(1-k_2^-\right)+\tilde{\rho}\left(k_1^-+\epsilon_1\right)-\sqrt{1-\left(k_1^-+\epsilon_1\right)^2}-\epsilon_2\end{bmatrix}=\mathbb{0},$$

where $\mathcal{D}_\epsilon\subset[0,1-k_1^-)\times[0,1-k_2^-)\subset\mathbb{R}^2$ is an open set. The domain of E is open, since both $\mathcal{D}_\epsilon$ and $\mathbb{R}^4$ are open and the Cartesian product of two open sets is open[7].

Note that Proposition 5.1 implies that $E(\mathbb{0},\mathbb{0})=\mathbb{0}$. The existence of ϵ that solves (5.19) is thus equivalent to the existence of a general (local) solution to $E(\epsilon,\mu)=\mathbb{0}$.

Proposition 5.2. Given a sufficiently small μ, there exists $\mathcal{U}$, a nonempty open subset of $\mathcal{D}_\epsilon\times\mathbb{R}^4$ such that $(\mathbb{0}_2,\mathbb{0}_4)\in\mathcal{U}$, and every $(\epsilon,\mu)\in\mathcal{U}$ satisfies $E(\epsilon,\mu)=\mathbb{0}$.

Proof. Clearly E is a C^1 function, so we can compute its Jacobian evaluated at some (ϵ,μ) in its domain as

$$\begin{aligned}
J_E(\epsilon,\mu)&=\left[\begin{array}{c|c}J_{E,\epsilon}(\epsilon,\mu) & J_{E,\mu}(\epsilon,\mu)\end{array}\right]\\
&=\left[\begin{array}{cc|cccc}\dfrac{\partial E_1}{\partial\epsilon_1}&\dfrac{\partial E_1}{\partial\epsilon_2}&\dfrac{\partial E_1}{\partial g}&\dfrac{\partial E_1}{\partial b_c}&\dfrac{\partial E_1}{\partial\bar{t}}&\dfrac{\partial E_1}{\partial\theta_{\mathrm{s}}}\\ \dfrac{\partial E_2}{\partial\epsilon_1}&\dfrac{\partial E_2}{\partial\epsilon_2}&\dfrac{\partial E_2}{\partial g}&\dfrac{\partial E_2}{\partial b_c}&\dfrac{\partial E_2}{\partial\bar{t}}&\dfrac{\partial E_2}{\partial\theta_{\mathrm{s}}}\end{array}\right].
\end{aligned}\tag{5.22}$$

[7]This fact can be easily shown based on the discussion in [41].

After evaluating the Jacobian at the point $(\epsilon, \mu) = (\mathbb{0}_2, \mathbb{0}_4)$, we get

$$J_{E,\epsilon}(\mathbb{0},\mathbb{0}) = \begin{bmatrix} -1 & \dfrac{-\gamma_P}{\left(1-k_2^-\right)^2} \\ \dfrac{k_1^-}{\sqrt{1-\left(k_1^-\right)^2}} & \dfrac{-\gamma_Q}{\left(1-k_2^-\right)^2} - 1 \end{bmatrix},$$

$$J_{E,\mu}(\mathbb{0},\mathbb{0}) = \begin{bmatrix} \dfrac{2+k_2^-}{b} & \dfrac{\gamma_P}{2b\left(1-k_2^-\right)} & -\dfrac{\gamma_P}{1-k_2^-} & -1 \\ \dfrac{k_1^-}{b} & \dfrac{\gamma_Q}{2b\left(1-k_2^-\right)} & -\dfrac{\gamma_Q}{1-k_2^-} & -k_1^- \end{bmatrix}.$$

We can also compute

$$\begin{aligned} \det J_{E,\epsilon}(\mathbb{0},\mathbb{0}) &= \left(1 - \frac{-\gamma_Q}{\left(1-k_2^-\right)^2}\right) - \left(\frac{-\gamma_P}{\left(1-k_2^-\right)^2}\right)\left(\frac{k_1^-}{\sqrt{1-\left(k_1^-\right)^2}}\right) \\ &= \frac{\sqrt{1-\left(k_1^-\right)^2}\left(1-k_2^-\right)^2 + \gamma_Q\sqrt{1-\left(k_1^-\right)^2} + k_1^-\gamma_P}{\left(1-k_2^-\right)^2\sqrt{1-\left(k_1^-\right)^2}}. \end{aligned} \tag{5.23}$$

Recall from the previous section the intervals from which k_1^- and k_2^- can take values, we can conclude that the denominator of (5.23) is always nonzero by construction. Thus, $J_{E,\epsilon}(\mathbb{0},\mathbb{0})$ is invertible if and only if the numerator of (5.23) is also nonzero, or equivalently,

$$\left(\left(1-k_2^-\right)^2 + \gamma_Q\right)\sqrt{1-\left(k_1^-\right)^2} = -k_1^-\gamma_P. \tag{5.24}$$

Recall from the previous section that k_1^- and k_2^- only depend on the loading levels γ_P, γ_Q, so we have

$$\left(1-k_2^-\right)^2 = \gamma_Q + \frac{1}{2} + \sqrt{\frac{1}{4} + \gamma_Q - \gamma_P^2}, \tag{5.25a}$$

$$\sqrt{1-\left(k_1^-\right)^2} = \sqrt{1 - \frac{\gamma_P^2}{\left(1-k_2^-\right)^2}} = \sqrt{\frac{\frac{1}{2} + \gamma_Q - \gamma_P^2 - \sqrt{\frac{1}{4} + \gamma_Q - \gamma_P^2}}{\gamma_Q + \frac{1}{2} + \sqrt{\frac{1}{4} + \gamma_Q - \gamma_P^2}}}. \tag{5.25b}$$

Expanding and squaring both sides of (5.24) using the explicit expressions (5.25a)–

(5.25b) and re-arranging the equation, we get

$$\begin{aligned}
0 &= \left(2\gamma_Q + \frac{1}{2} + \sqrt{\frac{1}{4} + \gamma_Q - \gamma_P^2}\right)^2 \left(\frac{\frac{1}{2} + \gamma_Q - \gamma_P^2 - \sqrt{\frac{1}{4} + \gamma_Q - \gamma_P^2}}{\gamma_Q + \frac{1}{2} + \sqrt{\frac{1}{4} + \gamma_Q - \gamma_P^2}}\right) \\
&\quad - \frac{\gamma_P^4}{\gamma_Q + \frac{1}{2} + \sqrt{\frac{1}{4} + \gamma_Q - \gamma_P^2}} \\
0 &= \left(2\gamma_Q + \frac{1}{2} + \sqrt{\frac{1}{4} + \gamma_Q - \gamma_P^2}\right)^2 \left(\frac{1}{2} + \gamma_Q - \gamma_P^2 - \sqrt{\frac{1}{4} + \gamma_Q - \gamma_P^2}\right) - \gamma_P^4 \\
0 &= \frac{1}{2}\left(3 - 6\gamma_P^2 + 8\gamma_Q^2 + 6\gamma_Q\right)\left(\frac{1}{4} + \gamma_Q - \gamma_P^2\right) \\
&\quad + \left(3\gamma_Q^2 - 4\gamma_P^2\gamma_Q + \frac{3}{2}\gamma_Q + \frac{3}{16}\right)\sqrt{\frac{1}{4} + \gamma_Q - \gamma_P^2} \qquad (5.26)
\end{aligned}$$

if and only if $J_{E,\epsilon}(\mathbb{0}, \mathbb{0})$ is singular. Note that the first half of the right-hand side of (5.26) can be rewritten as

$$\left(3\left(\frac{1}{4} + \gamma_Q - \gamma_P^2\right) + \frac{3}{4} + 4\gamma_Q^2\right)\left(\frac{1}{4} + \gamma_Q - \gamma_P^2\right),$$

which is strictly positive. Recall that Assumption 5.2 also implies that $\gamma_P^2 < 1/4$ when $\gamma_Q \leq (-1/4, 0]$, so the second half of the right-hand side of (5.26) can be rewritten as

$$\left(5\gamma_Q\left(\frac{1}{4} + \gamma_Q - \gamma_P^2\right) + \gamma_Q\left(\frac{1}{4} - \gamma_P^2\right) + \frac{3}{16}\right)\sqrt{\frac{1}{4} + \gamma_Q - \gamma_P^2},$$

and it is also strictly positive. Thus, the right-hand side is always strictly positive and (5.26) is never true, so $J_{E,\epsilon}(\mathbb{0}, \mathbb{0})$ is always invertible. Then, by the implicit function theorem, there exists a nonempty open set $\mathcal{U} = \mathcal{U}_\epsilon \times \mathcal{U}_\mu$ that includes $(\epsilon, \mu) = (\mathbb{0}, \mathbb{0})$, on which there exists a unique C^1 function $g : \mathcal{U}_\mu \subset \mathbb{R}^4 \to \mathbb{R}^2$ such that $E(g(\mu), \mu) = \mathbb{0}_2$ for all $\mu \in \mathcal{U}_\mu$, and $g(\mathbb{0}_4) = \mathbb{0}_2$. □

Having shown the existence of the desired ϵ when μ is sufficiently small, we can easily construct it by solving $E(\epsilon, \mu) = \mathbb{0}$ with a root-finding algorithm such as Newton-Raphson; the details are omitted here. An immediate consequence of Proposition 5.2 is that any sufficiently small μ guarantees the existence of an ϵ such that $\mathcal{A}_\epsilon^-$ is an F_μ-invariant set. As a result, by Brouwer's fixed-point theorem, there exists at least one solution to the power flow problem in $\mathcal{A}_\epsilon^-$.

5.3.2 Condition for Contractivity

Similar to the steps taken in the previous section, we now check whether F_μ is a contraction on $\mathcal{A}_\epsilon^-$ given a fixed, sufficiently small μ; if so, then we can conclude that there exists a unique solution to the full, two-bus power flow problem, and that the FPPF algorithm always converges to this solution.

The Jacobian of F_μ evaluated at any $\xi_k \in \mathcal{A}_\epsilon^-$ is

$$J_\mu(\xi_k) = \begin{bmatrix} \dfrac{\partial \mathcal{P}_\mu}{\partial \psi_k} & \dfrac{\partial \mathcal{P}_\mu}{\partial x_k} \\ \dfrac{\partial \mathcal{Q}_\mu}{\partial \psi_k} & \dfrac{\partial \mathcal{Q}_\mu}{\partial x_k} \end{bmatrix} = J_{\mathbb{0}}(\xi_k) + \Delta J(\xi_k) = \begin{bmatrix} \dfrac{\partial \mathcal{P}_{\mathbb{0}}}{\partial \psi_k} & \dfrac{\partial \mathcal{P}_{\mathbb{0}}}{\partial x_k} \\ \dfrac{\partial \mathcal{Q}_{\mathbb{0}}}{\partial \psi_k} & \dfrac{\partial \mathcal{Q}_{\mathbb{0}}}{\partial x_k} \end{bmatrix} + \begin{bmatrix} \delta_{11} & \delta_{12} \\ \delta_{21} & \delta_{22} \end{bmatrix}.$$

Clearly, Proposition 5.1 implies that $\Delta J(\xi_k) = \mathbb{0}$ when $\mu = \mathbb{0}$, and we can write

$$\begin{aligned}
\delta_{11} &\coloneqq \frac{\partial \mathcal{P}_\mu}{\partial \psi_k} = \frac{\tilde{\rho}\psi_k}{\sqrt{1-\psi_k^2}} \\
\delta_{12} &\coloneqq \frac{\partial \mathcal{P}_\mu}{\partial x_k} - \frac{\partial \mathcal{P}_{\mathbb{0}}}{\partial x_k} = \frac{(k_\mu - 1)\gamma_P}{(x_k+1)^2} + \rho \\
\delta_{21} &\coloneqq \frac{\partial \mathcal{Q}_\mu}{\partial \psi_k} = -\frac{\tilde{\rho}\psi_k}{\sqrt{1-\psi_k^2}} \left(\tilde{\rho} + \frac{\rho(x_k+1)^2 - \tilde{\rho}\sqrt{1-\psi_k^2} - k_\mu \gamma_P}{\sqrt{1 - \left(\rho(x_k+1) - \tilde{\rho}\sqrt{1-\psi_k^2} - \frac{k_\mu \gamma_P}{x_k+1}\right)^2}} \right) \\
\delta_{22} &\coloneqq \frac{\partial \mathcal{Q}_\mu}{\partial x_k} - \frac{\partial \mathcal{Q}_{\mathbb{0}}}{\partial x_k} = -\frac{(k_\mu - 1)\gamma_Q}{(x_k+1)^2} - \tilde{\rho}\left(\rho + \frac{k_\mu \gamma_P}{(x_k+1)^2}\right) \\
&\quad + \frac{\left(\rho + \frac{k_\mu \gamma_P}{(x_k+1)^2}\right)\left(\rho(x_k+1) - \tilde{\rho}\sqrt{1-\psi_k^2} - \frac{k_\mu \gamma_P}{x_k+1}\right)}{\sqrt{1 - \left(\rho(x_k+1) - \tilde{\rho}\sqrt{1-\psi_k^2} - \frac{k_\mu \gamma_P}{x_k+1}\right)^2}} \\
&\quad - \frac{\gamma_P^2}{(x_k+1)^2\sqrt{(x_k+1)^2 - \gamma_P^2}}.
\end{aligned}$$

While these terms look overwhelming, we can easily verify by inspection that for realistic values of μ, they are all well-defined and real-valued. Furthermore, the δ_{ij} entries are the results of elementary operations—such as element-wise addition and function composition—on standard continuous functions in μ, and thus are themselves continuous in μ. Recall that Theorem 5.2 states that it is possible find a constant $d < 1$ such that $\|J_{\mathbb{0}}\|_\infty \leq d$. Then by continuity, for sufficiently small μ, we can also find a $d' < 1$ such that $\|J_\mu\|_\infty \leq d'$ and conclude that F_μ must be a contraction on $\mathcal{A}_\epsilon^-$ in the ℓ_∞ norm. Thus, we can conclude that there must exist a unique power flow solution in the set $\mathcal{A}_\epsilon^-$.

In summary, in this section, we have analyzed the full FPPF algorithm on a lossy two-bus system with a phase-shifting transformer and a Π-model transmission line. We used the $F_{\mathbb{0}}$-invariant $\mathcal{A}^-$ set from Section 5.2 to construct an F_μ-invariant set $\mathcal{A}^-_\epsilon$, in which the desired solution to the two-bus power flow problem exists. The constant ϵ characterizes how much the $\mathcal{A}^-_\epsilon$ set expands from the $\mathcal{A}^-$ set when the perturbation vector μ is nonzero, and we used the implicit function theorem to prove the existence of such ϵ given a sufficiently small μ. Finally, given a sufficiently small μ, we have shown that the FPPF algorithm is a contraction on the $\mathcal{A}^-_\epsilon$ set, once again based on the nominal system analysis in the previous section using a continuity argument. In this case, we can guarantee that the FPPF algorithm always converges to the desired high voltage solution by starting from any point in the $\mathcal{A}^-_\epsilon$ set.

Chapter 6

Numerical Results

Having concluded our theoretical work, in this chapter we provide comprehensive numerical simulations of the FPPF algorithm.

In Section 6.1, we discuss the construction of the power flow data in Algorithm 1, and the recovery of the bus voltage values V, θ from the FPPF variables v, ψ. In Section 6.2, we examine some numerical behaviors of the FPPF algorithm, in particular the effect of update order on the convergence as briefly discussed in 4.2, and its sensitivity to high network branch R/X ratios. In Section 6.3, we present some simulation results using different standard systems of various sizes, loading profiles and network parameters.

All subsequent simulations are conducted on MATLAB, using test cases from the MATPOWER library [42]–[44].

6.1 Computational Remarks and Software Implementation

In this section, we discuss the construction of relevant network matrices and required data for FPPF iterations, as well as other caveats and issues relevant to the software implementation. The known "power flow data" in Algorithm 1 includes the following:

(i) network admittance matrix Y, which can be computed using built-in function `makeYbus` in MATPOWER, and it is modified to re-order the buses in conformity with the $\mathcal{N}_L, \mathcal{N}_G$ partitions and return the incidence matrix A;

(ii) network incidence matrix A, from which the "from"/"to" partitions A^+, A^- and the cycle matrix C can be computed. In particular, since C contains only elements from $\{-1, 0, 1\}$, we compute it using the `null(A, 'r')` command, in which the `'r'` option generates a rational basis for $\ker A$. This process is the most time-consuming step; as such, the C matrix for all large systems (with 300

buses or more) are computed once only and saved for future use, and they only need to be re-computed if the network topology changes[1];

(iii) bus voltage data, in particular the generator voltages V_G to evaluate the open-circuit voltage V°, from which the nodal stiffness matrix S can be computed;

(iv) branch stiffness matrices D_G^+, D_G^-, D_B^+ and D_B^- can be computed using (3.8);

(v) the bus participation factor α and the full rank R matrix whose columns form an orthonormal basis to $\alpha^\perp$. Since standard power flow algorithms and test cases available on MATPOWER do not support the distributed slack bus modelling by default, we use the traditional single slack bus model in the simulations, i.e., R is constructed by removing the column, whose the position of the 1 element is the slack bus number, from the identity matrix;

(vi) the right inverse $M_B^\dagger$ and the "compressed" weighted cycle matrix K, whose columns form a basis for M_B. Unlike the true cycle matrix C, the elements of K are not limited to $\{-1, 0, 1\}$. To maximize the sparsity of K, it is computed using the LUQ decomposition[2] [46], which is considerably faster than the cycle matrix computation. The right inverse $M_B^\dagger$ is computed using `sparse(lsqminnorm(M_B, eye(n+m-1)))`.

The matrices above are sparse wherever possible. The bus number re-ordering process mentioned in (i) is nontrivial. To satisfy the $\mathcal{N}_L, \mathcal{N}_G$ partitions, we must re-label the bus number (the `BUS_I` field of the bus data [35, Table B-1]) of all the load buses (`BUS_TYPE` $= 1$) as $1, ..., n$, and re-label the bus number of all the generator buses (`BUS_TYPE` $= 2$) as $n+1, ..., m$. In order to convert between the original bus numbering and the $\mathcal{N}_L, \mathcal{N}_G$ partition bus numbering, we need to build and store a lookup table (alternatively, a sparse permutation matrix). By convention, the test systems on MATPOWER has a single reference bus (`BUS_TYPE` $= 3$), which is also doubled as the slack bus in standard algorithms, so we also need to record its original and re-named bus number separately.

In addition, on certain large systems, multiple generators may be connected to a single bus, which corresponds to multiple rows in the generator data [35, Table B-2] having the same `GEN_BUS` data. If this setup occurs, we aggregate all the power generations into a single generator to properly compute the bus power injections, and remove all others from the system.

Recall from Chapter 4.2 that we also need to update the Jacobian of the cycle matrix and find its inverse J_{cycle}^{-1} at every iteration of the FPPF algorithm. We also

[1] From a purely computational perspective, we do not *require* the C matrix, since all we need is a full column rank matrix whose columns span the null space of A.

[2] See [45] for a detailed explanation of the LUQ decomposition algorithm.

need the inverse of the nodal stiffness matrix S^{-1} for the v update. Both of these can be computed much more efficiently with the `mldivide` command [3]

After the FPPF converges, we can recover V from v by (3.6) and θ from ψ by computing $\theta = \left(A^{\mathsf{T}}\right)^{\dagger} \mathbf{arcsin}\left(\psi\right)$ as long as $\psi \in [-1,1]^{|\mathcal{E}|}$, with the pseudoinverse again computed using the `mldivide` command. Finally, to ensure the reference bus has 0 voltage phase angle, we subtract from all θ_i its current value before returning the final V, θ vectors.

6.2 Numerical Behaviors of the FPPF Algorithm

In this section, we discuss the numerical behaviors of the FPPF algorithm; in particular, we show that the order we use to compute the next iteration variables has a small but non-negligible effect on the iterations required for convergence, and that the FPPF algorithm is sensitive to high network R/X ratios. For all of these cases, we set the desired power balance mismatch tolerance to be 10^{-8} p.u., which is the default Matpower convergence criterion. We also set the initial condition to be the "flat-start" voltage profile, i.e., $V_L = \mathbb{1}_n$ and $\theta = \mathbb{0}_{n+m}$.

6.2.1 Effects of Update Order

As mentioned in Chapter 4.2, there are six total possible update orders to compute ψ^{k+1}, v^{k+1} and x_c^{k+1} using the current ψ^k, v^k and x_c^k. Conducting a theoretical analysis to understand the differences between all these update orders would be a painstaking undertaking beyond the scope of this thesis, so we present the numerical results from selected standard test systems instead, which nonetheless offer some qualitative insight. Each system's maximum branch R/X ratio is capped to be 0.8, as explained in the next section.

Figure 6.1 shows the number of iterations FPPF requires to converge and the power balance mismatch at each iteration for all six update orders. The legend entries indicate the update order. For example, ψ-x_c-v means that ψ^{k+1} is first computed using ψ^k, v^k and x_c^k, then x_c^{k+1} is computed using ψ^{k+1}, v^k and x_c^k, and finally, v^{k+1} is computed using ψ^{k+1}, v^k and x_c^{k+1}. We can observe two major facts from Figure 6.1. First, the difference between the update orders are not significant, and the total iterations required to converge for each update order differs by only a few iterations. Second, the ψ-x_c-v and x_c-ψ-v orders seem to take consistently more iterations than the rest of the update orders to converge, and initially the power balance mismatch *increases* before it decreases again. However, updating v before ψ seems to provide

[3] Although it is not pursued here, the computations can be further optimized with heuristics such as the approximate minimum degree permutation [47], which is used in the NR implementation on Matpower.

consistently faster and smoother convergence behaviors. In fact, on the RTE 1951 and RTE 6468 bus systems, updating ψ before v leads to convergence failure. A potential reason for this phenomenon is that initially, updating ψ first may give it too large of a "kick" and the power balance mismatch would increase, but updating v before ψ steers the update of ψ in the right direction. However, more work is required to prove or disprove this conjecture. Nonetheless, we choose the v-x_c-ψ update order for the remaining simulations.

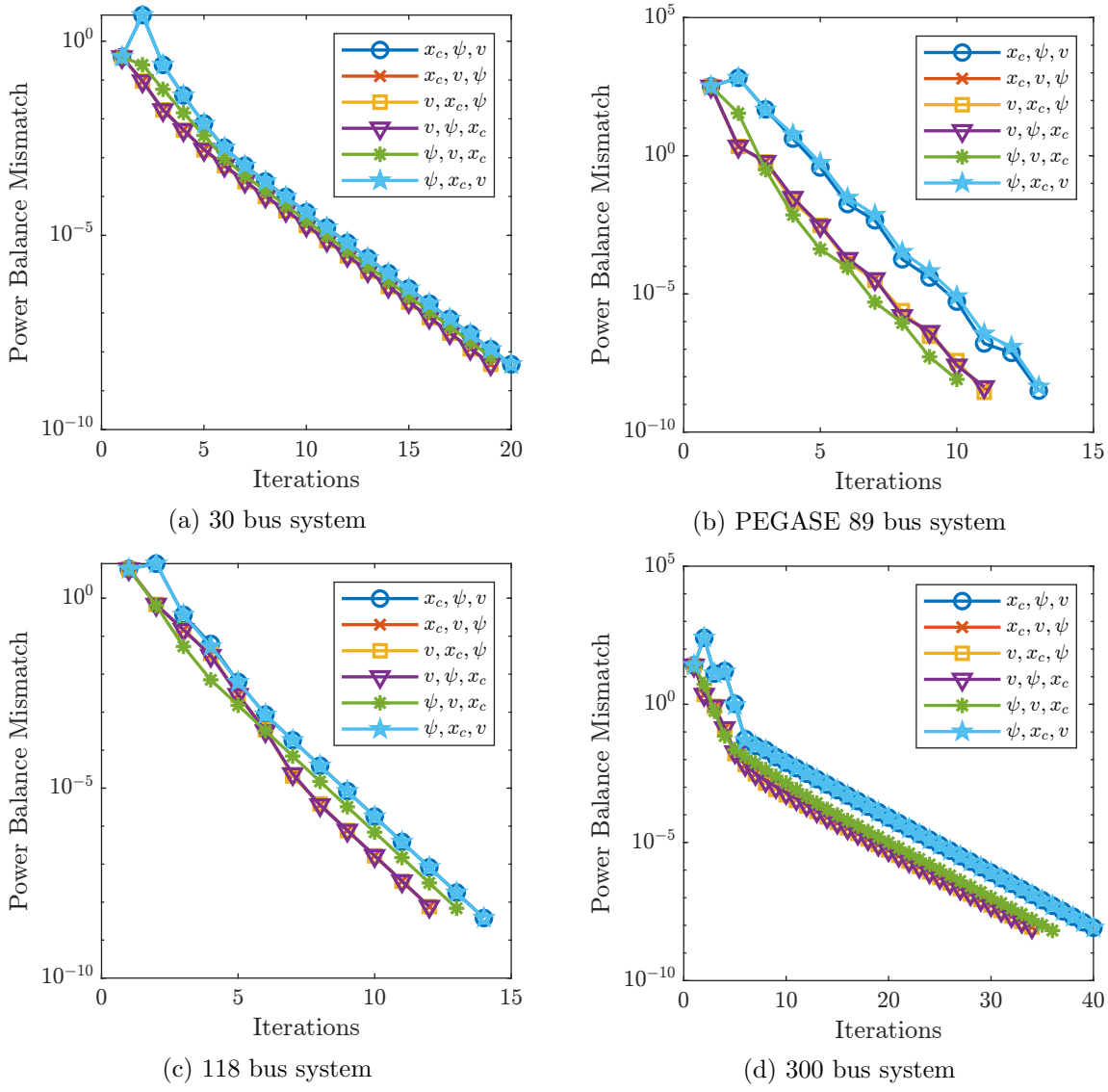

(a) 30 bus system

(b) PEGASE 89 bus system

(c) 118 bus system

(d) 300 bus system

Figure 6.1: Effect of update order on mismatch trajectories of FPPF

6.2.2 Sensitivity to Network R/X Ratio

While practical transmission networks generally have low branch R/X ratios, test systems on Matpower occasionally have branches with unrealistically high R/X ratios (e.g., due to equivalencing [48]). The FPPF algorithm is unfortunately sensitive to these branches, and on certain cases it does not converge with the default branch R/X parameters. Table 6.1 lists the branches with unrealistically high R/X ratios in the 300 bus system and the PEGASE 2869 bus system, where FPPF fails with the default branch parameters. The R and X values are taken directly from the test case data, in which parallel branches are combined into a single equivalent branch.

Table 6.1: Branches with high R/X ratios

Test case	Branch	R (p.u.)	X (p.u.)	R/X ratio
300 bus system	(9003, 9044)	0.07378	0.06352	1.16152
	(9021, 9023)	1.10680	0.95278	1.16165
	(9044, 9004)	0.03832	0.02894	1.32412
PEGASE 2869	(1216, 5233)	0.000430	0.000380	1.13158
	(3095, 2951)	0.003211	0.001760	1.82443
	(4318, 1338)	0.002967	0.002901	1.02275
	(6047, 5271)	0.001012	0.000802	1.26210
	(8209, 1998)	0.000690	0.000479	1.44050

Note that these problematic branches account for only a tiny portion of the total branches, since the 300 bus system has 411 total branches and the PEGASE 2869 bus system has 4582 total branches. However, these branches are sufficient to cause the FPPF iterations to violate the implicit constraint that $\|\psi\|_\infty \leq 1$, and result in convergence failure. It is not totally clear to us the precise mechanism through which few branches with high R/X ratios generates an iteration that violates this constraint, but it is not a trivial issue to fix. For example, the algorithm still fails even if we restrict the violating element(s) of ψ to be some $c \in [0, 1]$ in each iteration.

Consequently, we cap the branch R/X ratios on these test cases, and investigate the change in FPPF's convergence behavior as we vary the R/X ratio cap. Figure 6.2 shows the power balance mismatch trajectories of FPPF on both cases. Clearly, FPPF takes more iterations to converge as we increase the R/X ratio cap. Note that the first few power balance mismatches are close for all the R/X ratio caps, before they disperse and the convergence becomes slower as R/X ratio cap grows. Figure 6.3 shows the distribution of branch R/X ratios for both test systems, and verifies

that indeed the vast majority of the branches have low R/X ratios.

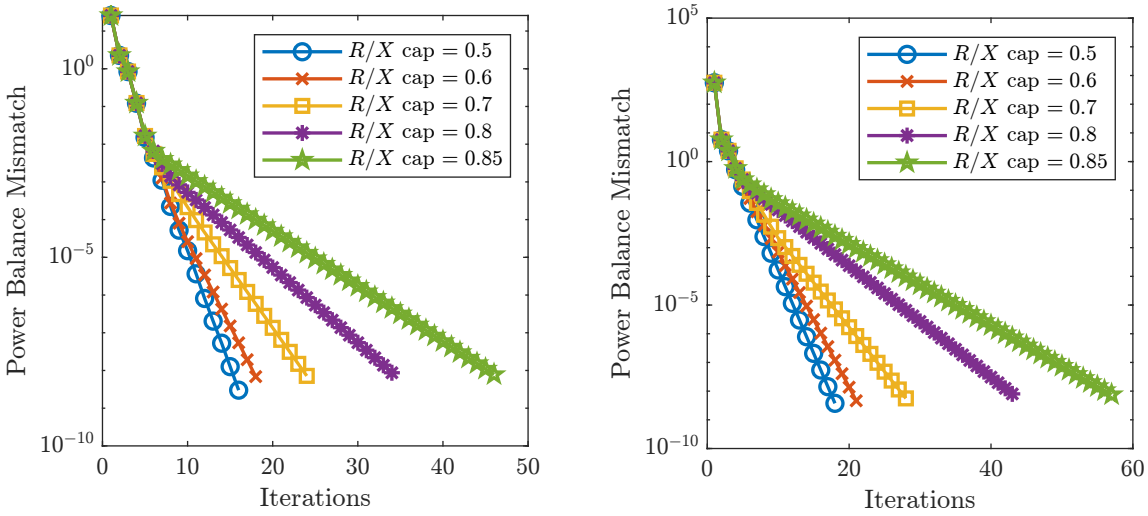

(a) 300 bus system (b) PEGASE 2869 bus system

Figure 6.2: Mismatch trajectories of FPPF with different R/X ratio caps

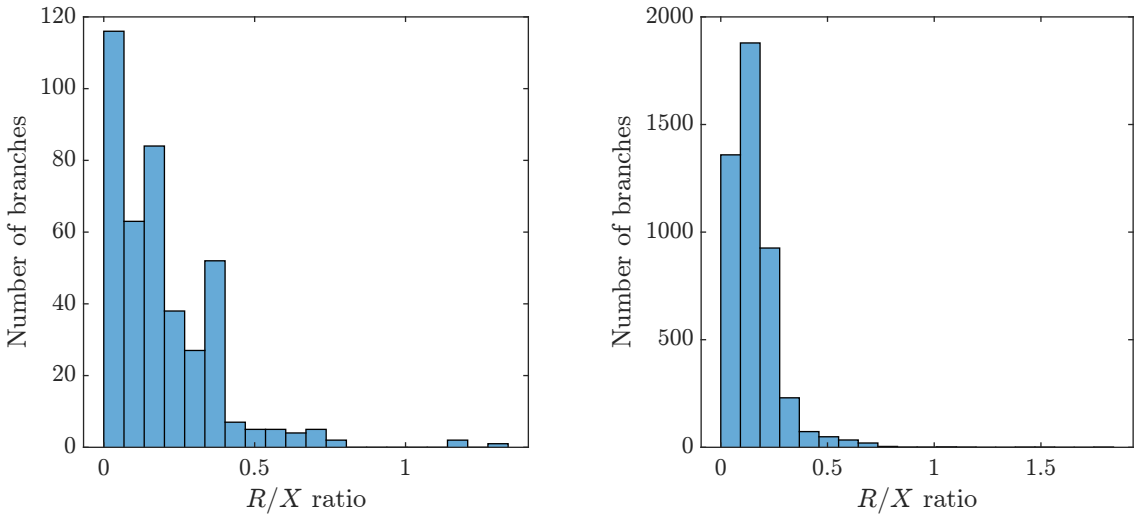

(a) 300 bus system (b) PEGASE 2869 bus system

Figure 6.3: Distribution of branch R/X ratios

With a step size of 0.01, we computed that the minimum R/X ratio cap for convergence failure to be 1.00 and 1.01 for the 300 bus system and PEGASE 2869 system, respectively. Consequently, we choose to cap the branch R/X ratios on all test cases at 0.8, since it is a generous upper bound for realistic transmission systems, and FPPF can converge on all test cases in a reasonable number of iterations in order to compare against classic power flow algorithms such as Newton-Raphson (NR) and the fast decoupled load flow (FDLF) in the next section. This modification does not

create an unfair advantage for FPPF over NR or FDLF, since their convergence rates also deteriorate as the network R/X ratio increases [49]. By not further decreasing the bound on maximum R/X ratio, we also minimally modify the system since only fewer than 1% of the branches are modified in general.

6.3 Comparison to Standard Power Flow Algorithms

In this section, we compare the FPPF algorithm against the standard NR and FDLF (the XB version), both of which are available in Matpower. We focus on two aspects of the algorithm performance: (i) iterations required for convergence, and (ii) sensitivity to the initial bus voltage values. We also set the maximum iteration count to be 100 for all three algorithms.

6.3.1 Iterations Required for Convergence

Here, we compare the number of iterations each algorithm requires to converge using the flat-start initial condition. We present the simulation results based on two loading scenarios: (i) base loading, which is the default values on the test systems, and (ii) high loading, which is computed by continuation power flow (CPF) using the `cpf` command on Matpower [35, Chapter 5]. For the latter scenario, the base power generation and demand are set to be 90% of the way to the power flow insolvability boundary. Table 6.2 shows the number of iterations each algorithm takes to converge. If the algorithm fails to converge, then the corresponding entry is marked as "/".

Table 6.2: Iterations required to converge

	Base loading			High loading		
Test case	NR	FDLF	FPPF	NR	FDLF	FPPF
9 bus system	4	6	8	5	29	22
30 bus system	3	11	18	6	28	22
PEGASE 89	4	9	10	6	26	23
118 bus system	4	11	11	6	33	25
300 bus system	5	15	33	6	33	33
PEGASE 1354	5	11	42	5	25	42
RTE 1888	/	61	33	/	76	33
RTE 1951	/	55	32	/	58	32
RTE 2868	/	49	43	/	46	44
PEGASE 2869	5	11	42	6	29	42
PEGASE 9241	6	17	46	6	23	47

We can make the following observations based on the data from Table 6.2. First, when NR converges successfully, it consistently outperforms both FDLF and FPPF due to its quadratic convergence rate. Figures 6.4–6.7 demonstrate that both FDLF and FPPF have a linear convergence rate, and the iterations required by both algorithms are comparable. Curiously, we can see that the power balance mismatch of FPPF seems to closely match that of FDLF for the first few iterations, before it takes a turn and decrease at a smaller but still linear rate for all except the 118 bus system with high loading, which does not have a smooth decaying trajectory but nonetheless converges.

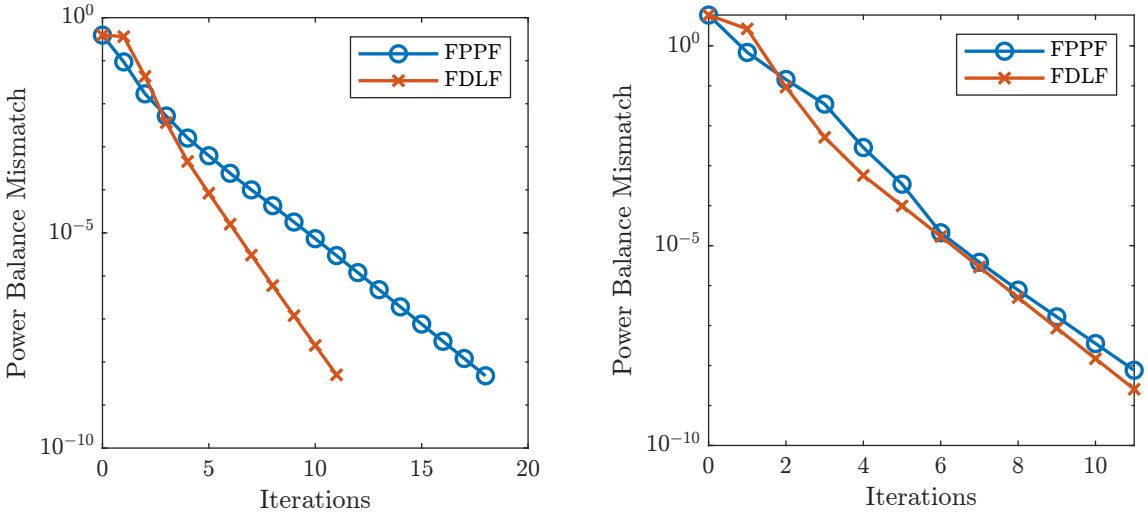

(a) 30 bus system (b) 118 bus system

Figure 6.4: Mismatch trajectory of FDLF and FPPF on small systems (base loading)

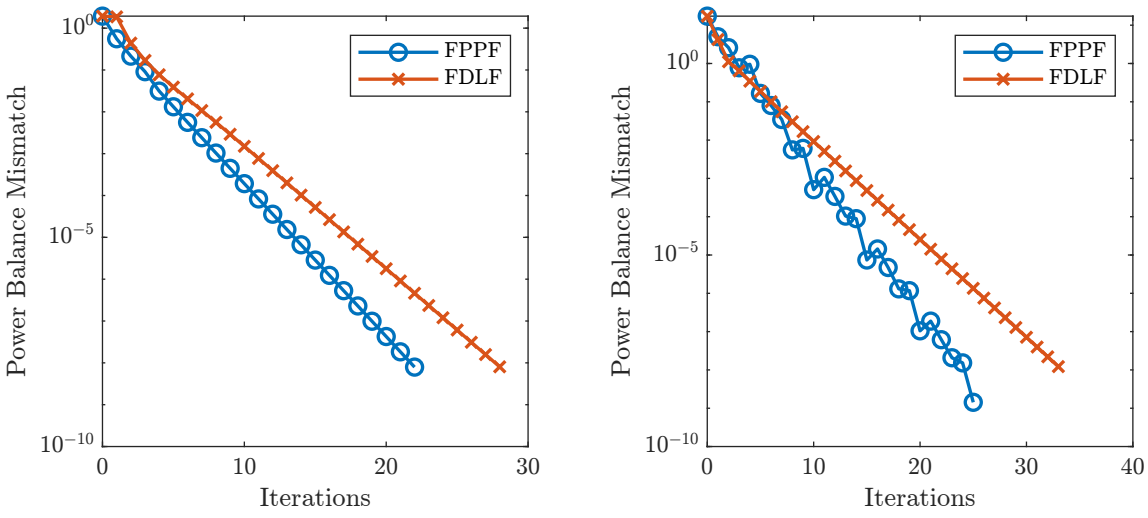

(a) 30 bus system (b) 118 bus system

Figure 6.5: Mismatch trajectory of FDLF and FPPF on small systems (high loading)

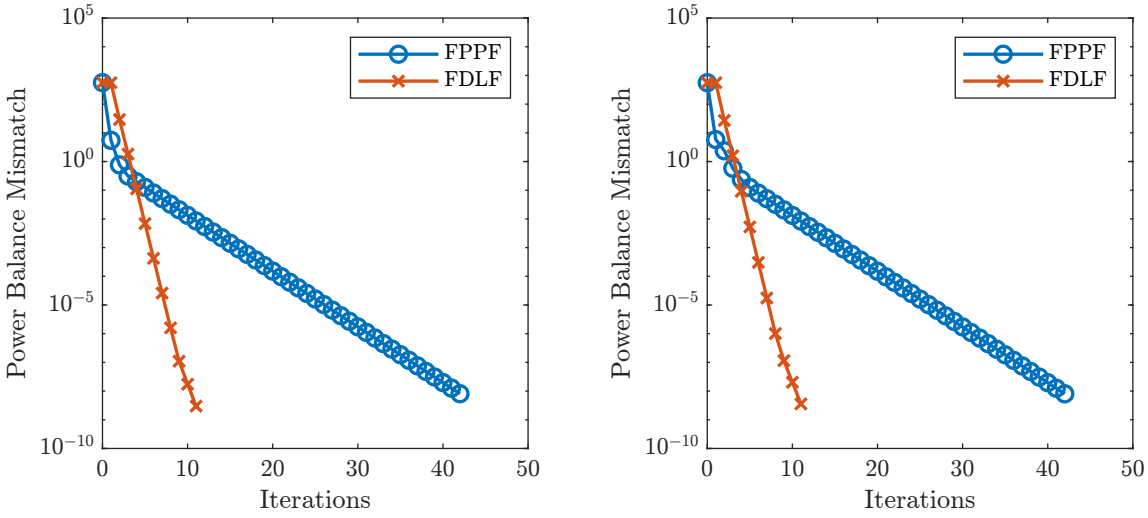

(a) PEGASE 1354 bus system (b) PEGASE 2869 bus system

Figure 6.6: Mismatch trajectory of FDLF and FPPF on large systems (base loading)

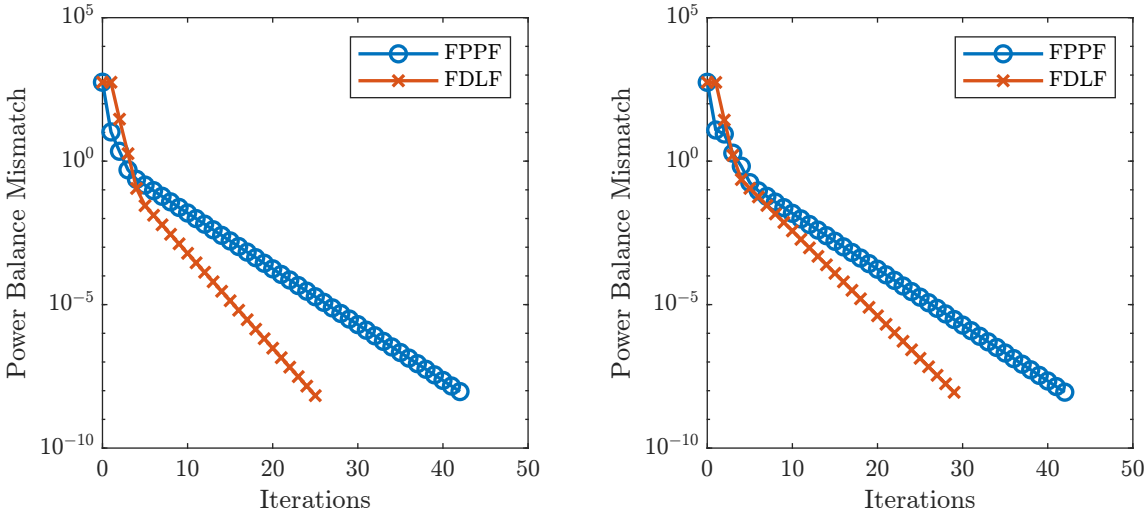

(a) PEGASE 1354 bus system (b) PEGASE 2869 bus system

Figure 6.7: Mismatch trajectory of FDLF and FPPF on large systems (high loading)

Second, on large systems (with 300 buses or more), FPPF requires almost identical iterations to converge for both base and high loading levels; however, FDLF requires nearly twice of the base loading iterations to converge on systems with high loading. That is, FDLF is more sensitive to the system loading level than FPPF is.

Aside from these, NR struggles to converge on all the RTE systems, even though it is able to converge on the PEGASE 9241 bus system, which is the largest system tested. FPPF also outperforms FDLF on these systems, even though it takes more iterations than FDLF to converge in almost all other systems in base loading. This

fact potentially has more to do with the inherent properties of these RTE systems than the algorithms themselves, which may warrant further investigations. We emphasize that the initial condition for these tests is the "flat-start" condition, and is generally not the best for NR due to its fractal convergence regions. With this caveat in mind, it then seems plausible for NR to fail on both base and high loading scenarios in the RTE systems while CPF computations successfully result in a non-unity scaling factor for the high loading scenario.

6.3.2 Sensitivity to Initialization

Finally, we test each algorithm's sensitivity to bus voltage initialization. While we did not pursue the development of sufficient and necessary condition(s) for FPPF to be a contraction, we can expect that if it is a contraction on a large set of bus voltages, then its convergence success rate would be insensitive to the initial conditions (ICs).

We adopt the random initialization scheme for voltage magnitudes introduced [3]. For a fixed "IC spread" constant $\delta \in (0, 1)$ as well as a fixed random number generator seed, we generate 1000 random samples of initial voltage magnitudes $V_{L,\text{init}}^{[k]} \in \mathbb{R}^n$, where the superscript $[k]$ represents the k-th sample. Each element of $V_{L,\text{init}}^{[k]}$ is sampled from a uniform distribution on the interval $[1 - \delta, 1 + \delta]$, and we set the initial load bus voltage magnitude $V_L^0 = V_{L,\text{init}}^{[k]}$, for $k = 1, ..., 1000$ while keeping $\theta = \mathbb{0}_{n+m}$.

We first compute the known high voltage solution using NR with flat-start voltages, then compare this solution against the ones returned by NR, FDLF and FPPF using the random voltage initializations. If the solution returned does not match the known solution up to a small tolerance, or if the algorithm fails, then the sample is marked as unsuccessful, otherwise it is successful. Tables 6.3–6.4 demonstrates each algorithm's success rate for different δ on the 30 and 118 bus systems.

Table 6.3: Algorithm success rate (%) under random V_L^0 for the 30 bus system

	Base loading			High loading		
δ	NR	FDLF	FPPF	NR	FDLF	FPPF
0.1	100.0	100.0	100.0	100.0	100.0	100.0
0.2	97.2	100.0	100.0	97.8	100.0	100.0
0.3	34.2	100.0	100.0	39.5	100.0	100.0
0.4	2.7	100.0	100.0	3.7	100.0	100.0
0.5	0.1	100.0	100.0	0.1	100.0	100.0
0.7	0.0	100.0	100.0	0.0	100.0	100.0
0.9	0.0	100.0	100.0	0.0	87.3	95.9
0.95	0.0	100.0	100.0	0.0	75.5	88.2

Table 6.4: Algorithm success rate (%) under random V_L^0 for the 118 bus system

	Base loading			High loading		
δ	NR	FDLF	FPPF	NR	FDLF	FPPF
0.1	100.0	100.0	100.0	100.0	100.0	100.0
0.2	98.8	100.0	100.0	98.8	100.0	100.0
0.3	65.6	100.0	100.0	66.7	100.0	100.0
0.4	6.9	100.0	100.0	7.7	100.0	100.0
0.5	0.0	100.0	100.0	0.0	100.0	100.0
0.7	0.0	100.0	100.0	0.0	100.0	100.0
0.9	0.0	100.0	100.0	0.0	98.7	100.0
0.95	0.0	100.0	100.0	0.0	89.0	98.9

Evidently, NR is the least robust against the random voltage magnitude initializations; with a small δ, it performs on par with FPPF and FDLF, but its convergence success rate drastically decreases as δ increases. This observation matches the well-known fact that the convergence of NR is extremely sensitive to the initial condition selection. Additionally, FDLF performs almost as well as FPPF until δ gets close to 1 in the high loading scenario, where a small number of samples fail to converge[4]. For each $V_{L,\text{init}}^{[k]}$ that results in FPPF failing to converge, FPPF fails due to the violation of the implicit constraint that $\|\psi\|_\infty \leq 1$ during the fixed-point iterations, similar to the case discussed in Section 6.2.2. That is, when FPPF converges, it always converges to the known high voltage solution.

However, when a similar random initialization is implemented for voltage phases (e.g., sampling from $[-\pi\delta/4, \pi\delta/4]$), FPPF becomes much more sensitive and consistently fail to converge due to $\|\psi\|_\infty > 1$. We offer a brief analysis on a potential cause of this constraint violation, as well as a possible solution to address this issue in our concluding remarks in Chapter 7.

[4]The source code that generated [3, Table II] contained a small typo, so FDLF was mistakenly shown to have the same results as NR.

Chapter 7

Conclusions and Future Work

In this thesis, we have derived a new algorithm for the AC power flow problem by extending the lossless FPPF algorithm to accommodate network loss, phase-shifting transformers, transmission line Π-model parameters, and the distributed slack bus model. As a first step in the theoretical analysis of the algorithm, we studied a version of it on the two-bus system and presented sufficient conditions on the existence and uniqueness of the desired solution. We have also demonstrated the performance of the proposed full FPPF algorithm on standard test cases.

This thesis has three major components. The first one is the derivation of an equivalent fixed-point reformulation of the conventional power flow equations, and the full FPPF algorithm based on this reformulation in Chapter 4. These results relied on concepts and techniques from algebraic graph theory, matrix algebra and power system modelling discussed in Chapters 2–3. One caveat of the full FPPF algorithm is that in the traditional nodal power injection model of the power flow equations, the domain of the voltage angle θ is virtually all of $\mathbb{R}^{n+m}$ (even though only a small subset of $\mathbb{R}^{n+m}$ makes practical sense). However, the domain of the related voltage angle quantity for our fixed-point reformulation, ψ, is implicitly constrained to be in $[-1, 1]^{|\mathcal{E}|}$ in order to keep the fixed-point reformulations real-valued.

The second component is a first step in a rigorous theoretical analysis of the full FPPF algorithm in Chapter 5. We studied the two-bus power flow problem with a physically realistic branch model, and provided sufficient conditions for the FPPF algorithm to be a contraction on a methodically constructed closed and convex norm ball in $\mathbb{R}^2$. This analysis relies on the lossless system results extensively studied in the literature, which we have attempted to build upon. Crucially, we employed the implicit function theorem to show the existence of the desired high voltage solution, and argued by continuity for the contractivity.

The final component consists of the extensive numerical simulations we conducted

to test the performance of the full FPPF algorithm in Chapter 6, where we showed that it can reliably obtain the high voltage solution under the mild assumption that network has realistic R/X ratios. Overall, we showed that the full FPPF algorithm is comparable to FDLF, with FDLF being potentially more computationally efficient, and FPPF being less sensitive to loading level changes. Additionally, while FPPF has a lower order of convergence compared to NR, it is much more robust given random initial conditions.

Finally, as mentioned in Chapter 2, a tangential contribution of this thesis is the construction of the asymmetrically weighted incidence matrix Γ, which is motivated by the presence of phase-shifting transformers in the system. While the preliminary rank properties of Γ that we derived in Appendix A are novel to the best of our knowledge, they have no applications in the context of this thesis, thanks to the R matrix that "compressed" the active power flow equations and removed the slack bus power injections from the analysis. However, this matrix could be potentially useful for other problems involving complex networked system modelling and analysis.

Future Work

Numerically, violation of the $\|\psi\|_\infty \leq 1$ constraint, whether due to high R/X ratio or large initial θ values, seems to be the most significant drawback of the FPPF algorithm. Further analysis and numerical techniques could be employed to address or circumvent this problem, for example:

- investigate the precise mechanism through which one or few branches with high R/X ratio(s), or large initial θ values creates the infeasible update that violates this constraint;
- examine whether this constraint violation is a "transient" phenomenon of the algorithm, i.e., whether the voltage variables and the cycle slack variable eventually become real-valued given sufficient iterations;

Additionally, the cycle constraint computations at every FPPF iteration can be made more efficient with a pseudo-Newton update scheme, and the `mldivide` command for solving systems of linear equations can be accelerated by using heuristics such as the approximate minimal degree permutation. A complexity analysis of the FPPF algorithm can also be conducted for further comparison against NR and FDLF.

Theoretically, the sufficient conditions we obtained in Chapter 5.3 could be tightened, e.g., through better manipulations of the invariance inequalities. They could also be extended to general radial systems using similar approaches as in [4]. If this extension is possible, then further extensions to the meshed systems could be attempted. In addition, we could revise the fixed-point reformulation in Chapter 4

to explicitly account for branches with high R/X ratios, which could address the non-convergence caused by the $\|\psi\|_\infty \leq 1$ constraint violation. Since the right-hand side of (4.2b) encodes some R/X information from the $M_B^\dagger$, $[G_{ii}]$ and Γ_G matrices, it seems plausible that branches with high R/X ratios can cause the ψ update to violate the constraint. We could revise the reformulation by, for example, replacing M_B with another matrix, which includes not just the information from B but also the G matrix, and could "cancel out" the loss terms captured by the $[G_{ii}]$ and Γ_G matrices to a certain degree.

If the FPPF algorithm is implemented for other applications that require power flow solutions, e.g., contingency analysis, then there is one caveat: changes in the system topology necessitate that the graph matrices A, C both to be re-computed. While computing C is expensive in general, it can be achieved efficiently under certain circumstances. For example, if only a few nearby edges in the graph are removed to represent out-of-service transmission lines, then we can choose a small subgraph $\mathcal{G}'$ that contains these edges and cut it off from the rest of the graph $\mathcal{G}$. We can then compute the new cycle vectors in the subgraph $\mathcal{G}'$ to form the updated cycle matrix C, which would be much faster than computing C from scratch since the cycles in the rest of the graph are not impacted.

Finally, while the construction of the asymmetrically weighted matrix Γ is an unambiguous extension of the typical incidence matrix of a directed graph A, the notion of bidirected graph and its properties are still somewhat fuzzy. As such, the way we defined the bidirected graph and its properties can be polished and made compatible with standard algebraic graph theory language. Even though they are tangentially related to this thesis, we can explore the connections between Γ and other standard directed graph matrices such as the Laplacian matrix (which can be constructed using A), and Kirchhoff's voltage and current laws (which can be written using A, the nodal voltage and current injection and branch potential difference and current flow). We can also investigate its potential applications in other complex networks with bidirected and asymmetrical information or commodity flow, other than the AC transmission networks with phase-shifting transformers.

Bibliography

[1] J. Glover, T. Overbye, and M. Sarma, *Power System Analysis and Design*, 5th ed. Cengage Learning, 2016, ISBN: 9781305632134.

[2] J. W. Simpson-Porco, "Lossy DC power flow," *IEEE Transactions on Power Systems*, vol. 33, no. 3, pp. 2477–2485, 2018.

[3] ——, "A theory of solvability for lossless power flow equations – Part I: Fixed-point power flow," *IEEE Transactions on Control of Network Systems*, vol. 5, no. 3, pp. 1361–1372, 2018.

[4] ——, "A theory of solvability for lossless power flow equations – Part II: Conditions for radial networks," *IEEE Transactions on Control of Network Systems*, vol. 5, no. 3, pp. 1373–1385, 2018.

[5] R. Delabays, S. Jafarpour, and F. Bullo, "Multistability and Paradoxes in Lossy Oscillator Networks," arXiv:2202.02439, Feb. 2022.

[6] A. J. Korsak, "On the question of uniqueness of stable load-flow solutions," *IEEE Transactions on Power Apparatus and Systems*, vol. PAS-91, no. 3, pp. 1093–1100, 1972. DOI: 10.1109/TPAS.1972.293463.

[7] F. F. Wu and S. Kumagai, "Limits on power injections for power flow equations to have secure solutions," EECS Department, University of California, Berkeley, Tech. Rep. UCB/ERL M80/19, Apr. 1980. [Online]. Available: http://www2.eecs.berkeley.edu/Pubs/TechRpts/1980/28467.html.

[8] ——, "Steady-state security regions of power systems," *IEEE Transactions on Circuits and Systems*, vol. 29, no. 11, pp. 703–711, 1982. DOI: 10.1109/TCS.1982.1085091.

[9] J. Thorp, D. Schulz, and M. Ilić-Spong, "Reactive power-voltage problem: Conditions for the existence of solution and localized disturbance propagation," *International Journal of Electrical Power & Energy Systems*, vol. 8, no. 2, pp. 66–74, 1986.

[10] M. Ilic, "Network theoretic conditions for existence and uniqueness of steady state solutions to electric power circuits," in *1992 IEEE International Symposium on Circuits and Systems (ISCAS)*, vol. 6, 1992, pp. 2821–2828. DOI: 10.1109/ISCAS.1992.230611.

[11] J. W. Simpson-Porco, F. Dörfler, and F. Bullo, "Voltage collapse in complex power grids," *Nature Communications*, vol. 7, no. 1, p. 10 790, Feb. 2016. [Online]. Available: https://doi.org/10.1038/ncomms10790.

[12] F. Dörfler, M. Chertkov, and F. Bullo, "Synchronization in complex oscillator networks and smart grids," *Proceedings of the National Academy of Sciences*, vol. 110, no. 6, pp. 2005–2010, 2013. [Online]. Available: https://www.pnas.org/doi/abs/10.1073/pnas.1212134110.

[13] B. Cui and X. A. Sun, *Solvability of power flow equations through existence and uniqueness of complex fixed point*, 2019. arXiv: 1904.08855 [cs.SY].

[14] S. Bolognani and S. Zampieri, "On the existence and linear approximation of the power flow solution in power distribution networks," *IEEE Transactions on Power Systems*, vol. 31, no. 1, pp. 163–172, 2015.

[15] D. K. Molzahn and I. A. Hiskens, "A survey of relaxations and approximations of the power flow equations," *Foundations and Trends in Electric Energy Systems*, vol. 4, no. 1-2, pp. 1–221, 2019. [Online]. Available: http://dx.doi.org/10.1561/3100000012.

[16] J. Meisel and R. D. Barnard, "Application of fixed-point techniques to load-flow studies," *IEEE Transactions on Power Apparatus and Systems*, vol. PAS-89, no. 1, pp. 136–140, 1970. DOI: 10.1109/TPAS.1970.292681.

[17] F. F. Wu, "Theoretical study of the convergence of the fast decoupled load flow," *IEEE transactions on power apparatus and systems*, vol. 96, no. 1, pp. 268–275, 1977.

[18] C. Wang, A. Bernstein, J.-Y. Le Boudec, and M. Paolone, "Explicit conditions on existence and uniqueness of load-flow solutions in distribution networks," *IEEE Transactions on Smart Grid*, vol. 9, no. 2, pp. 953–962, 2016.

[19] A. Bernstein and E. Dall'Anese, "Linear power-flow models in multiphase distribution networks," in *2017 IEEE PES Innovative Smart Grid Technologies Conference Europe (ISGT-Europe)*, 2017, pp. 1–6. DOI: 10.1109/ISGTEurope.2017.8260205.

[20] K. Dvijotham, S. Low, and M. Chertkov, "Convexity of energy-like functions: Theoretical results and applications to power system operations," Tech. Rep., Jan. 2015. [Online]. Available: https://www.osti.gov/biblio/1168707.

[21] K. Dvijotham, E. Mallada, and J. W. Simpson-Porco, "High-voltage solution in radial power networks: Existence, properties and equivalent algorithms," *IEEE Control Systems Letters*, vol. 1, no. 2, pp. 322–327, 2017.

[22] R. Penrose, "A generalized inverse for matrices," *Mathematical Proceedings of the Cambridge Philosophical Society*, vol. 51, no. 3, pp. 406–413, 1955. DOI: 10.1017/S0305004100030401.

[23] R. Horn and C. Johnson, *Matrix Analysis*, 2nd ed. Cambridge University Press, 2013.

[24] F. Dörfler, J. W. Simpson-Porco, and F. Bullo, "Electrical networks and algebraic graph theory: Models, properties, and applications," *Proceedings of the IEEE*, vol. 106, no. 5, pp. 977–1005, 2018.

[25] A. Berman and R. J. Plemmons, *Nonnegative Matrices in the Mathematical Sciences*, ser. Computer science and applied mathematics. San Diego, CA: Academic Press, Dec. 1979.

[26] K. R. Davidson and A. P. Donsig, *Real Analysis and Applications*, 1st ed. Springer New York, 2009.

[27] C. C. Pugh, *Real Mathematical Analysis*, 2nd ed. Springer Cham, 2015.

[28] T. M. Apostol, *Mathematical Analysis*, 2nd ed. Pearson Education, Inc., 1971.

[29] S. Boyd and L. Vandenberghe, *Convex Optimization*. Cambridge University Press, 2009.

[30] O. de Oliveira, "The implicit and the inverse function theorems: Easy proofs," *Real Anal. Exchange*, vol. 39, no. 1, p. 207, 2014.

[31] K. Conrad, *The contraction mapping theorem*. [Online]. Available: https://kconrad.math.uconn.edu/blurbs/analysis/contraction.pdf.

[32] T. von Petersdorff, *AMSC/CMSC 666 Numerical Analysis: Fixed point iteration and contraction mapping theorem*, https://terpconnect.umd.edu/~petersd/666/fixedpoint.pdf, Accessed: 2022-05-07.

[33] T. Kavitha, C. Liebchen, K. Mehlhorn, *et al.*, "Cycle bases in graphs characterization, algorithms, complexity, and applications," *Computer Science Review*, vol. 3, no. 4, pp. 199–243, 2009, ISSN: 1574-0137. DOI: https://doi.org/10.1016/j.cosrev.2009.08.001. [Online]. Available: https://www.sciencedirect.com/science/article/pii/S1574013709000483.

[34] C. Balbuena, D. Ferrero, X. Marcote, and I. Pelayo, "Algebraic properties of a digraph and its line digraph," *Journal of Interconnection Networks*, vol. 4, no. 4, pp. 377–393, 2003.

[35] R. D. Zimmerman and C. E. Murillo-Sanchez, *MATPOWER User's Manual, Version 7.1*, 2020.

[36] N. Deo, *Graph Theory with Applications to Engineering & Computer Science*. New York: Dover Publications, 2016.

[37] T. Van Cutsem and C. Vournas, *Voltage Stability of Electric Power Systems*. Boston, MA: Springer, 1998.

[38] A. J. Wood, B. F. Wollenberg, and G. B. Sheble, *Power Generation, Operation, and Control*, 3rd ed. Chichester, England: Wiley-Blackwell, Dec. 2013.

[39] S. V. Dhople, Y. C. Chen, A. Al-Digs, and A. D. Domínguez-García, "Reexamining the distributed slack bus," *IEEE Transactions on Power Systems*, vol. 35, no. 6, pp. 4870–4879, 2020. DOI: 10.1109/TPWRS.2020.2987325.

[40] F. Dörfler, "Dynamics and Control in Power Grids and Complex Oscillator Networks," Student thesis, University of California Santa Barbara, Sep. 2013.

[41] N. Overmars, *Is the Cartesian product of two open sets open?* Mathematics Stack Exchange, Version: 2020/10/17. [Online]. Available: https://math.stackexchange.com/q/653106.

[42] C. Josz, S. Fliscounakis, J. Maeght, and P. Panciatici, *Ac power flow data in MATPOWER and QCQP format: ITesla, RTE snapshots, and PEGASE*, 2016. arXiv: 1603.01533 [math.OC].

[43] S. Fliscounakis, P. Panciatici, F. Capitanescu, and L. Wehenkel, "Contingency ranking with respect to overloads in very large power systems taking into account uncertainty, preventive, and corrective actions," *IEEE Transactions on Power Systems*, vol. 28, no. 4, pp. 4909–4917, 2013. DOI: 10.1109/TPWRS.2013.2251015.

[44] R. D. Zimmerman, C. E. Murillo-Sánchez, and R. J. Thomas, "Matpower: Steady-state operations, planning, and analysis tools for power systems research and education," *IEEE Transactions on Power Systems*, vol. 26, no. 1, pp. 12–19, 2011. DOI: 10.1109/TPWRS.2010.2051168.

[45] N. Bou-Rabee, *How can one construct a sparse null space basis using recursive lu decomposition?* MathOverflow, version: 2016-11-07. [Online]. Available: https://mathoverflow.net/q/254095.

[46] P. Kowal, *Nullspace of a sparse matrix*, May 28, 2022. [Online]. Available: https://www.mathworks.com/matlabcentral/fileexchange/11120-null-space-of-a-sparse-matrix.

[47] P. R. Amestoy, T. A. Davis, and I. S. Duff, "An approximate minimum degree ordering algorithm," *SIAM Journal on Matrix Analysis and Applications*, vol. 17, no. 4, pp. 886–905, 1996.

[48] R. D. Zimmerman, *Re: High branch R/X ratio in MATPOWER cases*, Nov. 2021. [Online]. Available: https://www.mail-archive.com/matpower-l@cornell.edu/msg07883.html.

[49] ——, *Re: impact of R/X ratio*, Jul. 2016. [Online]. Available: https://www.mail-archive.com/matpower-l@cornell.edu/msg05247.html.

Appendix A

The Asymmetrically Weighted Incidence Matrix

In this chapter, we develop some rank properties for the asymmetrically weighted incidence matrix, defined in Chapter 2.2. We assume that the bidirected graph $\mathcal{G}$ is weakly connected (in the sense of forward edges), and that both edge weight vectors w^+, w^- are element-wise strictly positive. Recall that given A, the incidence matrix of the associated directed graph and its partitions A^+ and A^-, the *asymmetrically weighted incidence matrix* is constructed as

$$\Gamma := A^+[w^+] - A^-[w^-].$$

Recall that the incidence matrix A of a weakly connected directed graph with n nodes always satisfies $\operatorname{rank}(A) = \operatorname{rank}(A[w]) = n-1$ for any nonzero weight vector w. Since Γ shares the identical sparsity patterns as A and $A[w]$, we study the following problem: *when does a bidirected graph have an asymmetrically weighted incidence matrix with full rank?* Note that the results derived here can be easily generalized to weight vectors of all negative weights, since these results rely only on the fact that there are no sign variations in the edge weight elements.

A.1 Rank Properties

We now discuss the rank of the asymmetrically weighted incidence matrix. First, we compute $\operatorname{rank}(\Gamma)$ for a simple asymmetrically weighted bidirected graphs in Figure A.1 with different weighting patterns to motivate the general results that follow.

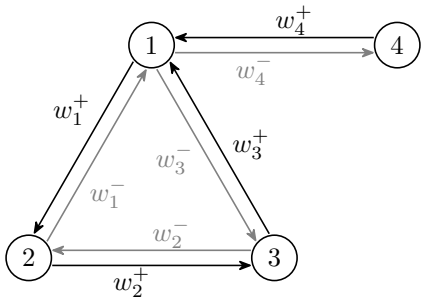

Figure A.1: Example of an asymmetrically weighted bidirected graph

Example A.1. For the bidirected graph in Figure A.1, we can check that

$$\Gamma = \begin{bmatrix} w_1^+ & 0 & -w_3^- & -w_4^- \\ -w_1^- & w_2^+ & 0 & 0 \\ 0 & -w_2^- & w_3^+ & 0 \\ 0 & 0 & 0 & w_4^+ \end{bmatrix}.$$

We compute $\operatorname{rank}(\Gamma)$ for four different weighting patterns:

(i) Suppose $w_1^+ \neq w_1^-$, but $w_2^+ = w_2^- =: w_2$, $w_3^+ = w_3^- =: w_3$, and $w_4^+ = w_4^- =: w_4$. Then, suppose $x \in \ker \Gamma$ and $x \neq \mathbb{0}$, we have

$$\begin{bmatrix} w_1^+ & 0 & -w_3 & -w_4 \\ -w_1^- & w_2 & 0 & 0 \\ 0 & -w_2 & w_3 & 0 \\ 0 & 0 & 0 & w_4 \end{bmatrix} \begin{bmatrix} x_1 \\ x_2 \\ x_3 \\ x_4 \end{bmatrix} = \begin{bmatrix} 0 \\ 0 \\ 0 \\ 0 \end{bmatrix} \implies \begin{cases} w_1^+ x_1 = w_3 x_3 + w_4 x_4 \\ w_1^- x_1 = w_2 x_2 \\ w_2 x_2 = w_3 x_3 \\ w_4 x_4 = 0 \end{cases}.$$

Since the weights are strictly positive and $x \neq \mathbb{0}$, we must have $w_1^+ = w_1^-$, which is a contradiction. Therefore, $\ker \Gamma$ constructed using this weighting pattern has a trivial kernel and $\operatorname{rank}(\Gamma) = 4$.

(ii) Suppose $w_4^+ \neq w_4^-$ but all others are identical, similar to case (i). If $x \in \ker \Gamma$, then

$$\begin{bmatrix} w_1 & 0 & -w_3 & -w_4^- \\ -w_1 & w_2 & 0 & 0 \\ 0 & -w_2 & w_3 & 0 \\ 0 & 0 & 0 & w_4^+ \end{bmatrix} \begin{bmatrix} x_1 \\ x_2 \\ x_3 \\ x_4 \end{bmatrix} = \begin{bmatrix} 0 \\ 0 \\ 0 \\ 0 \end{bmatrix}.$$

However, in this case, we can verify that for all $k \in \mathbb{R}$,

$$x = k \begin{bmatrix} \frac{1}{w_1} & \frac{1}{w_2} & \frac{1}{w_3} & 0 \end{bmatrix}^\mathsf{T}$$

satisfies $x \in \ker \Gamma$. Thus we conclude that $\operatorname{rank}(\Gamma) = 3$.

(iii) Suppose $w^+ \neq w^-$ element-wise, but $w_1^+ = w_3^- =: v_1, w_2^+ = w_1^- =: v_2$, and $w_3^+ = w_2^- =: v_3$, If $x \in \ker \Gamma$, then

$$\begin{bmatrix} v_1 & 0 & -v_1 & -w_4^- \\ -v_2 & v_2 & 0 & 0 \\ 0 & -v_3 & v_3 & 0 \\ 0 & 0 & 0 & w_4^+ \end{bmatrix} \begin{bmatrix} x_1 \\ x_2 \\ x_3 \\ x_4 \end{bmatrix} = \begin{bmatrix} 0 \\ 0 \\ 0 \\ 0 \end{bmatrix},$$

and we can verify that $x = k\begin{bmatrix} 1 & 1 & 1 & 0 \end{bmatrix}^\mathsf{T}$ for any constant k satisfies the equality above, and conclude that $\operatorname{rank}(\Gamma) = 3$ as well.

(iv) Again suppose that $w^+ \neq w^-$, but $w_1^+ = 2w_1^-$ and $w_2^+ = \frac{1}{2}w_2^-$ while $w_3^+ = w_3^- =: w_3$ and $w_4^+ = w_4^- =: w_4$. If $x \in \ker \Gamma$, then

$$\begin{bmatrix} 2w_1^- & 0 & -w_3 & -w_4 \\ -w_1^- & w_2^+ & 0 & 0 \\ 0 & -2w_2^+ & w_3 & 0 \\ 0 & 0 & 0 & w_4 \end{bmatrix} \begin{bmatrix} x_1 \\ x_2 \\ x_3 \\ x_4 \end{bmatrix} = \begin{bmatrix} 0 \\ 0 \\ 0 \\ 0 \end{bmatrix}$$

and we can pick any

$$x = k\begin{bmatrix} \dfrac{w_3}{2w_1^-} & \dfrac{w_3}{2w_2^+} & 1 & 0 \end{bmatrix}^\mathsf{T}$$

for the equality above to holds, and conclude that $\operatorname{rank}(\Gamma) = 3$ too in this case.

The key difference between cases (i) and (ii) is that the asymmetrical edge weight is placed in the cycle $\{e_1, e_2, e_3\}$ in (i) but not in (ii), and the key difference between (i) and (iii) is that, in (iii), the elements of w^- that correspond to the cycle $\{e_1, e_2, e_3\}$ is constructed by "right-shifting" the corresponding elements of w^+ by one. We can alternatively express this relationship using a "weighted" permutation matrix, i.e., $w^- = Pw^+$, where

$$P = \begin{bmatrix} 0 & 0 & w_3^-/w_3^+ & 0 \\ w_1^-/w_1^+ & 0 & 0 & 0 \\ 0 & w_2^-/w_2^+ & 0 & 0 \\ 0 & 0 & 0 & w_4^-/w_4^+ \end{bmatrix}.$$

Note that the top left 3×3 submatrix of P performs the shifting operation. Observe that, however, in both cases (iii) and (iv) where Γ is rank-deficient, for the cycle $\{e_1, e_2, e_3\}$, the product of edge weights in the forward direction is the same as that in the backward direction, that is, $\prod_i^3 w_i^+ = \prod_i^3 w_i^-$.

Given the four cases discussed above and the observations we made, we attempt to state some general results about rank (Γ). First, we generalize the standard result that rank $(A) = n - 1$ to rank (Γ).

Lemma A.1. *If $\mathcal{G}$ is weakly connected, then* rank $(\Gamma) \geq n - 1$.

Proof. Analogous to the proof given in [36, Theorem 9.6], we prove by induction, and denote $\mathcal{G}$ and its Γ matrix with a subscript (k) as needed, which represents the number of nodes. The nontrivial base case is when $n = 2$, for which

$$\Gamma_{(2)} = \begin{bmatrix} w_1^+ & w_1^- \end{bmatrix}^\mathsf{T}, \quad \text{or} \quad \Gamma_{(2)} = \begin{bmatrix} w_1^- & w_1^+ \end{bmatrix}^\mathsf{T},$$

and rank $\left(\Gamma_{(2)}\right) = 1$ in either case since $w_1^+, w_1^- \neq 0$.

For the inductive step, we assume rank $\left(\Gamma_{(n)}\right) \geq n - 1$ up to $n = k$, and prove rank $\left(\Gamma_{(k+1)}\right) \geq k$. First, since $\mathcal{G}_{(k+1)}$ is weakly connected, its underlying undirected graph $\mathcal{G}^u_{(k+1)}$ is connected, and it has a spanning tree $\mathcal{S}^u = (\mathcal{N}, \mathcal{E}^u_T)$, where $|\mathcal{E}_T| = k \leq m$. We denote the corresponding bidirected tree as $\mathcal{S} = (\mathcal{N}, \mathcal{E}_T)$. Next, we relabel the edges of $\mathcal{G}_{(k+1)}$ such that edges $e_1, ..., e_k \in \mathcal{E}_T$, and rename the nodes such that node $k + 1$ is incident to a node $i \in \{1, ..., k\}$ via the forward edge $e_k = (i, k + 1)$. This process only shuffles the rows and columns of the $\Gamma_{(k+1)}$ so that its first k columns correspond to $e_1, ..., e_k$ and does not change its rank and nullity. Let $\delta_{ik} \in \mathbb{R}^{k-1}$ denote the vector with w_k^+ in its i-th entry and zero everywhere else. Then, the matrix $\Gamma_{(k+1)}$ has the following form

$$\left[\begin{array}{c|c|c|c|c} \Gamma_{(k)} & \delta_{ik} & * & \cdots & * \\ \hline \mathbb{0}_k^\mathsf{T} & -w_k^- & & & \end{array}\right],$$

where the columns $*$ represent the edges in $\mathcal{E} \setminus \mathcal{E}_T$ and are not important here. The first block

$$\begin{bmatrix} \Gamma_{(k)} \\ \mathbb{0}_k^\mathsf{T} \end{bmatrix}$$

has at least $k - 1$ linearly independent columns, since rank $\left(\Gamma_{(k)}\right) \geq k - 1$ by the inductive assumption. Since $w_k^- \neq 0$, the column

$$\begin{bmatrix} \delta_{ik} \\ -w_k^- \end{bmatrix}$$

is linearly independent from all the columns in the first block. That is, the submatrix

$$\left[\begin{array}{c|c} \Gamma_{(k)} & \delta_{ik} \\ \hline \mathbb{0}_k^\mathsf{T} & -w_k^- \end{array}\right]$$

has at least k linearly independent columns, so rank $\left(\Gamma_{(k+1)}\right) \geq k$. □

Remark A.1. Since Γ is a wide matrix with n rows, rank (Γ) is either $n-1$ or n. In particular, if $\mathcal{G}$ is a tree, then it has full rank $n-1$.

Recall from Chapter 2.2 that a bidirected graph can be constructed from a directed graph by treating all edges e_k as the forward edge e_k^+ and adding a backward edge e_k^- where appropriate. The same procedure applies in the weighted graph context, although an additional nonzero backward edge weight w_k^- must be chosen. In the same spirit, we can construct a *bidirected cycle* from a directed cycle, in both weighted and unweighted contexts.

Now, we prove a useful result that helps us establish Lemma A.3, which establishes the full rank condition for a weighted bidirected cycle.

Lemma A.2. *Given strictly positive edge weight vectors w^+, w^-, there exist nonzero constants $\{t_i\}_{i=1}^n$ such that*

$$\frac{t_1}{w_1^+} = \frac{t_2}{w_1^-}, \frac{t_2}{w_2^+} = \frac{t_3}{w_2^-}, \cdots, \frac{t_n}{w_n^+} = \frac{t_1}{w_n^-}, \tag{A.1a}$$

if and only if

$$\prod_{i=1}^n w_i^+ = \prod_{i=1}^n w_i^-. \tag{A.1b}$$

Proof. We first show (A.1b) implies (A.1a). Suppose (A.1b) holds, then any $t \in \mathbb{R}$ implies

$$t = t \cdot 1 \implies t = t\left(\frac{\prod_{i=1}^n w_i^+}{\prod_{i=1}^n w_i^-}\right) = t\frac{w_n^+ w_{n-1}^+ \cdots w_1^+}{w_n^- w_{n-1}^- \cdots w_1^-}.$$

We pick an arbitrary $t_1 \neq 0$ and clearly the equality above holds for t_1. Then, we recursively define

$$t_2 \coloneqq t_1\frac{w_1^-}{w_1^+}, \;\; t_3 \coloneqq t_2\frac{w_2^-}{w_2^+}, \;\; \cdots, \;\; t_n \coloneqq t_{n-1}\frac{w_{n-1}^-}{w_{n-1}^+},$$

all of which are well-defined since the weights w_i^+ are nonzero; additionally they are nonzero given $t_1 \neq 0$ and the strictly positive weights. Expanding the t_n term and inserting an identity element using (A.1b), we get

$$t_n = t_1\frac{\prod_{i=1}^{n-1} w_i^-}{\prod_{i=1}^{n-1} w_i^+} = t_1\frac{\prod_{i=1}^n w_i^+}{\prod_{i=1}^n w_i^-}\frac{\prod_{i=1}^{n-1} w_i^-}{\prod_{i=1}^{n-1} w_i^+} = t_1\frac{w_n^+}{w_n^-}.$$

Re-arrange these terms and we recover (A.1a). Next, we prove the converse statement. Suppose that there exist $t_1, ..., t_n \neq 0$ such that (A.1a) holds, then we can re-arrange

the terms as

$$t_1 = t_2\frac{w_1^+}{w_1^-} = \left(t_3\frac{w_2^+}{w_2^-}\right)\frac{w_1^+}{w_1^-} = \cdots = \left(\left(\left(t_1\frac{w_n^+}{w_n^-}\right)\cdots\right)\frac{w_2^+}{w_2^-}\right)\frac{w_1^+}{w_1^-} = t_1\frac{\prod_{i=1}^n w_i^-}{\prod_{i=1}^n w_i^+}$$

which implies (A.1b). □

Lemma A.3. *If $\mathcal{G}$ is a bidirected cycle, then rank$(\Gamma) = n$ if and only if the weights w^+, w^- satisfy*

$$\prod_{i=1}^n w_i^+ \neq \prod_{i=1}^n w_i^-. \tag{A.2}$$

Proof. If $\mathcal{G}$ is a bidirected cycle, then its nodes and edges can be relabeled, i.e., its asymmetrically weighted incidence matrix can be shuffled into the following form, without affecting its rank:

$$\Gamma = \begin{bmatrix} w_1^+ & 0 & \cdots & 0 & -w_n^- \\ -w_1^- & w_2^+ & \cdots & 0 & 0 \\ 0 & -w_2^- & \cdots & 0 & 0 \\ \vdots & \vdots & \ddots & \vdots & \vdots \\ 0 & 0 & \cdots & -w_{n-1}^- & w_n^+ \end{bmatrix}.$$

First, we show that rank $(\Gamma) = n$ implies (A.2) by equivalently proving its contraposition, i.e., we show that (A.1b) implies $\det\Gamma = 0$ and thus rank $(\Gamma) \neq n$. Suppose that (A.1b) holds, then by Lemma A.2, there exist nonzero t_i for $i = 1, ..., n$ such that

$$\frac{t_1}{w_1^+} = \frac{t_2}{w_1^-}, \frac{t_2}{w_2^+} = \frac{t_3}{w_2^-}, \cdots, \frac{t_n}{w_n^+} = \frac{t_1}{w_n^-},$$

which can be equivalently written as

$$w_1^+ = \frac{t_1}{t_2}w_1^-, w_2^+ = \frac{t_2}{t_3}w_2^-, \cdots, w_n^+ = \frac{t_n}{t_1}w_n^-.$$

Thus, substitute the expressions above, we have

$$\det\begin{bmatrix} \frac{t_1}{t_2}w_1^- & 0 & \cdots & 0 & -w_n^- \\ -w_1^- & \frac{t_2}{t_3}w_2^- & \cdots & 0 & 0 \\ 0 & -w_2^- & \cdots & 0 & 0 \\ \vdots & \vdots & \ddots & \vdots & \vdots \\ 0 & 0 & \cdots & -w_{n-1}^- & \frac{t_n}{t_1}w_n^- \end{bmatrix} = \frac{1}{\prod_{i=1}^n w_i^-}\det\underbrace{\begin{bmatrix} \frac{t_1}{t_2} & 0 & \cdots & 0 & -1 \\ -1 & \frac{t_2}{t_3} & \cdots & 0 & 0 \\ 0 & -1 & \cdots & 0 & 0 \\ \vdots & \vdots & \ddots & \vdots & \vdots \\ 0 & 0 & \cdots & -1 & \frac{t_n}{t_1} \end{bmatrix}}_{\tilde{\Gamma}},$$

which is well-defined since w_i^- and t_i are all nonzero. However, observe that

$$-\frac{t_2}{t_1}\begin{bmatrix}\frac{t_1}{t_2}\\-1\\0\\\vdots\\0\end{bmatrix}-\frac{t_3}{t_1}\begin{bmatrix}0\\\frac{t_2}{t_3}\\-1\\\vdots\\0\end{bmatrix}-\cdots-\frac{t_n}{t_1}\begin{bmatrix}0\\0\\\vdots\\\frac{t_{n-1}}{t_n}\\-1\end{bmatrix}=\begin{bmatrix}-1\\0\\0\\\vdots\\\frac{t_n}{t_1}\end{bmatrix},$$

that is, the last column of $\tilde{\Gamma}$ can be written as a linear combination of the first $n-1$ columns, so $\det\tilde{\Gamma}=0$, and Γ itself is rank deficient.

We now show the converse direction by contradiction. Suppose that (A.2) holds, but there always exists exactly one nonzero $x\in\ker\Gamma$. Then, $\operatorname{rank}(\Gamma)=n-1$ by the rank-nullity theorem (by Lemma A.1 there cannot exist more than one such x), and

$$\Gamma x=\begin{bmatrix}w_1^+&0&\cdots&0&-w_n^-\\-w_1^-&w_2^+&\cdots&0&0\\0&-w_2^-&\cdots&0&0\\\vdots&\vdots&\ddots&\vdots&\vdots\\0&0&\cdots&-w_{n-1}^-&w_n^+\end{bmatrix}\begin{bmatrix}x_1\\x_2\\x_3\\\vdots\\x_n\end{bmatrix}=\mathbb{0}_n,$$

which implies

$$\begin{cases}w_1^+x_1-w_n^-x_n=0\\w_2^+x_2-w_1^-x_1=0\\\vdots\\w_n^+x_n-w_{n-1}^-x_{n-1}=0\end{cases}\implies\begin{cases}x_1=\dfrac{t_1}{w_1^+},\quad x_n=\dfrac{t_1}{w_n^-}\\x_2=\dfrac{t_2}{w_2^+},\quad x_1=\dfrac{t_2}{w_1^-}\\\qquad\vdots\qquad\qquad\vdots\\x_n=\dfrac{t_n}{w_n^+},\quad x_{n-1}=\dfrac{t_n}{w_n^-}\end{cases},\tag{A.3}$$

for some $t_1,...,t_n\neq 0$ (by Lemma 2.1, any $t_i=0$ would propagate and result in all t_i's being 0). Then, since $x_i=x_i$ for all $i=1,...,n$, by Lemma A.2 we must have

$$\prod_{i=1}^n w_i^-=\prod_{i=1}^n w_i^+,$$

which is a contradiction. □

Finally, we combine all the previous lemmas for a general asymmetrically weighted

bidirected graph with at least one cycle: suppose that $\mathcal{C}$, the cycle basis of $\mathcal{G}$, has at least one element $\mathrm{c} \in \mathbb{R}^m$, which traverses through the nodes in $\mathcal{N}_\mathrm{c} \subseteq \mathcal{N}$ via the edges in $\mathcal{E}_\mathrm{c} \subseteq \mathcal{E}$. Denote by $\mathcal{G}_\mathrm{c} \coloneqq (\mathcal{N}_\mathrm{c}, \mathcal{E}_\mathrm{c})$ the subgraph induced by the cycle c, and it is associated with the asymmetrically weighted incidence matrix Γ_c.

Theorem A.1. *Suppose $\mathcal{G}$ has a nonempty cycle basis $\mathcal{C}$. Then,* $\operatorname{rank}(\Gamma) = n$ *if and only if there exists at least one* $\mathrm{c} \in \mathcal{C}$ *such that*

$$\prod_{i=1}^{|\mathcal{N}_\mathrm{c}|} w_i^- \neq \prod_{i=1}^{|\mathcal{N}_\mathrm{c}|} w_i^+. \tag{A.4}$$

Proof. We first cut $\mathcal{G}$ into two disjoint subgraphs, with edges in the (nonempty) cutset denoted by χ, where $|\chi| = d < m$. The first subgraph $\mathcal{G}_\mathrm{c}$ corresponds to a cycle c that satisfies (A.4), if it exists. Let $|\mathcal{N}_\mathrm{c}| = |\mathcal{E}_\mathrm{c}| = \ell \leq n$. The second subgraph is $\mathcal{G}_{\not\mathrm{c}} \coloneqq (\mathcal{N}_{\not\mathrm{c}}, \mathcal{E}_{\not\mathrm{c}})$, where $\mathcal{N}_{\not\mathrm{c}} \coloneqq \mathcal{N} \setminus \mathcal{N}_\mathrm{c}$ and $\mathcal{E}_{\not\mathrm{c}} \coloneqq \mathcal{E} \setminus (\mathcal{E}_\mathrm{c} \cup \chi)$. In addition, let $\Gamma_{\not\mathrm{c}}$ denote the asymmetrically weighted incidence matrix for $\mathcal{G}_{\not\mathrm{c}}$, and let $\Gamma_\chi \in \mathbb{R}^{n \times d}$ be the matrix whose columns represent the edges in the cutset χ.

Next, we can re-label the nodes and edges of $\mathcal{G}$, and correspondingly shuffle the rows and columns of Γ such that $\mathcal{N}_\mathrm{c} = \{1, ..., \ell\}$, $\mathcal{N}_{\not\mathrm{c}} = \{\ell + 1, ..., n\}$, $\mathcal{E}_\mathrm{c} = \{e_1, ..., e_\ell\}$, $\chi = \{e_{\ell+1}, ..., e_{\ell+d}\}$, and $\mathcal{E}_{\not\mathrm{c}} = \{e_{\ell+d+1}, ..., e_m\}$. That is, the matrix Γ can be shuffled into the following form

$$\left[\begin{array}{c|c|c} \Gamma_\mathrm{c} & \multirow{2}{*}{Γ_χ} & \multirow{2}{*}{$\mathbb{0}_{\ell \times (m-\ell-d)}$} \\ \hline \mathbb{0}_{(n-\ell)\times \ell} & & \Gamma_{\not\mathrm{c}} \end{array}\right] =: \left[Z_\mathrm{c} \;\middle|\; \Gamma_\chi \;\middle|\; Z_{\not\mathrm{c}}\right], \tag{A.5}$$

where the zero blocks exist due to the fact that $\mathcal{N}_\mathrm{c} \cap \mathcal{N}_{\not\mathrm{c}} = \varnothing$. We can make several observations from (A.5). First and most importantly, by Lemma A.3 the matrix Γ_c has rank ℓ, i.e., Z_c has ℓ linearly independent columns, if and only if (A.4) holds. Next, since the cutset χ is nonempty, Γ_χ contains at least one column, which is linearly independent from all columns in Z_c and $Z_{\not\mathrm{c}}$ by construction. Finally, by Lemma A.1, $\operatorname{rank}(Z_{\not\mathrm{c}}) = \operatorname{rank}(\Gamma_{\not\mathrm{c}}) \geq n - \ell - 1$. Thus, together, Γ contains at least $\ell + 1 + (n - \ell - 1) = n$ linearly independent columns, i.e., $\operatorname{rank}(\Gamma) \geq n$ if and only if (A.4) holds. However, by Remark A.1, $\operatorname{rank}(\Gamma)$ is either $n - 1$ or n. Therefore, we conclude that $\operatorname{rank}(\Gamma) = n$ if and only if (A.4) holds. □

Appendix B

Power Flow Equation Vectorization Example

In this appendix, we use a concrete example to demonstrate the procedure to vectorize the power flow equations given in Section 3.3. Consider the bidirected graph model of a simple four-bus system in Figure B.1, where the nodes are labelled in accordance with the $\mathcal{N}_L, \mathcal{N}_G$ partition (the blue circles represent load buses and the red squares represent generator buses), and only the forward edges are shown and labelled. We assume that all the branches are modelled by the Π-model and the system contains at least one phase-shifting transformer.

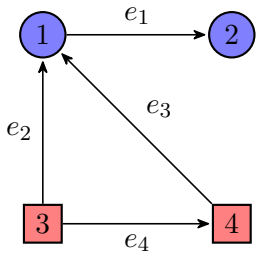

Figure B.1: The bidirected graph model of a simple four-bus system

The incidence matrix and the "from" and "to" incidence matrices are as follows:

$$A = \begin{bmatrix} 1 & -1 & -1 & 0 \\ -1 & 0 & 0 & 0 \\ 0 & 1 & 0 & 1 \\ 0 & 0 & 1 & -1 \end{bmatrix}, \quad A^+ = \begin{bmatrix} 1 & 0 & 0 & 0 \\ 0 & 0 & 0 & 0 \\ 0 & 1 & 0 & 1 \\ 0 & 0 & 1 & 0 \end{bmatrix}, \quad A^- = \begin{bmatrix} 0 & 1 & 1 & 0 \\ 1 & 0 & 0 & 0 \\ 0 & 0 & 0 & 0 \\ 0 & 0 & 0 & 1 \end{bmatrix},$$

and the branch stiffness matrices defined in (3.8) are as follows:

$$D_G^+ = \operatorname{diag}\left(\begin{bmatrix} V_1^\circ V_2^\circ G_{12} \\ V_3^\circ V_1^\circ G_{31} \\ V_4^\circ V_1^\circ G_{41} \\ V_3^\circ V_4^\circ G_{34} \end{bmatrix}\right), \quad D_G^- = \operatorname{diag}\left(\begin{bmatrix} V_1^\circ V_2^\circ G_{21} \\ V_3^\circ V_1^\circ G_{13} \\ V_4^\circ V_1^\circ G_{14} \\ V_3^\circ V_4^\circ G_{43} \end{bmatrix}\right),$$

$$D_B^+ = \operatorname{diag}\left(\begin{bmatrix} V_1^\circ V_2^\circ B_{12} \\ V_3^\circ V_1^\circ B_{31} \\ V_4^\circ V_1^\circ B_{41} \\ V_3^\circ V_4^\circ B_{34} \end{bmatrix}\right), \quad D_B^- = \operatorname{diag}\left(\begin{bmatrix} V_1^\circ V_2^\circ B_{21} \\ V_3^\circ V_1^\circ B_{13} \\ V_4^\circ V_1^\circ B_{14} \\ V_3^\circ V_4^\circ B_{43} \end{bmatrix}\right).$$

The normalized load voltages is $v = [v_1 \quad v_2]^\mathsf{T}$, so we can write $g(v) = [v_1 \quad v_2 \quad 1 \quad 1]^\mathsf{T}$, and $h(v) = [v_1 v_2 \quad v_1 \quad v_1 \quad 1]^\mathsf{T}$.

We focus on vectorizing the active power flow equations, since the reactive power flow equations can be vectorized almost identically. As such, the relevant asymmetrically weighted incidence matrices are $|\Gamma_G|$ and Γ_B, which can be written as

$$|\Gamma_G| = \begin{bmatrix} V_1^\circ V_2^\circ G_{12} & V_1^\circ V_3^\circ G_{13} & V_1^\circ V_4^\circ G_{14} & 0 \\ V_1^\circ V_2^\circ G_{21} & 0 & 0 & 0 \\ 0 & V_1^\circ V_3^\circ G_{31} & 0 & V_3^\circ V_4^\circ G_{34} \\ 0 & 0 & V_1^\circ V_4^\circ G_{41} & V_3^\circ V_4^\circ G_{43} \end{bmatrix},$$

$$\Gamma_B = \begin{bmatrix} V_1^\circ V_2^\circ B_{12} & -V_1^\circ V_3^\circ B_{13} & -V_1^\circ V_4^\circ B_{14} & 0 \\ -V_1^\circ V_2^\circ B_{21} & 0 & 0 & 0 \\ 0 & V_1^\circ V_3^\circ B_{31} & 0 & V_3^\circ V_4^\circ B_{34} \\ 0 & 0 & V_1^\circ V_4^\circ B_{41} & -V_3^\circ V_4^\circ B_{43} \end{bmatrix}.$$

The standard active power flow equations (3.1a) are written as follows:

$$\begin{aligned} P_1 &= V_1^2 G_{11} + V_1 V_2 G_{12} \cos(\theta_1 - \theta_2) + V_1 V_2 B_{12} \sin(\theta_1 - \theta_2) \\ &\quad + V_1 V_3 G_{13} \cos(\theta_1 - \theta_3) + V_1 V_2 B_{13} \sin(\theta_1 - \theta_3) \\ &\quad + V_1 V_4 G_{14} \cos(\theta_1 - \theta_4) + V_1 V_2 B_{14} \sin(\theta_1 - \theta_4). && \text{(B.1a)} \\ P_2 &= V_2^2 G_{22} + V_2 V_1 G_{21} \cos(\theta_2 - \theta_1) + V_2 V_1 B_{21} \sin(\theta_2 - \theta_1), && \text{(B.1b)} \\ P_3 &= V_3^2 G_{33} + V_3 V_1 G_{31} \cos(\theta_3 - \theta_1) + V_3 V_1 B_{31} \sin(\theta_3 - \theta_1) \\ &\quad + V_3 V_4 G_{34} \cos(\theta_3 - \theta_4) + V_3 V_4 B_{34} \sin(\theta_3 - \theta_4), && \text{(B.1c)} \\ P_4 &= V_4^2 G_{44} + V_4 V_1 G_{41} \cos(\theta_4 - \theta_1) + V_4 V_1 B_{41} \sin(\theta_4 - \theta_1) \\ &\quad + V_4 V_3 G_{43} \cos(\theta_4 - \theta_3) + V_4 V_3 B_{43} \sin(\theta_4 - \theta_3). && \text{(B.1d)} \end{aligned}$$

We can group the cosine terms on the right-hand sides of (B.1) as follows:

$$\begin{bmatrix} V_1V_2G_{12}\cos(\theta_1-\theta_2)+V_1V_3G_{13}\cos(\theta_1-\theta_3)+V_1V_4G_{14}\cos(\theta_1-\theta_4) \\ V_2V_1G_{21}\cos(\theta_2-\theta_1) \\ V_3V_1G_{31}\cos(\theta_3-\theta_1)+V_3V_4G_{34}\cos(\theta_3-\theta_4) \\ V_4V_1G_{41}\cos(\theta_4-\theta_1)+V_4V_3G_{43}\cos(\theta_4-\theta_3)+ \end{bmatrix}, \tag{B.2}$$

and the sine terms as follows:

$$\begin{bmatrix} V_1V_2B_{12}\sin(\theta_1-\theta_2)+V_1V_2B_{13}\sin(\theta_1-\theta_3)+V_1V_2B_{14}\sin(\theta_1-\theta_4) \\ V_2V_1B_{21}\sin(\theta_2-\theta_1) \\ V_3V_1B_{31}\sin(\theta_3-\theta_1)+V_3V_4B_{34}\sin(\theta_3-\theta_4) \\ V_4V_1B_{41}\sin(\theta_4-\theta_1)+V_4V_3B_{43}\sin(\theta_4-\theta_3) \end{bmatrix}. \tag{B.3}$$

The necessity of both D_G^+ and D_G^- (respectively, D_B^+ and D_B^-) is reflected in the equations above where both G_{ij} and G_{ji} (resp. B_{ij} and B_{ji}) are present, and at least one branch (i,j) satisfies $G_{ij} \neq G_{ji}$ and $B_{ij} \neq B_{ji}$.

For the vectorization steps, we proceed term by term as discussed in Section 3.3. Vectorizing the squared voltage terms is straightforward and thus omitted. For the second term involving cosine, first, we can easily verify that

$$A^\mathsf{T}\theta = \begin{bmatrix} \theta_1-\theta_2 \\ \theta_3-\theta_1 \\ \theta_4-\theta_1 \\ \theta_3-\theta_4 \end{bmatrix}.$$

Since $\mathbf{cos}\left(A^\mathsf{T}\theta\right) = \mathbf{cos}\left(-A^\mathsf{T}\theta\right)$, we have

$$\mathbf{cos}\left(A^\mathsf{T}\theta\right) = \begin{bmatrix} \cos(\theta_1-\theta_2) \\ \cos(\theta_3-\theta_1) \\ \cos(\theta_4-\theta_1) \\ \cos(\theta_3-\theta_4) \end{bmatrix} = \begin{bmatrix} \cos(\theta_2-\theta_1) \\ \cos(\theta_1-\theta_3) \\ \cos(\theta_1-\theta_4) \\ \cos(\theta_4-\theta_3) \end{bmatrix}.$$

Then, we can verify that

$$|\Gamma_G|[h(v)] = \begin{bmatrix} V_1V_2G_{12} & V_1V_3G_{13} & V_1V_4G_{14} & 0 \\ V_1V_2G_{21} & 0 & 0 & 0 \\ 0 & V_1V_3G_{31} & 0 & V_3V_4G_{34} \\ 0 & 0 & V_1V_4G_{41} & V_3V_4G_{43} \end{bmatrix},$$

and $|\Gamma_G|[h(v)]\,\mathbf{cos}\left(A^\mathsf{T}\theta\right)$ results in precisely (B.2).

For the third term involving the sine terms, we can similarly verify that

$$\Gamma_B[h(v)] = \begin{bmatrix} V_1V_2B_{12} & -V_1V_3B_{13} & -V_1V_4B_{14} & 0 \\ -V_1V_2B_{21} & 0 & 0 & 0 \\ 0 & V_1V_3B_{31} & 0 & V_3V_4B_{34} \\ 0 & 0 & V_1V_4B_{41} & -V_3V_4B_{43} \end{bmatrix},$$

and that since $\mathbf{sin}\left(-A^\mathsf{T}\theta\right) = -\mathbf{sin}\left(A^\mathsf{T}\theta\right)$,

$$\mathbf{sin}\left(A^\mathsf{T}\theta\right) = \begin{bmatrix} \sin(\theta_1 - \theta_2) \\ \sin(\theta_3 - \theta_1) \\ \sin(\theta_4 - \theta_1) \\ \sin(\theta_3 - \theta_4) \end{bmatrix} = \begin{bmatrix} -\sin(\theta_2 - \theta_1) \\ -\sin(\theta_1 - \theta_3) \\ -\sin(\theta_1 - \theta_4) \\ -\sin(\theta_4 - \theta_3) \end{bmatrix}.$$

The negative signs in $\Gamma_B[h(v)]$ thus exactly cancels out the negative signs in the $\sin(\cdot)$ terms in the product $\Gamma_B[h(v)]\,\mathbf{sin}\left(A^\mathsf{T}\theta\right)$, which recovers (B.3).